

RS-04-083

June 11, 2004

U. S. Nuclear Regulatory Commission  
ATTN: Document Control Desk  
Washington, DC 20555-0001

Dresden Nuclear Power Station, Units 2 and 3  
Facility Operating License Nos. DPR-19 and DPR-25  
NRC Docket Nos. 50-237 and 50-249

Quad Cities Nuclear Power Station, Units 1 and 2  
Facility Operating License Nos. DPR-29 and DPR-30  
NRC Docket Nos. 50-254 and 50-265

**Subject:** Additional Information Regarding Potential Steam Dryer Loading at Dresden Nuclear Power Station

**Reference:** Letter from K. R. Jury (Exelon Generation Company, LLC) to U. S. NRC, "Commitments and Plans Related to Extended Power Uprate Operation," dated May 12, 2004

In the referenced letter, Exelon Generation Company, LLC (EGC) submitted the quantitative input to the technical assessment of the loadings of the Dresden Nuclear Power Station (DNPS), Units 2 and 3, steam dryers. In a conference call on May 26, 2004, the NRC requested EGC to submit similar information for the Quad Cities Nuclear Power Station (QCNPS), Unit 1, steam dryer to enable the NRC to compare the potential loading on the DNPS steam dryers to QCNPS Unit 1. The Attachment to this letter provides the requested information.

The attachment to this letter is the result of evaluations performed in December 2003 by Continuum Dynamics Incorporated. As described in the referenced letter, the models used for these evaluations have been revised as part of the Plan for Evaluation of Flow Effects. Additional steam line pressure data is being gathered at both DNPS units and will be evaluated using the improved model. The results of these evaluations will be used to update the DNPS operability evaluations, as appropriate. However, based on evaluations completed to date, EGC continues to conclude that the structural integrity of the DNPS steam dryers will not be compromised as a result of operation at EPU conditions.

ADD1

June 11, 2004  
U. S. Nuclear Regulatory Commission  
Page 2

If you have any questions concerning this submittal, please contact Mr. Kenneth M. Nicely, at (630) 657-2803.

Respectfully,



Patrick R. Simpson  
Manager – Licensing

Attachment:

Continuum Dynamics, Inc. Report No. 03-18, Revision 2, "Hydrodynamic Loads on Quad Cities Unit 1 Steam Dryer," dated May 2004

cc: Regional Administrator – NRC Region III  
NRC Senior Resident Inspector – Dresden Nuclear Power Station  
NRC Senior Resident Inspector – Quad Cities Nuclear Power Station

**ATTACHMENT**

**Continuum Dynamics, Inc. Report No. 03-18, Revision 2,  
"Hydrodynamic Loads on Quad Cities Unit 1 Steam Dryer," dated May 2004**

Hydrodynamic Loads on Quad Cities Unit 1 Steam Dryer

Final Report

Revision 2

Prepared by

Continuum Dynamics, Inc.  
34 Lexington Avenue  
Ewing, NJ 08618

Prepared under Purchase Order No. 64992 for

Exelon Generation LLC  
4300 Winfield Road  
Warrenville, IL 60555

Approved by



---

Alan Bilanin

May 2004

## Object

In plant measured pressure oscillation data in main steam lines of Quad Cities Unit 1 (QC1) are used to force a dynamic model of the steam system. The model is then used to predict the fluctuating pressures across components of the steam dryer in the reactor vessel. This effort provides Exelon with a dryer load definition which comes directly from measured data. The hydrodynamic load data then will be used by a structural analyst to assess the structural adequacy of the "as built" steam dryer in QC1.

## Physical Observations

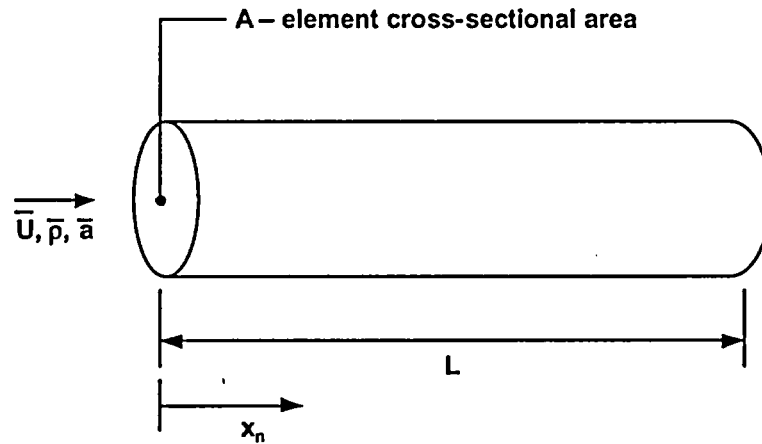
Analysis by others, of dryer failure at QC2 during the summer of 2003, used the observed fatigue dryer damage to back calculate a structural load which was consistent with this damage. Fatigue damage, however, is dependent upon both magnitude of load and frequency of application. The analysis was not able to identify discrete frequencies and therefore recommended that a flat spectrum be used with an amplitude which was determined to be consistent with the observed damage. This flat spectrum is equivalent to the assumption that the forcing is random, in spite of the fact that the subscale tests conducted by others indicated that discrete frequencies were observed in the steam lines and the reactor steam dome. Exelon obtained unsteady pressure data in the plant (QC1) during operation, and the effort reported herein is the analysis of these data. Contrary to the assumption of a flat loading spectrum, the data show that there are discrete deterministic phenomenon at work in the steam dome and main steam lines that are responsible for the loading on the dryer. This report quantifies this load from full scale test data.

## Modeling Considerations

Pulsation in a single phase compressible medium, where acoustic wavelengths are long compared to component dimensions and in particular long compared to transverse dimensions (directions perpendicular to the primary flow directions), lend themselves to an analysis methodology known as acoustic circuit analysis. If the analysis is restricted to frequencies below 50 Hz, acoustic wavelengths are approximately 30 feet in length and wavelengths are long compared to most components of interest.

Acoustic circuit analysis divides the system to be analyzed into elements which are characterized as sketched below in a length ( $L$ ), cross sectional area ( $A$ ), mean density ( $\bar{\rho}$ ), mean flow velocity ( $\bar{U}$ ) and mean acoustic speed ( $\bar{a}$ )

n<sup>th</sup>-element



It can be shown that the fluctuating pressure  $P'$  and velocity  $u'_n$  in this n<sup>th</sup> element must satisfy

$$P'_n = (A_n e^{ik_{1n} X_n} + B_n e^{ik_{2n} X_n}) e^{i\omega t}$$

$$u'_n = \frac{1}{\omega \rho} (A_n k_{1n} e^{ik_{1n} X_n} + B_n k_{2n} e^{ik_{2n} X_n}) e^{i\omega t}$$

where harmonic time dependence of the form  $e^{i\omega t}$ , has been assumed. The wave numbers  $k_{1n}$  and  $k_{2n}$  are the two complex roots of

$$k_n^2 + i4f_n \frac{|\bar{U}_n|}{D_n a} (\omega + \bar{U}_n k_n) - \frac{\omega}{a} (\omega + \bar{U}_n k_n) = 0$$

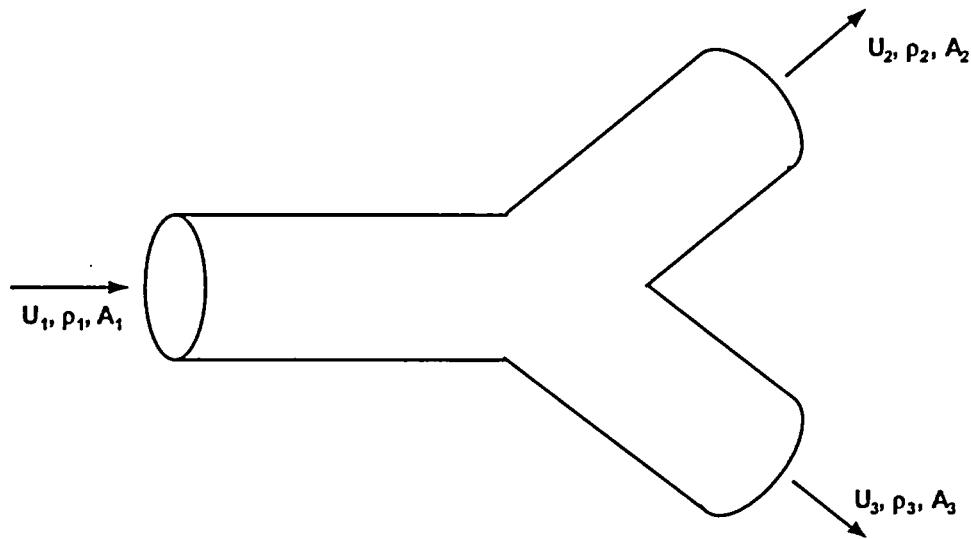
where  $f_n$  - Cranes pipe friction factor for element n  
 $D_n$  - hydrodynamic diameter for element n  
 $i = \sqrt{-1}$

$A_n$  and  $B_n$  are constants which are a function of frequency and are determined by satisfying continuity of pressure at element junctions and mass conservation at a junction.

Mass conservation at a junction requires that (see sketch below)

$$\rho_1 U_1 A_1 = \rho_2 U_2 A_2 + \rho_3 U_3 A_3$$

where ( )<sub>m</sub> refer to each segment.



The flow passages for the QCl reactor and main steam lines are discretized into 78 elements and the resulting system can be driven with prescribed shear layer motions at geometric discontinuities. These discontinuities exist in the steam delivery system where convective velocities are high.

One source of energy transfer from the main steam velocity to unsteady motion results from the impingement of the shear layer in the main steam line over the 30 inch diameter D ring junction. This oscillation of the shear layer over the cavity formed by D ring header has an empirically determined preferred frequency of oscillation ( $f$ ) of

$$f = 0.44 \frac{\bar{U}}{D}$$

The preferred driving frequency with a main steam velocity at this junction is 145 ft/sec and  $D = 2.5$  ft is 25.5 Hz. As will be shown, the plant data suggest that energy does indeed exist at this frequency in the main steam lines. The circuit analysis should tell whether the energy at this frequency can propagate into the reactor dome.



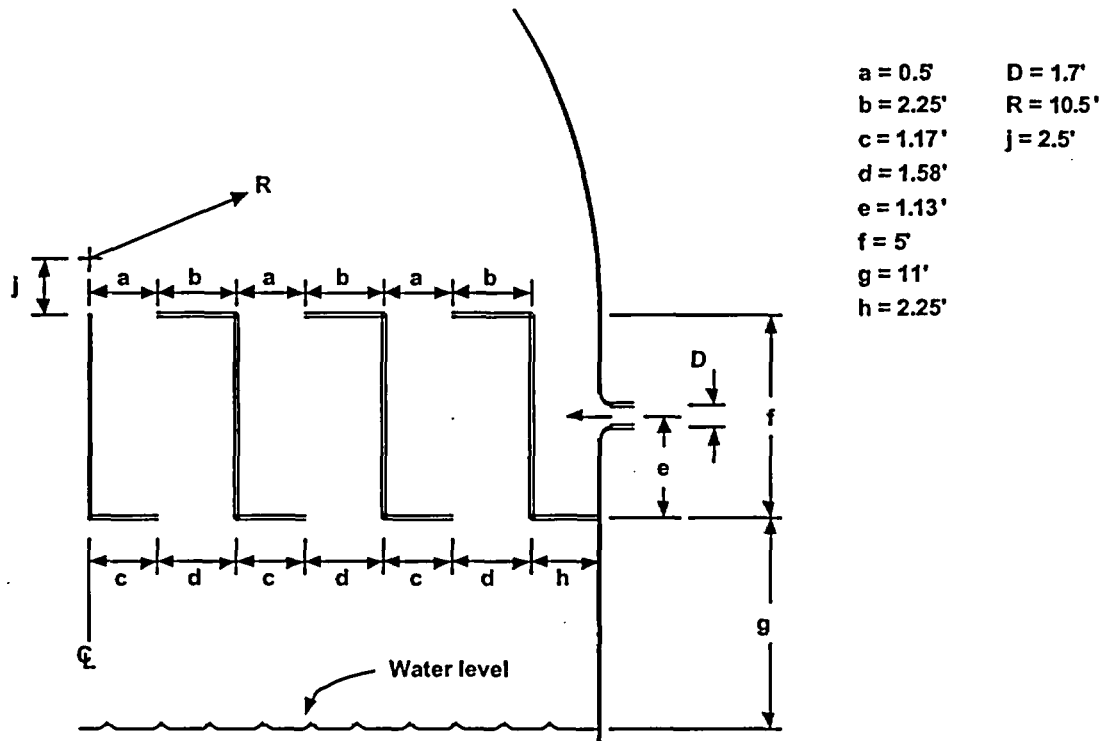


Figure 2: Steam dome and dryer dimensions.

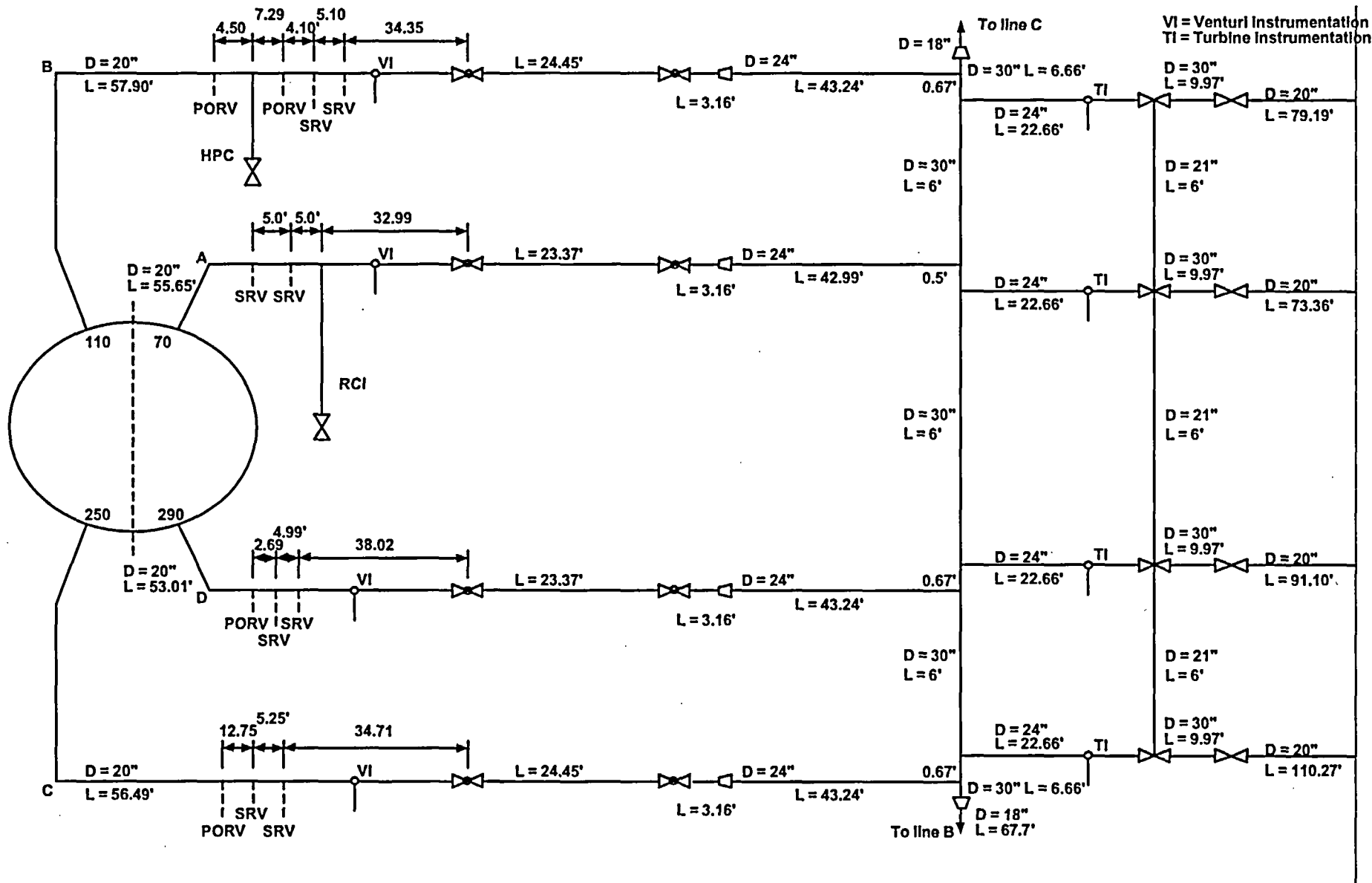


Figure 3: Piping geometry to be used in the circuit analysis (QC1).

## Input Pressure Data

Exelon has mounted pressure transducers on the main steam lines at the main steam venturi and upstream of the turbine (turbine instrument lines). The data sets provided are tabulated below on Table 1. All data provided were taken at the end of instrument lines whose lengths were specified. Lines were assumed filled with water and the data corrected for the instrument line effects of line length, acoustic speed, and losses along the line, by correcting the data in frequency space and then reconstructing the time signal at the instrument line location on the main steam line. Corrections are significant at frequencies associated with the 1/4, 3/4, 5/4, etc. standing wave frequencies of the instrument lines. The resulting pressure time histories and Power Spectral Density functions (PSDs) are shown on Figures 4 to 22. The respective captions on these figures are read as follows. From Figure 4-a, for example, the label "18B: 11.95 Turbine" denotes that the data set number is "18" (see Table 1) taken on the "B" steam line at a steam mass flow rate of  $11.95 \times 10^6$  lbm/hr. The sensor location is at the main steam line "turbine" location.

Note from Table 1 that one data set was provided at a low power setting ( $9.65 \times 10^6$  lbm/hr), but was not analyzed, since the corresponding turbine data were not recorded. In addition, one data set was provided at the highest power setting ( $11.95 \times 10^6$  lbm/hr), but was also not analyzed, since the phase information between the main steam lines was not recorded.

In an effort to illustrate the relationship between mean steam flow rate and pressure oscillation level, the rms pressure at the venturi on main steam line D was plotted as a function of mean steam flow rate on Figure 23 (the D line was chosen, since by observation the oscillations are largest in this line). The data point, at the mean steam flow rate of  $9.55 \times 10^6$  lbm/hr, and corresponding rms pressure of 6.9 psid, is suspect, since an examination of the pressure time history shows pressure spikes that do not appear to have any physical basis. Eliminating this data point from discussion leads to the conclusion that the rms pressure fluctuations on the D main steam line are an increasing function of mean steam flow rate.

From work with these data sets, it is known that the largest dryer loads are correlated with the highest rms pressure levels. It is therefore anticipated that the largest dryer load occurs in these data at a mean steam flow rate of  $11.95 \times 10^6$  lbm/hr. Unfortunately, at this flow rate, data have not been obtained simultaneously at each of the four venturi pressure transducers, and therefore dryer loads cannot be confidently computed at this flow rate. For this reason the dryer load definition will be deduced from data taken at a mean steam flow rate of  $11.75 \times 10^6$  lbm/hr. Until data are retaken at the flow rate of  $11.95 \times 10^6$  lbm/hr, it is suggested that the dryer load definition given in the Appendix be ratioed upward by 2.54, which is the increase in rms pressure at  $25 \pm 2$  Hz, at the main steam line D venturi at a mean steam flow rate of  $11.95 \times 10^6$  lbm/hr (Figure 6-b), over that at  $11.75 \times 10^6$  lbm/hr (Figure 14-d). This adjustment unfortunately adds additional uncertainty to the load definition.

Table 1  
SUMMARY OF QUAD CITIES 1 DATA SETS

Data Set #	Steam Flow (10 <sup>6</sup> lbm/hr)	Location	Date/Time	Data Rate (samples/sec)	Figure #	Comments
18	11.95	Turbine B & C	08/01 1713	2000	4-a, b	1
19	11.95	Turbine B & C	08/09 0806	500	5-a, b	1
20	11.95	Venturi B	08/04 2105	2000	6-a	1
20	11.95	Venturi D	08/04 2113	2000	6-b	1, 2
25	9.65	Venturi A, B, C & D	12/01 13:09	2000		3
26	9.55	Turbine A, B, C & D	12/01 13:15	2000	7-a, b, c, d	4
27	9.55	Venturi A, B, C & D	12/01 13:16	2000	8-a, b, c, d	2, 4
28	9.60	Turbine A, B, C & D	12/02 07:44	2000	9-a, b, c, d	4
29	9.60	Venturi A, B, C & D	12/02 07:45	2000	10-a, b, c, d	2, 4
42	10.23	Turbine A, B, C & D	12/30 08:37	2000	11-a, b, c, d	4
43	10.23	Venturi A, B, C & D	12/30 08:39	2000	12-a, b, c, d	2, 4
44	11.75	Turbine A, B, C & D	12/30 13:50	2000	13-a, b, c, d	5
45	11.75	Venturi A, B, C & D	12/30 13:31	2000	14-a, b, c, d	2, 5
46	10.48	Turbine A, B, C & D	12/30 09:22	2000	15-a, b, c, d	4
47	10.48	Venturi A, B, C & D	12/30 09:23	2000	16-a, b, c, d	2, 4
48	10.76	Turbine A, B, C & D	12/30 10:11	2000	17-a, b, c, d	4
49	10.76	Venturi A, B, C & D	12/30 10:12	2000	18-a, b, c, d	2, 4
50	11.17	Turbine A, B, C & D	12/30 11:08	2000	19-a, b, c, d	4
51	11.17	Venturi A, B, C & D	12/30 11:10	2000	20-a, b, c, d	2, 4
52	11.40	Turbine A, B, C & D	12/30 12:13	2000	21-a, b, c, d	4
53	11.40	Venturi A, B, C & D	12/30 12:14	2000	22-a, b, c, d	2, 4

Comment 1: not analyzed for dryer load

Comment 2: rms value computed on D venturi data

Comment 3: not used

Comment 4: analyzed for dryer load but not reported here

Comment 5: used for dryer load definition

## Model Validation

Referring to Table 1 there are eight data sets where the four venturi pressure fluctuations were recorded simultaneously, and the four turbine pressure fluctuations were recorded simultaneously. Therefore, at other power levels the phasing information is in general lost between instrument locations, and some approximation will be introduced into the analysis if these data were used. Unfortunately, the assumptions required to proceed introduce unquantifiable conservatism into the load, and it is now known that the phase relationship between fluctuations in the four main steam lines must be known. From Table 1 it may be seen that the pressures in the venturi instrument lines A through D were recorded simultaneously in Runs 27, 29, 43, 45, 47, 49, 51, and 53 with corresponding turbine data in Runs 26, 28, 42, 44, 46, 48, 50, and 52, respectively. The main steam venturi measurements were used to drive the circuit model of the system, and validation will be to predict the average root mean square pressure measured by the four turbine instruments at the same power settings. These averages are shown in Table 2.

It should be noted that the turbine instrumentation showed extremely narrow spikes at precisely 20 and 40 Hz. These spikes are believed to be induced by the strong electromagnetic field of the turbine. The spikes were removed from the data analyzed by dropping the Fourier coefficients of the time series between 19-21 and 39-41 Hz.

The model was inputted all of the venturi in phase data sets, and Cranes frictional damping was adjusted in the main steam lines until the average root mean square pressure was predicted at the turbine instrument lines. The four venturi data sets were used simultaneously in the acoustic circuit analysis, to determine sources at the main steam line D ring junction. The friction factors used are summarized in Table 3. The fact that only about a factor of 5% greater than that recommended by Cranes is judged to be a very favorable result of this analysis.

Table 2  
 SUMMARY OF QUAD CITIES 1 RMS PRESSURE VALUES AT THE TURBINE  
 INSTRUMENT LINES

Run	Steam Flow (10 <sup>6</sup> lbm/hr)	A Line P <sub>RMS</sub> (psid)	B Line P <sub>RMS</sub> (psid)	C Line P <sub>RMS</sub> (psid)	D Line P <sub>RMS</sub> (psid)	Average (psid)
26	9.55	2.01	2.03	2.62	2.39	2.26
28	9.60	1.95	2.17	3.07	2.39	2.43
42	10.23	2.17	2.07	2.42	2.44	2.30
44	11.75	2.38	2.69	3.88	3.22	3.10
46	10.48	2.15	2.43	2.89	2.35	2.47
48	10.76	2.41	2.58	2.87	2.60	2.62
50	11.17	2.40	2.55	3.23	2.94	2.80
52	11.40	2.61	2.78	3.28	3.05	2.94

Table 3  
 SUMMARY OF QUAD CITIES 1 DAMPING MODIFICATIONS TO PREDICT THE  
 RMS PRESSURE VALUES AT THE TURBINE INSTRUMENT LINES

Steam Flow (10 <sup>6</sup> lbm/hr)	Multiplier on Cranes	Turbine Inlet Predicted rms (psid)	Turbine Inlet Measured rms (psid)
9.55	1.05	4.06	2.26
9.60	1.05	2.46	2.43
10.23	1.05	2.27	2.30
10.48	1.05	2.49	2.47
10.76	1.05	2.86	2.62
11.17	1.05	2.79	2.80
11.40	1.05	2.93	2.94
11.75	1.05	3.23	3.10

## Results

The model (subject to the approximations and limitations described above) can now predict the pressure time histories in the reactor steam space as a function of position and time. Shown in Figure 24 is the prediction of steam dome pressure time history and PSD at a steam flow rate of  $11.75 \times 10^6$  lbm/hr. Note that the PSD levels are very low, and little energy exists in the 20-30 Hz frequency band.

## Dryer Hydrodynamic Forcing

Pressure differences are now computed across dryer components, and these loads and locations are described in the Appendix and are transmitted separately. In this section we will discuss these loads.

### Maximum Predicted Load on Dryer

The analysis discussed above shows the maximum predicted load occurs on the cover plate located at the  $270^\circ$  position. The differential pressure time history and associated PSD are shown in Figure 25. Here, clearly, is a strong load at approximately 25 Hz and 33 Hz, which should be compared with the pressure fluctuation in the steam dome (Figure 24) which is lower by nearly three orders of magnitude. This indicates excitation of the steam above and below the dryer in a mode that would be difficult to anticipate by inspection of the dryer and steam dome geometry. It is also noted that unless the phasing of fluctuations in the main steam lines were such that signals were out of phase in general, the steam dome is a pressure node in the system. The peak is sharp and centered about 25 Hz. The maximum load is predicted on the side of the dryer on which the most severe damage was observed.

Differential pressure loads for other dryer components computed at the center of the component are shown in Figures 26 to 32 for a steam flow rate of  $11.75 \times 10^6$  lbm/hr. In general the loads decrease radially inboard into the dryer components away from the main steam line inlets, but not monotonically. This again is an indication that the acoustic oscillation about the dryer assembly is complex.

### Dryer Loading as a Result of Damage

When the differential pressure is sufficiently high that a crack or hole develops across a dryer plate, an acoustic path is opened whereby the pressure signal can easily be transferred to an inner plate. As an exercise, the acoustic circuit analysis was modified to include a hole at the center of the  $270^\circ$  outer bank hood, and a calculation was undertaken to estimate the pressure reduction that could occur. Figure 33 summarizes the results of the calculation. A hole area of  $0.0001 \text{ ft}^2$  recovers the same results as an area of  $0 \text{ ft}^2$  (no hole in outer bank hood). The largest hole area decreases the normalized rms pressure difference across the outer bank hood by a factor of 4.0, while increasing the normalized rms pressure difference across the next internal bank hood by a factor of 3.3. The

normalized pressure difference is that which would be predicted across the outer bank hood when undamaged.

## Conclusions

1. The acoustic circuit analysis used with plant data
  - a) confirms that steam dryer hydrodynamic loads are highest at the highest reactor power setting.
  - b) predicts the maximum loading on the dryer occurs predominantly at a single frequency, 25 Hz in the 0 to 50 Hz frequency range. This is in agreement with the plant reactor pressure data included in Exelon's July 25, 2003 presentation to the NRC.
  - c) predicts that the loads on dryer components are largest for components nearest the main steam nozzles and decrease for components near the center of the reactor vessel.
  - d) does not determine the highest dryer load, since the data set at maximum mean steam flow rate of  $11.95 \times 10^6$  lbm/hr is incomplete.
  - e) predicts that the highest peak differential pressure to be found on any dryer component at a steam flow rate of  $11.75 \times 10^6$  lbm/hr is instantaneously 2.8 psid (Figure 25), with a rms differential pressure of 0.82 psid. If ratioed to account for a steam flow rate of  $11.95 \times 10^6$  lbm/hr, this rms differential pressure would become 2.08 psid.
2. While the load definition given herein is judged to be the best that could be obtained with existing data and plant description, improvement would result from obtaining data at maximum operating steam flow rates.

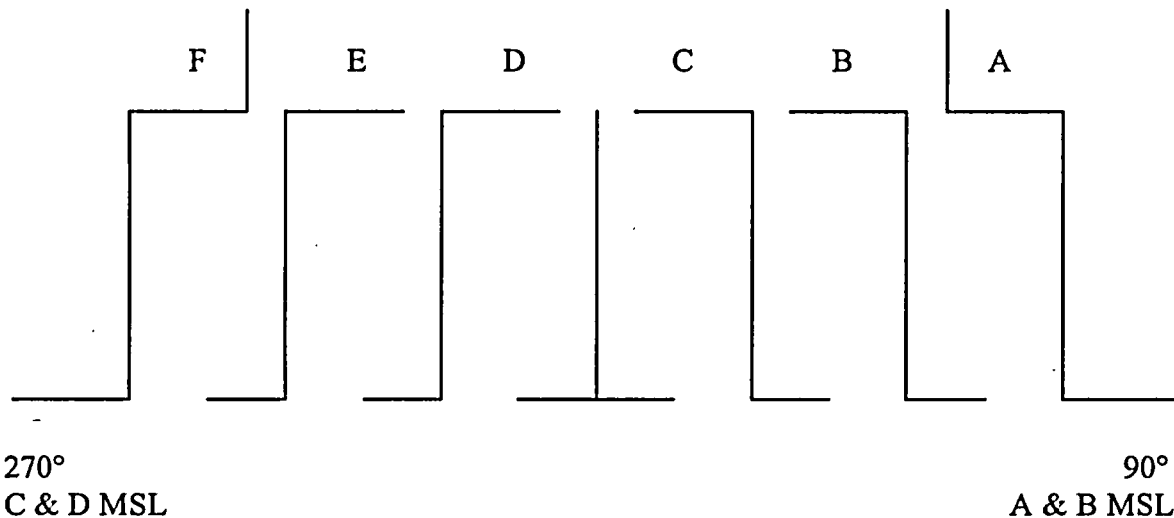
## Recommendations

As confidence grows that the loads transfer methodology is valid and appropriate, scoping work should be undertaken to ascertain required changes to the circuit analysis to make it appropriate to computer higher frequency dryer loads.

## APPENDIX

### PREDICTIONS OF PRESSURE TIME HISTORY IN THE STEAM DOME

Three ASCII data files contain the time history data for the predictions of differential pressure (psid) across the various plates in the dryer. A schematic of the geometry looks like this:



The pressure differences are computed by subtracting the pressure below the plate from the pressure above the plate (for horizontal plates), and subtracting the pressure to the right of the plate (in the above schematic) from the pressure to the left of the plate (for vertical plates).

The file time45bottom.txt contains the following columns of data for the power setting of  $11.75 \times 10^6$  lbm/hr:

#	Contents
1	time (sec) to 20.48 sec
2	pressure difference at the left edge of the 270° cover plate below entrance to MSL C
3	pressure difference at the right edge of the 270° cover plate below entrance to MSL C
4	pressure difference at the left edge of the 270° cover plate below entrance to MSL D
5	pressure difference at the right edge of the 270° cover plate below entrance to MSL D
6	pressure difference at the left edge of the F bottom plate
7	pressure difference at the right edge of the F bottom plate
8	pressure difference at the left edge of the E bottom plate
9	pressure difference at the right edge of the E bottom plate

- 10 pressure difference at the left edge of the D bottom plate
- 11 pressure difference at the right edge of the D bottom plate (center)
- 12 pressure difference at the left edge of the C bottom plate (center)
- 13 pressure difference at the right edge of the C bottom plate
- 14 pressure difference at the left edge of the B bottom plate
- 15 pressure difference at the right edge of the B bottom plate
- 16 pressure difference at the left edge of the A bottom plate
- 17 pressure difference at the right edge of the A bottom plate
- 18 pressure difference at the left edge of the 90° cover plate below entrance to MSL A
- 19 pressure difference at the right edge of the 90° cover plate below entrance to MSL A
- 20 pressure difference at the left edge of the 90° cover plate below entrance to MSL B
- 21 pressure difference at the right edge of the 90° cover plate below entrance to MSL B

The file time45vertical.txt contains the following columns of data for the power setting of  $11.75 \times 10^6$  lbm/hr:

- | #  | Contents   |
|----|--|
| 1  | time (sec) to 20.48 sec  |
| 2  | pressure difference at the top edge of the 270° outer hood opposite entrance to MSL C    |
| 3  | pressure difference at the bottom edge of the 270° outer hood opposite entrance to MSL C |
| 4  | pressure difference at the top edge of the 270° outer hood opposite entrance to MSL D    |
| 5  | pressure difference at the bottom edge of the 270° outer hood opposite entrance to MSL D |
| 6  | pressure difference at the top edge of the vertical plate between F and E                |
| 7  | pressure difference at the bottom edge of the vertical plate between F and E             |
| 8  | pressure difference at the top edge of the vertical plate between E and D                |
| 9  | pressure difference at the bottom edge of the vertical plate between E and D             |
| 10 | pressure difference at the top edge of the vertical plate between D and C                |
| 11 | pressure difference at the bottom edge of the vertical plate between D and C             |
| 12 | pressure difference at the top edge of the vertical plate between C and B                |
| 13 | pressure difference at the bottom edge of the vertical plate between C and B             |
| 14 | pressure difference at the top edge of the vertical plate between B and A                |
| 15 | pressure difference at the bottom edge of the vertical plate between B and A             |
| 16 | pressure difference at the top edge of the 90° outer hood opposite entrance to MSL A     |
| 17 | pressure difference at the bottom edge of the 90° outer hood opposite entrance to MSL A  |
| 18 | pressure difference at the top edge of the 90° outer hood opposite entrance to MSL B     |

- 19 pressure difference at the bottom edge of the 90° outer hood opposite entrance to MSL B

The file time45top.txt contains the following columns of data for the power setting of  $11.75 \times 10^6$  lbm/hr:

#	Contents
1	time (sec) to 20.48 sec
2	pressure difference at the left edge of the F top plate
3	pressure difference at the right edge of the F top plate
4	pressure difference at the left edge of the E top plate
5	pressure difference at the right edge of the E top plate
6	pressure difference at the left edge of the D top plate
7	pressure difference at the right edge of the D top plate (center)
8	pressure difference at the left edge of the C top plate (center)
9	pressure difference at the right edge of the C top plate
10	pressure difference at the left edge of the B top plate
11	pressure difference at the right edge of the B top plate
12	pressure difference at the left edge of the A top plate
13	pressure difference at the right edge of the A top plate
14	pressure difference on the 270° skirt
15	pressure difference at the 90° skirt

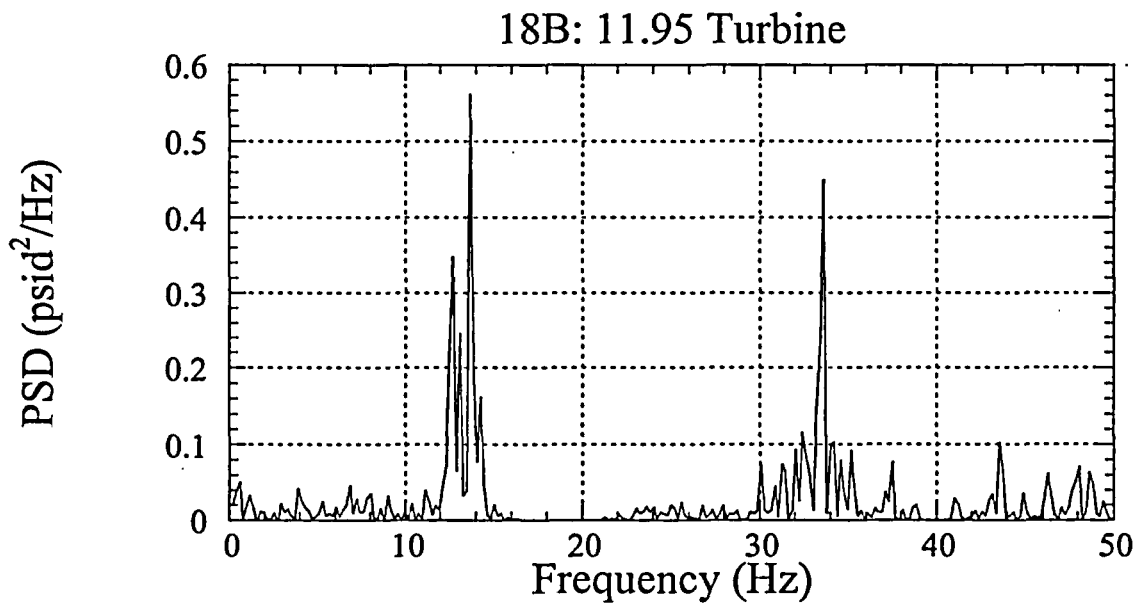
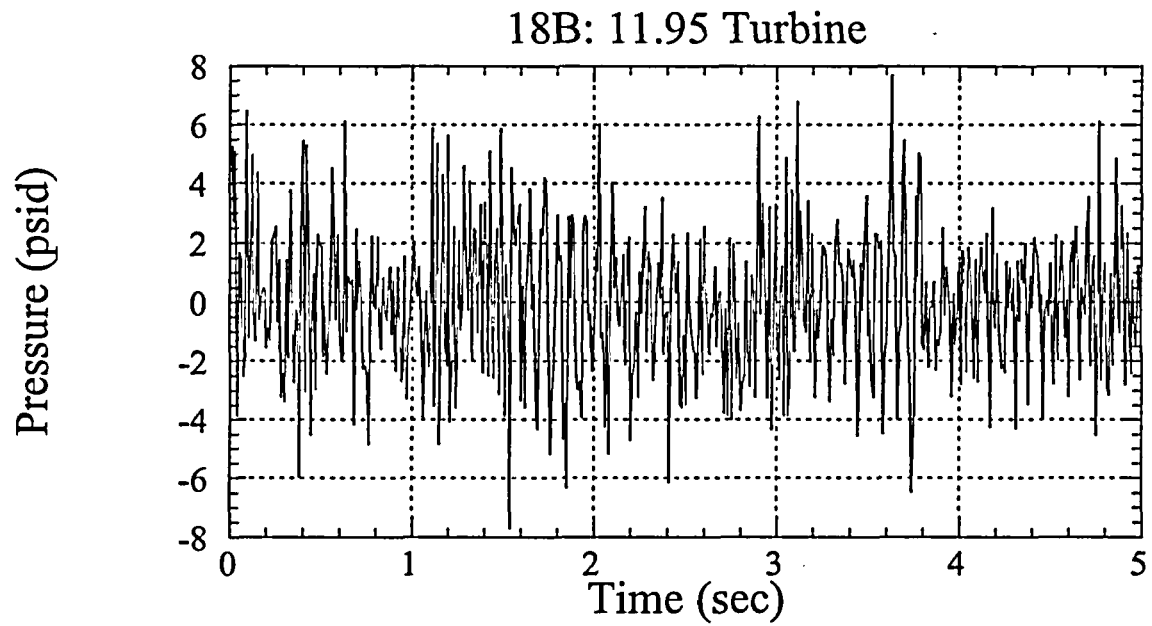


Figure 4-a

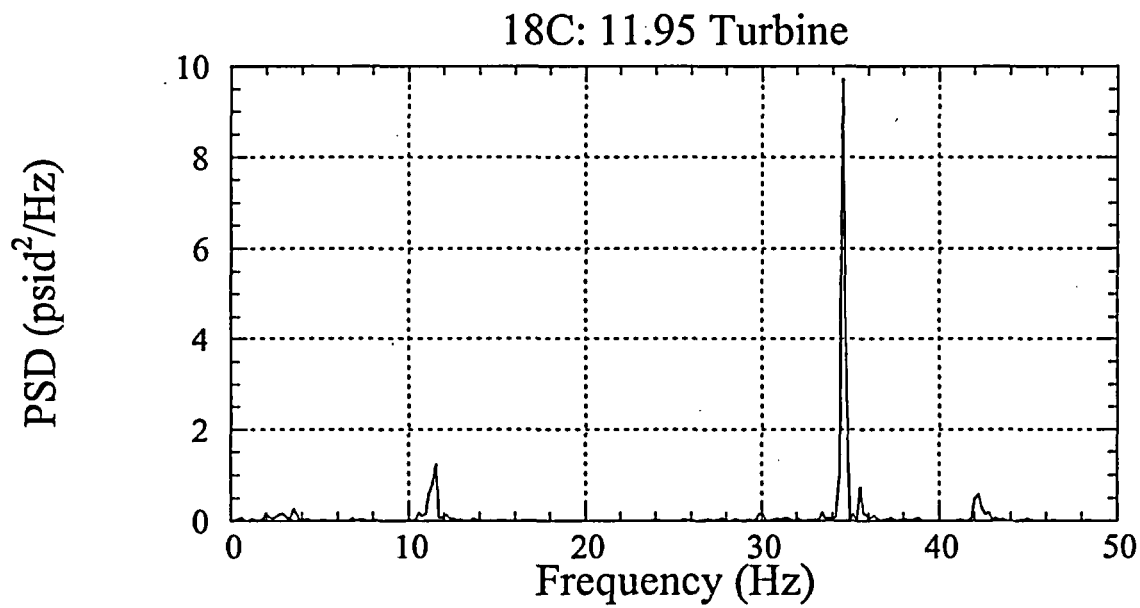
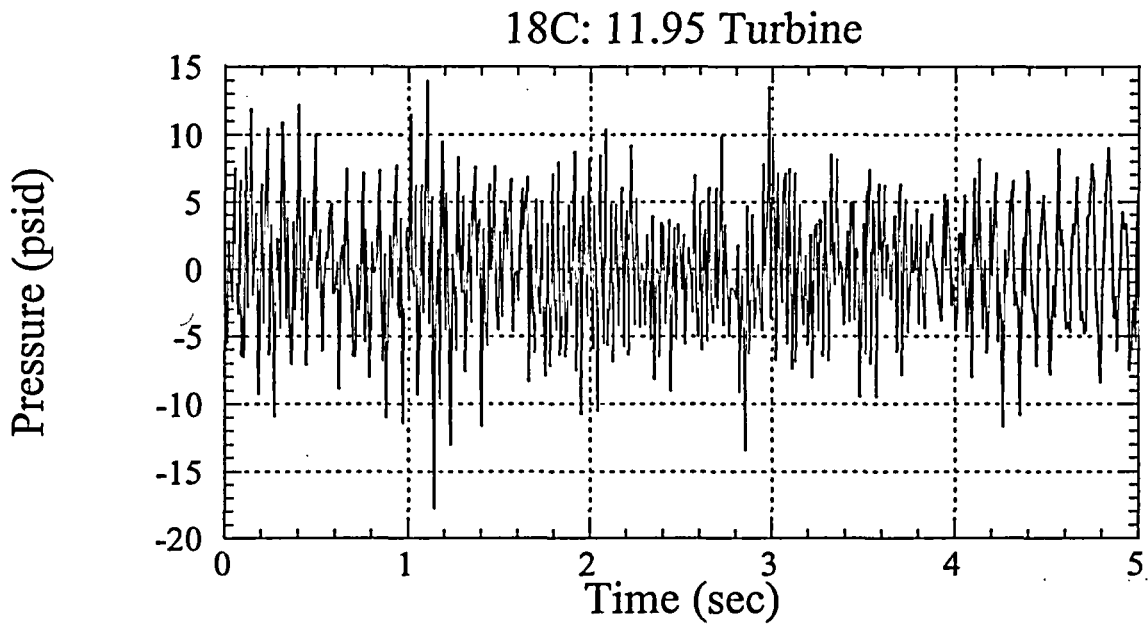


Figure 4-b

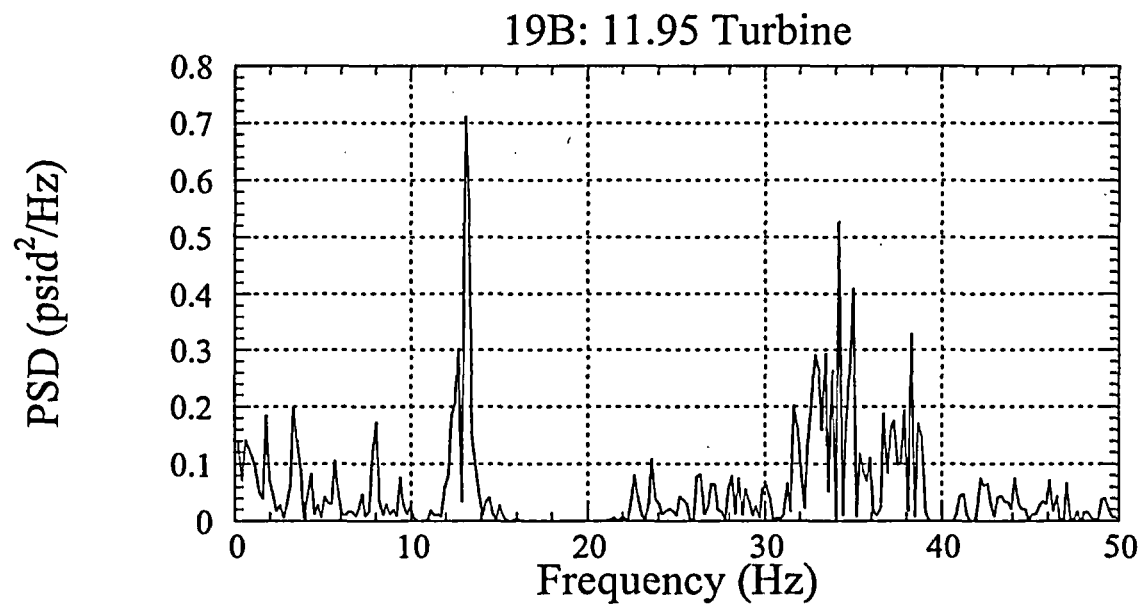
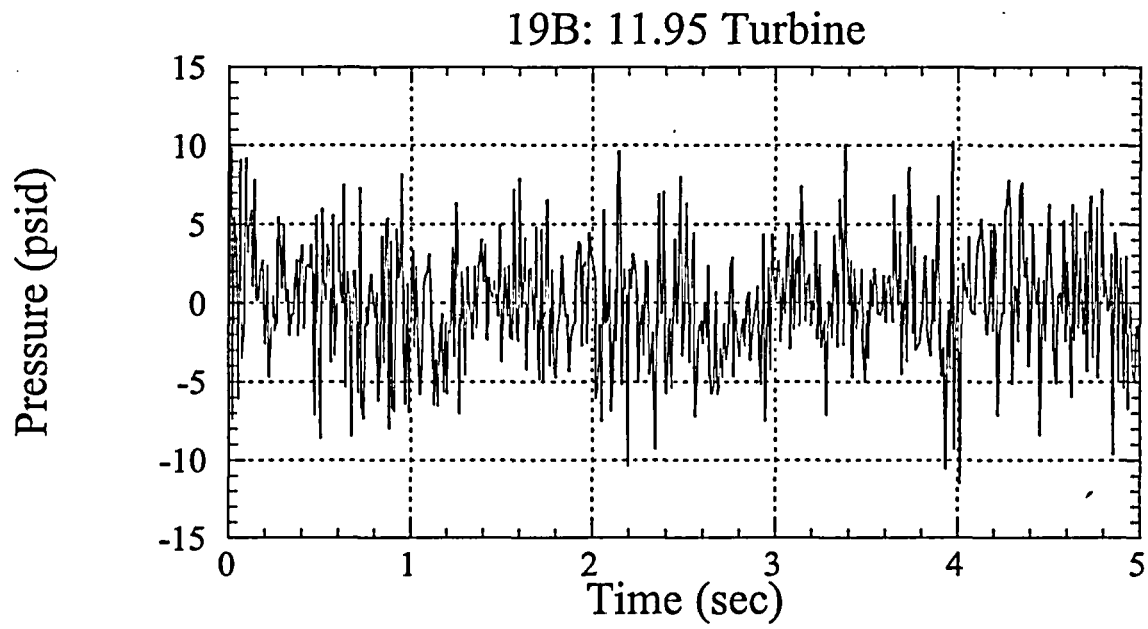


Figure 5-a

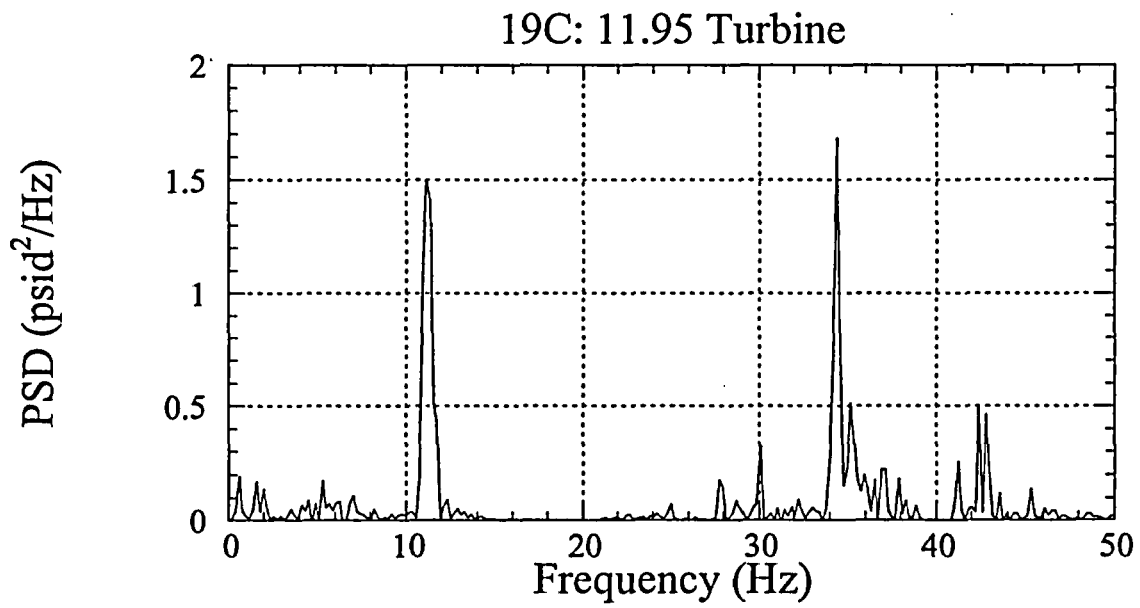
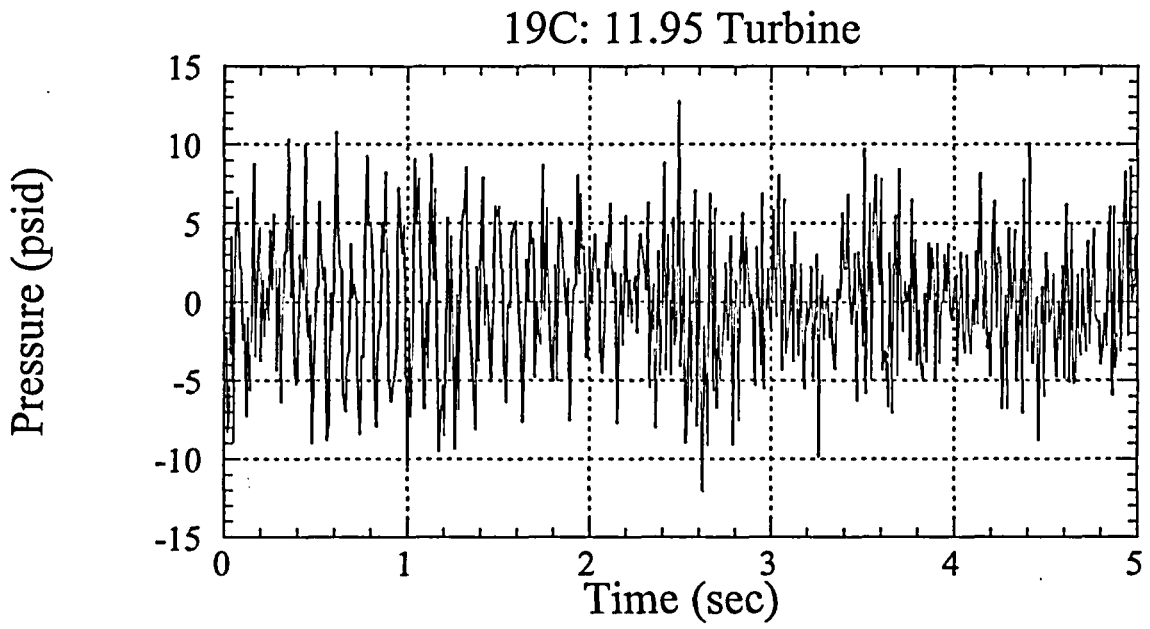


Figure 5-b

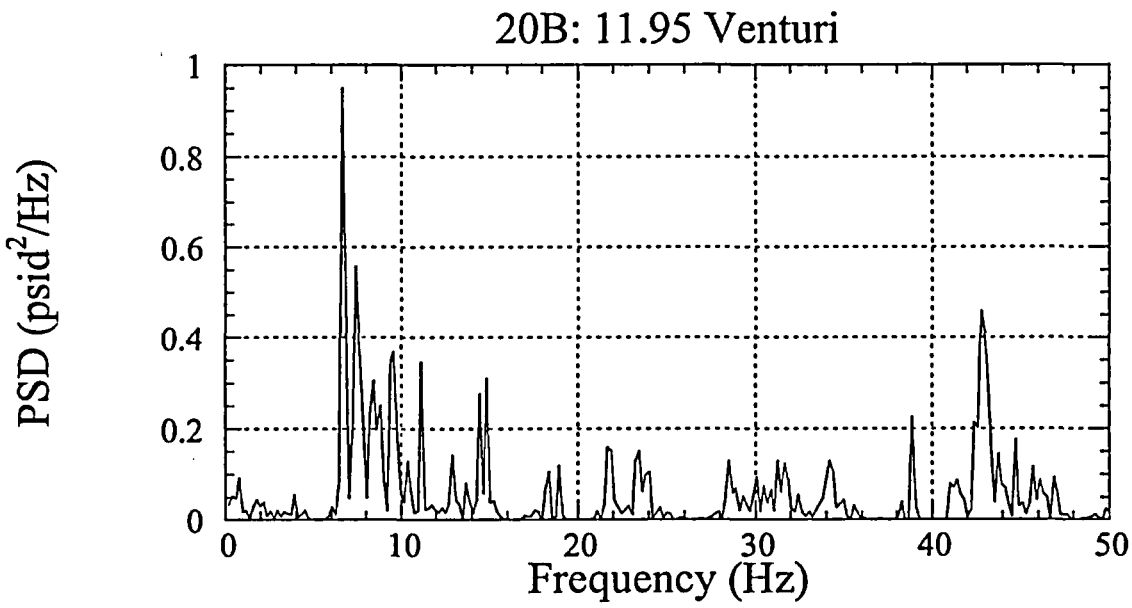
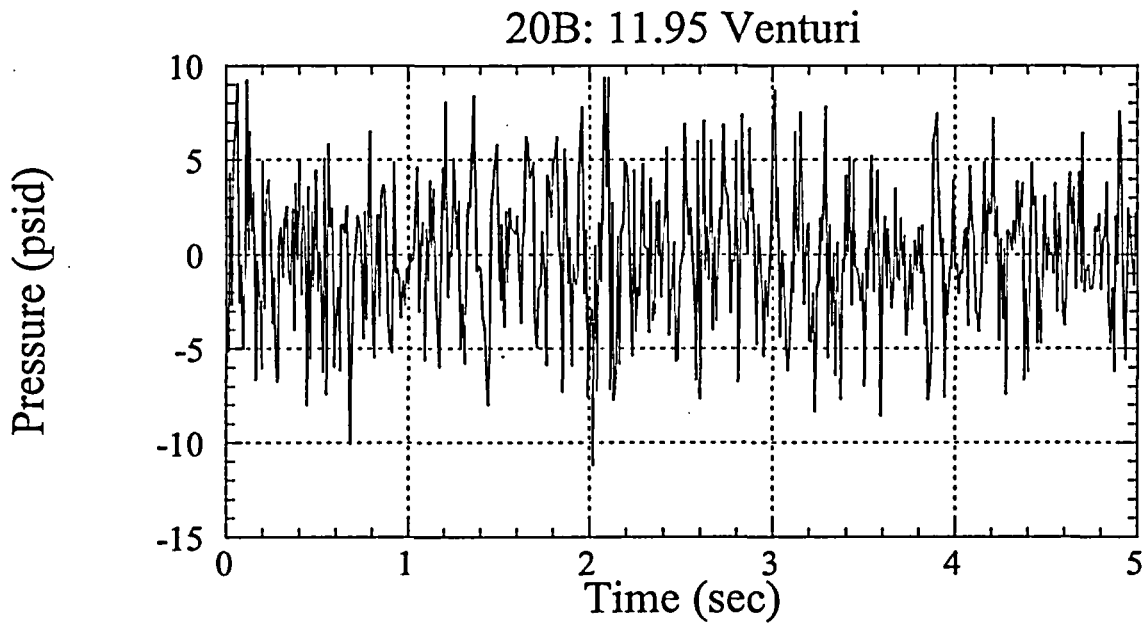


Figure 6-a

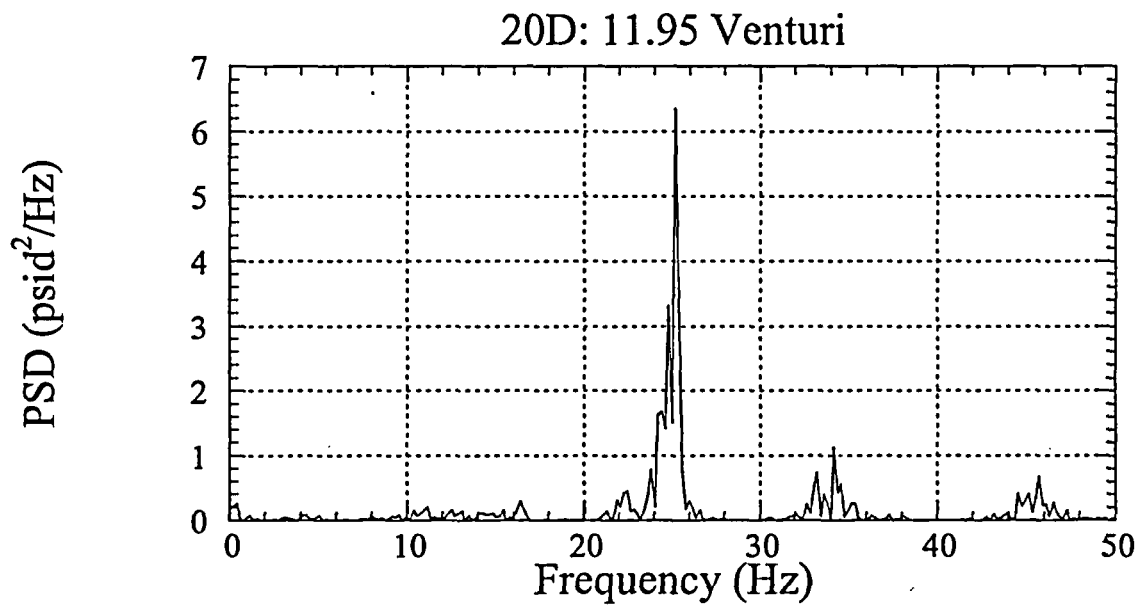
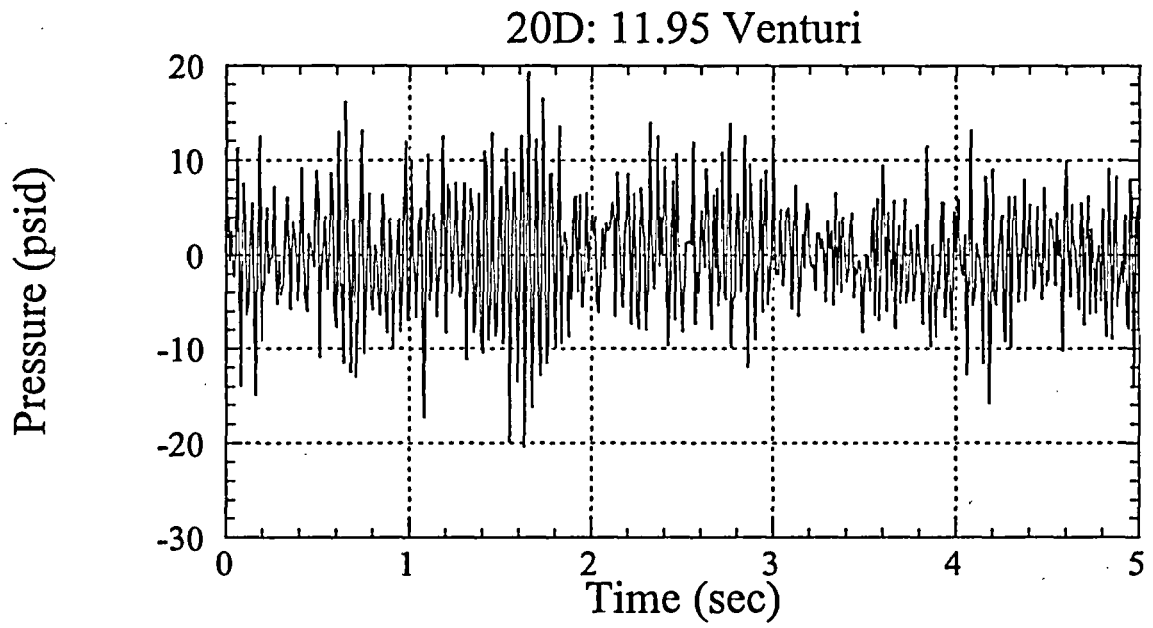


Figure 6-b

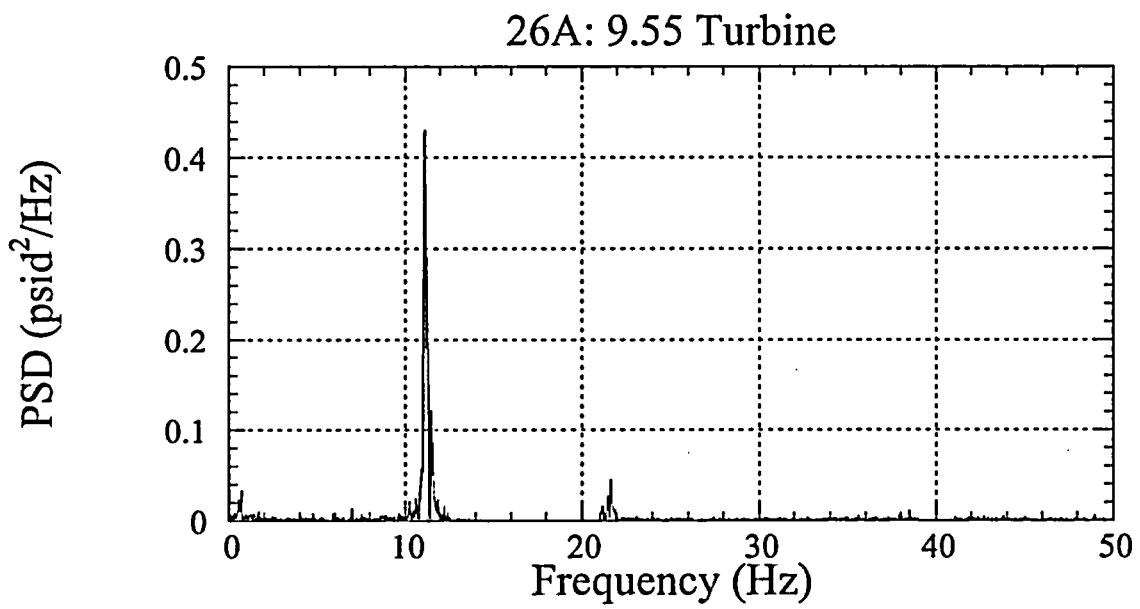
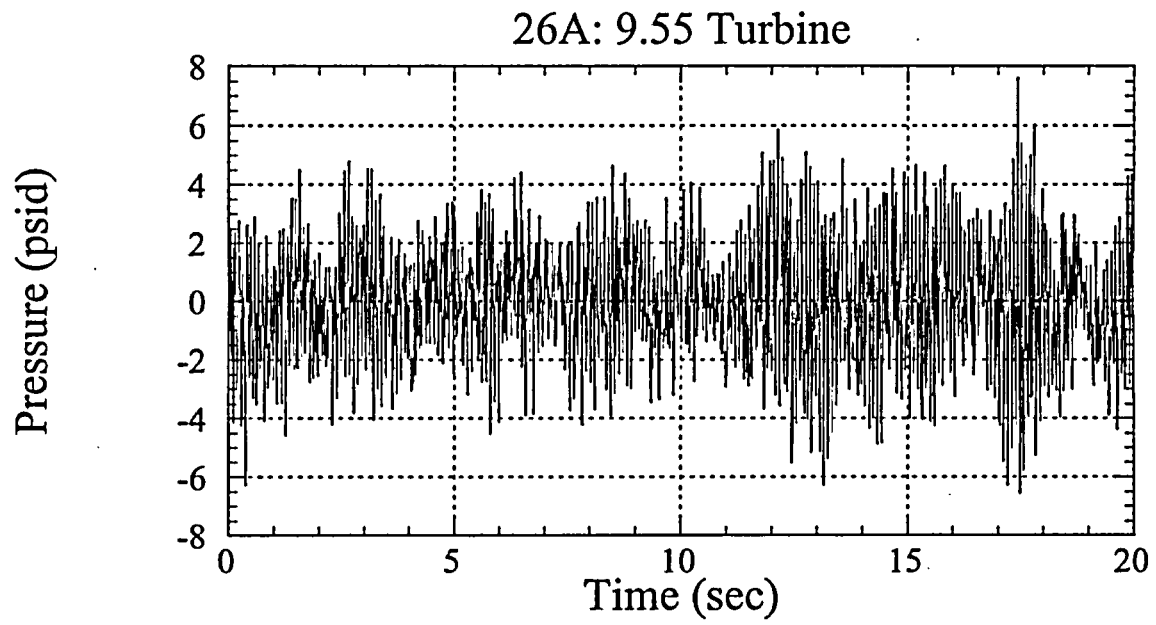


Figure 7-a

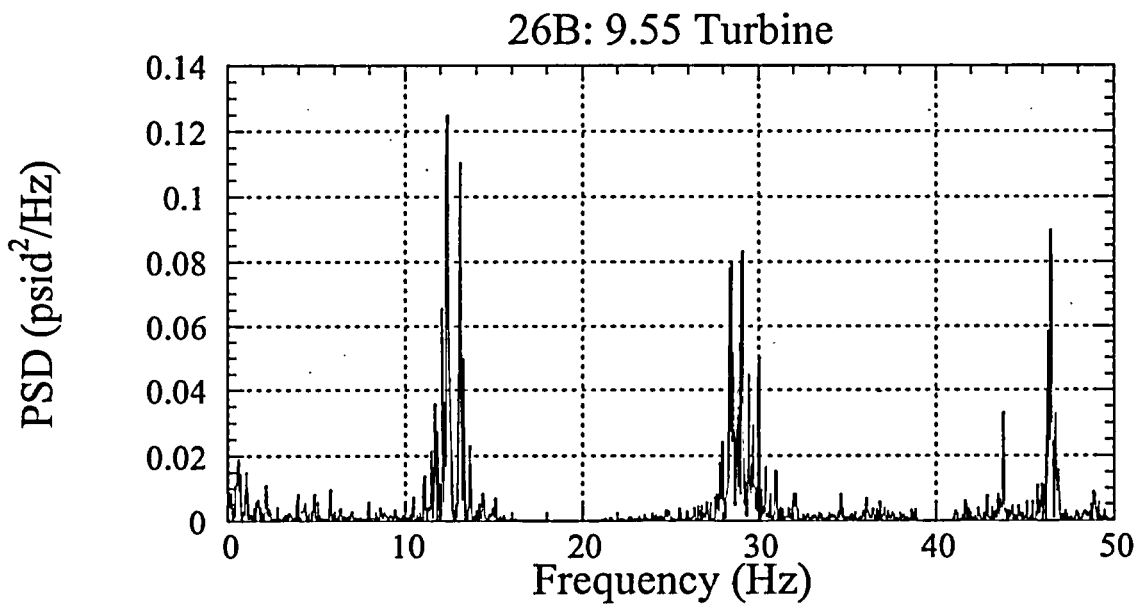
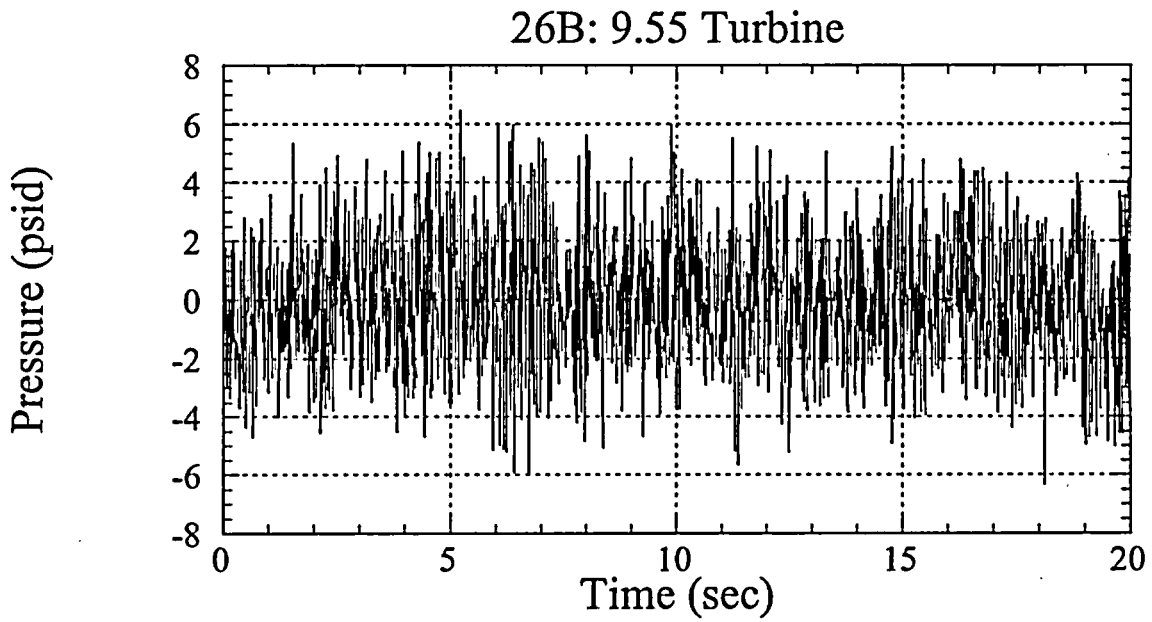


Figure 7-b

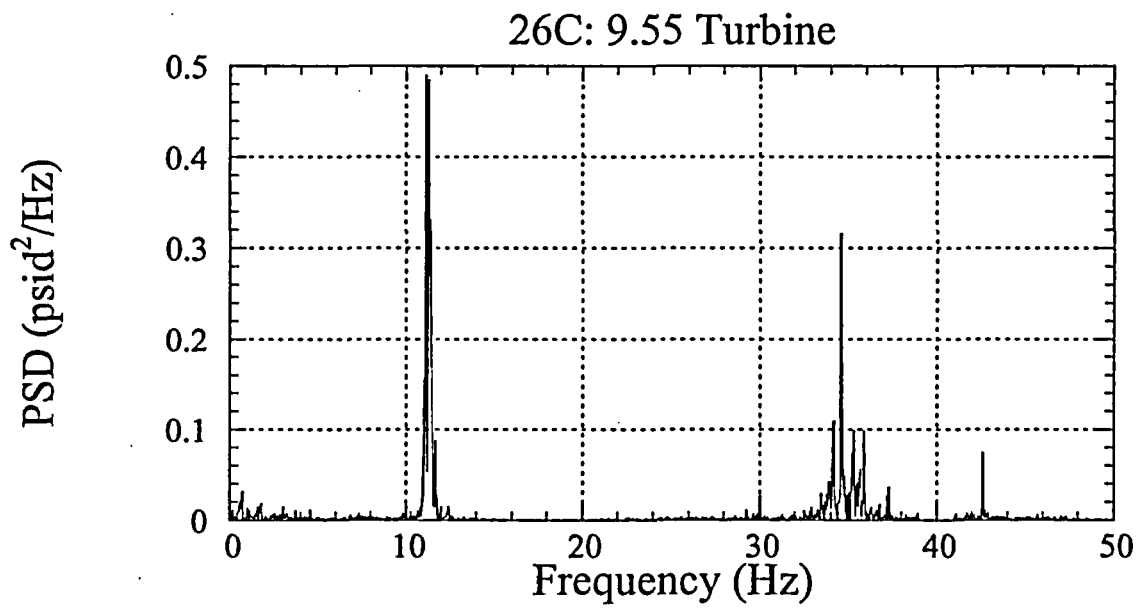
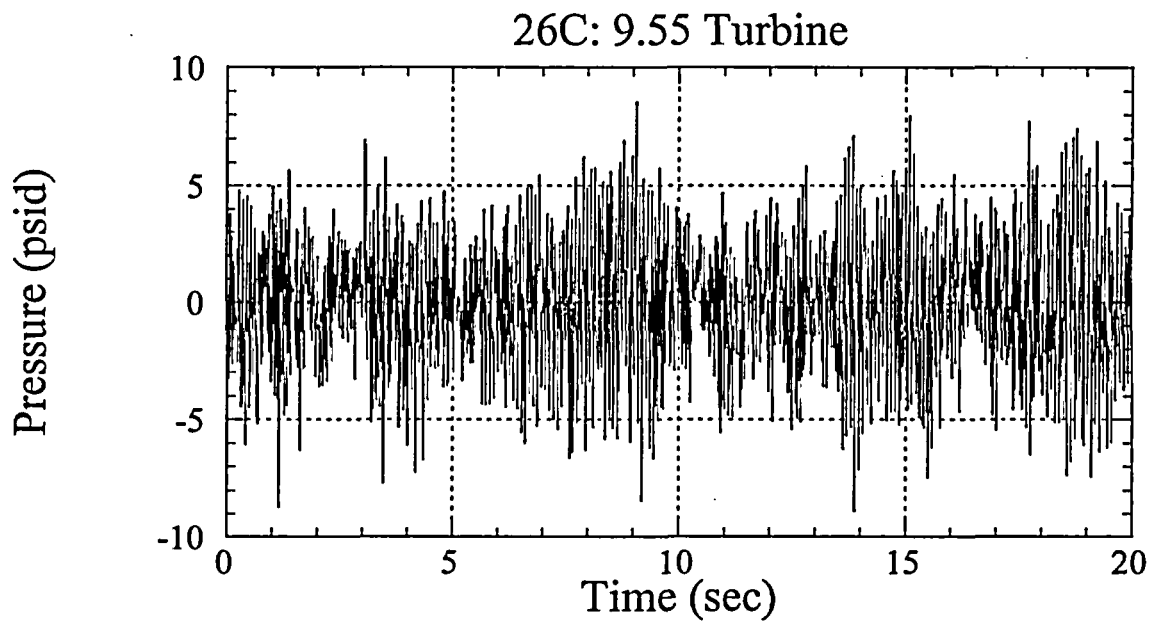


Figure 7-c

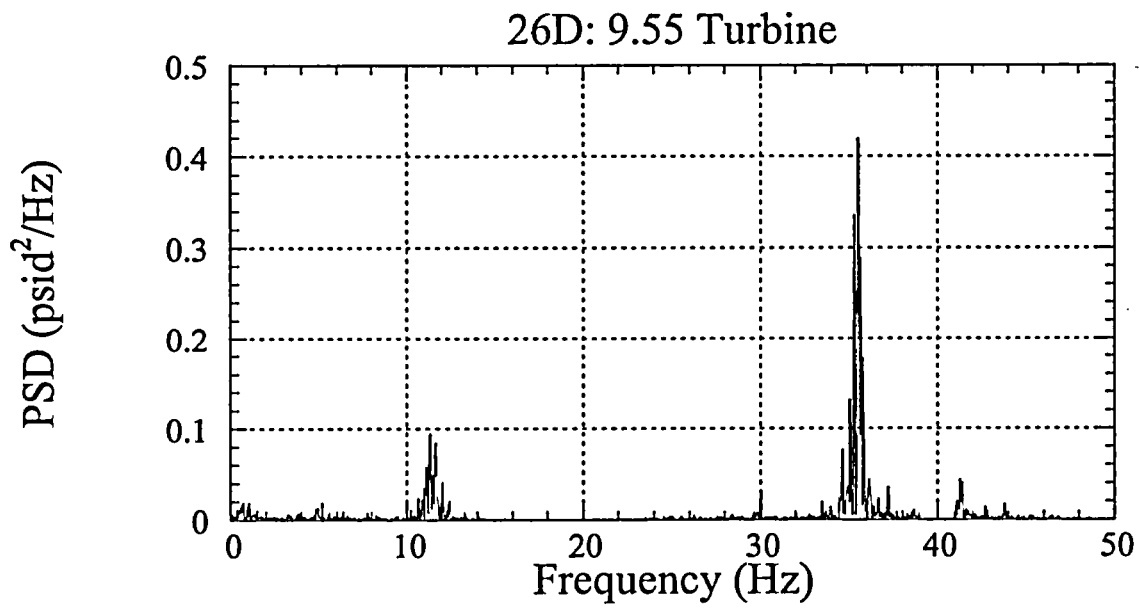
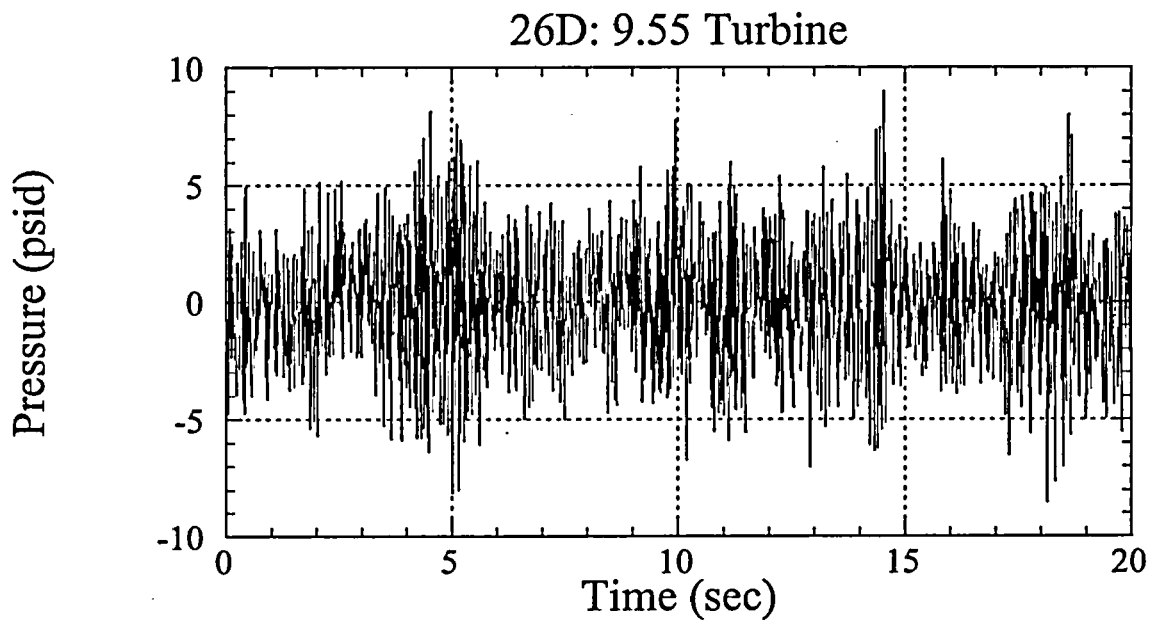


Figure 7-d

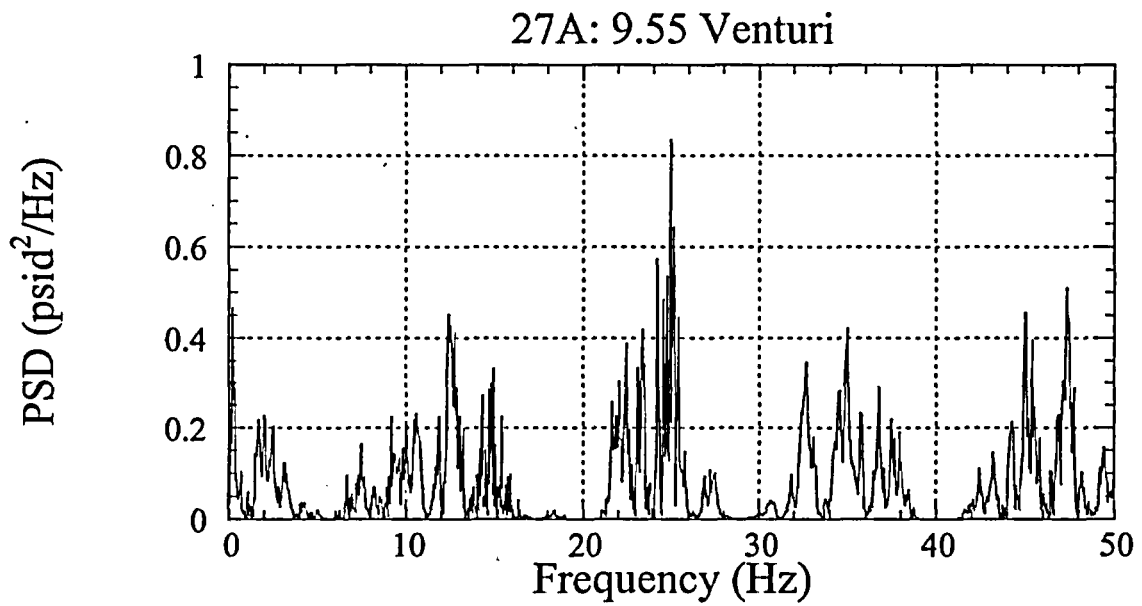
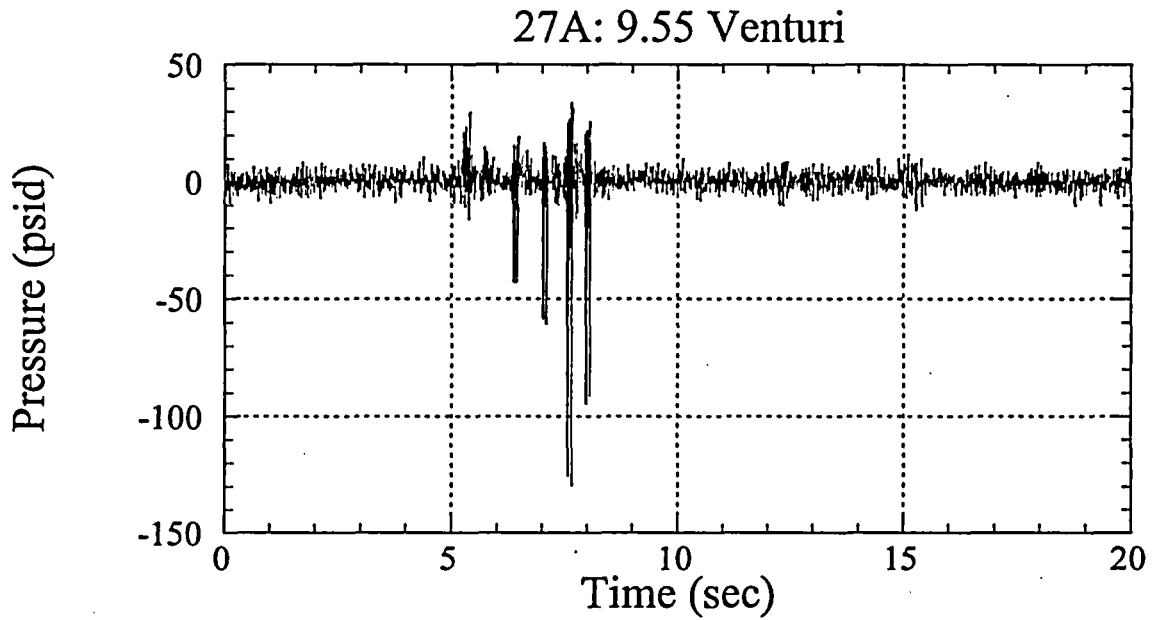


Figure 8-a

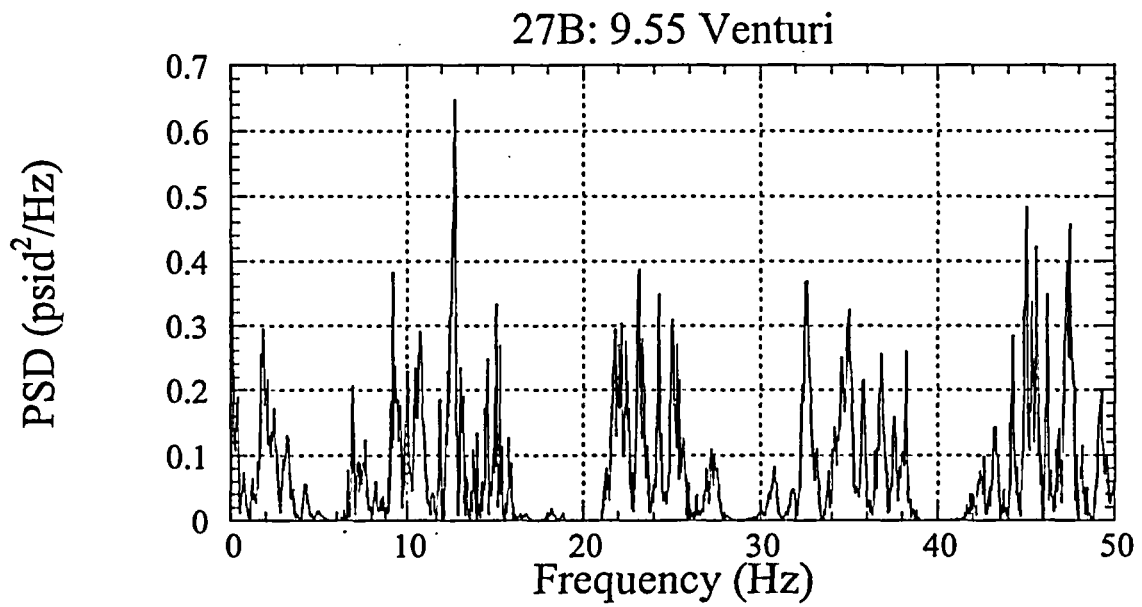
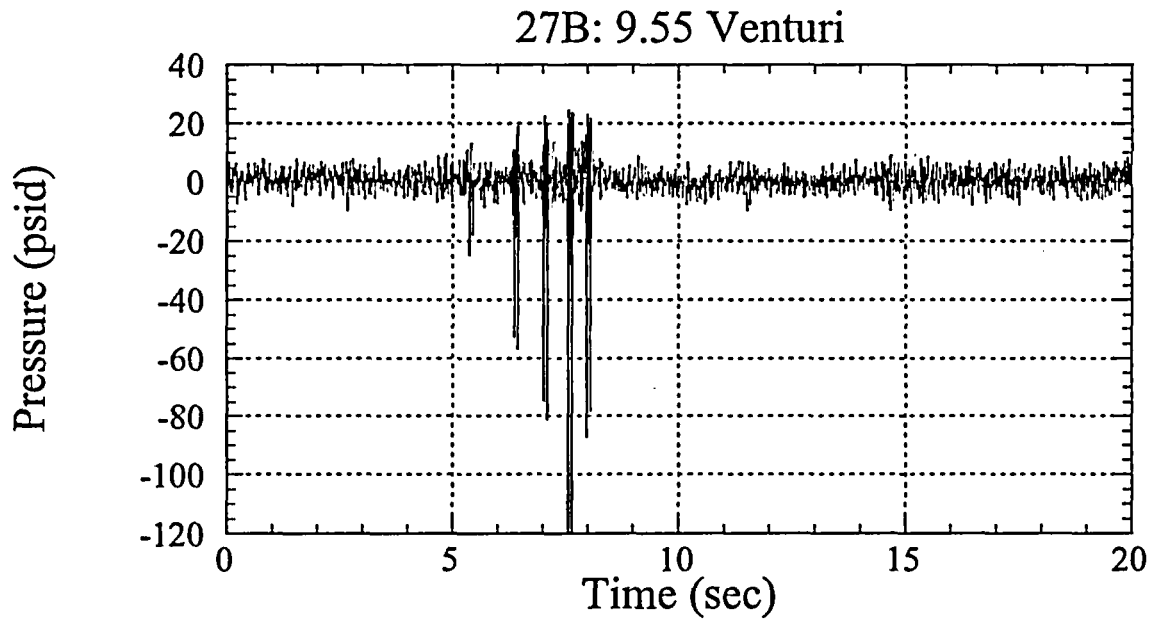


Figure 8-b

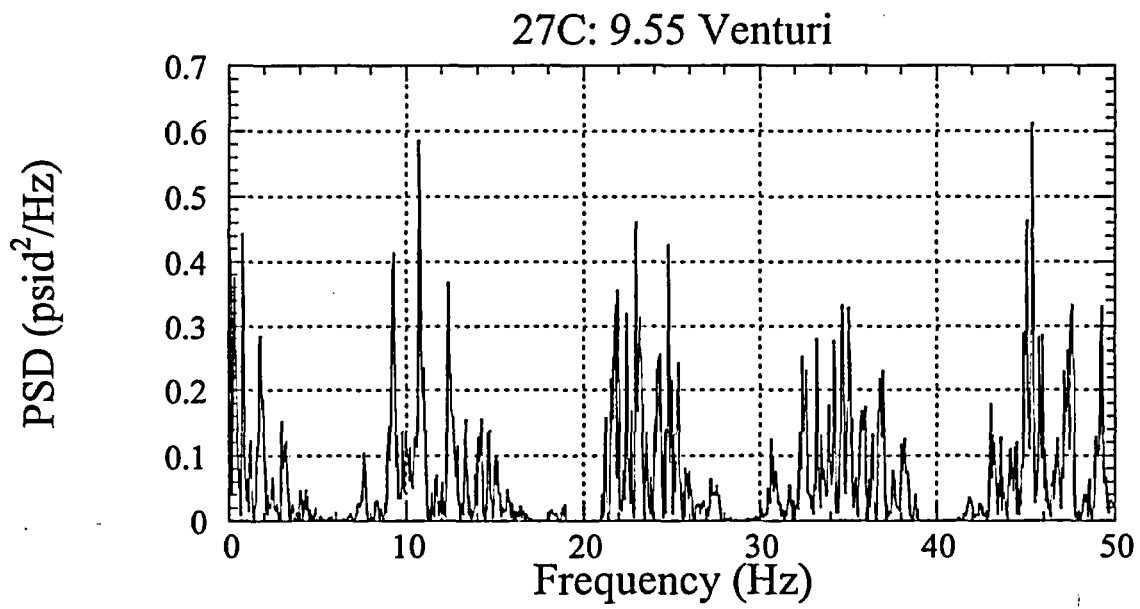
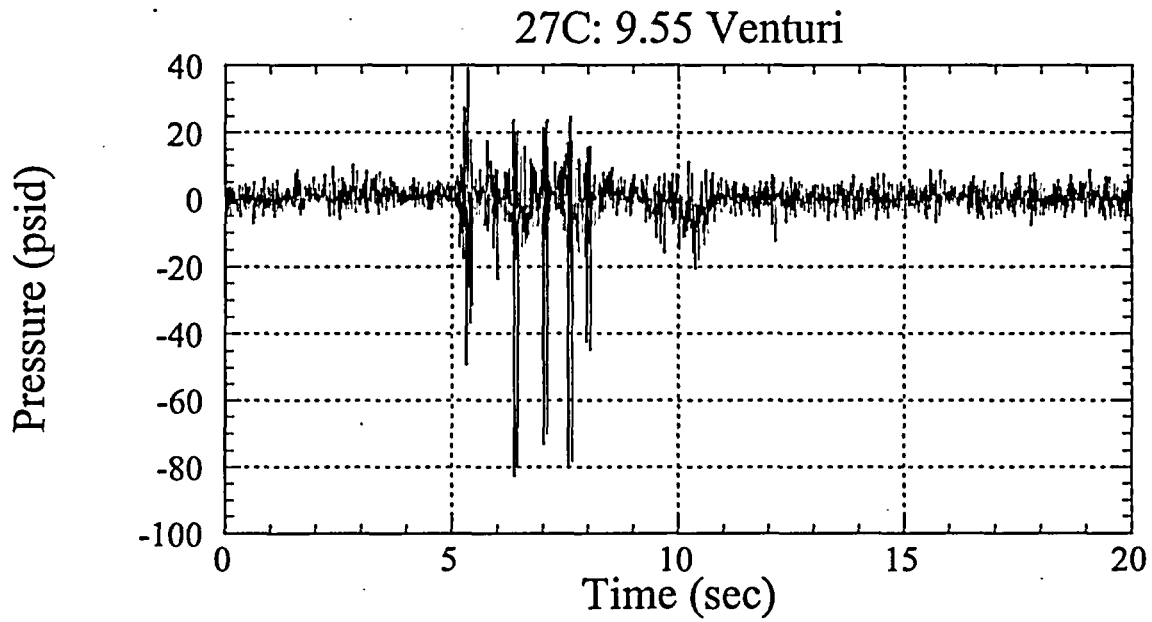


Figure 8-c

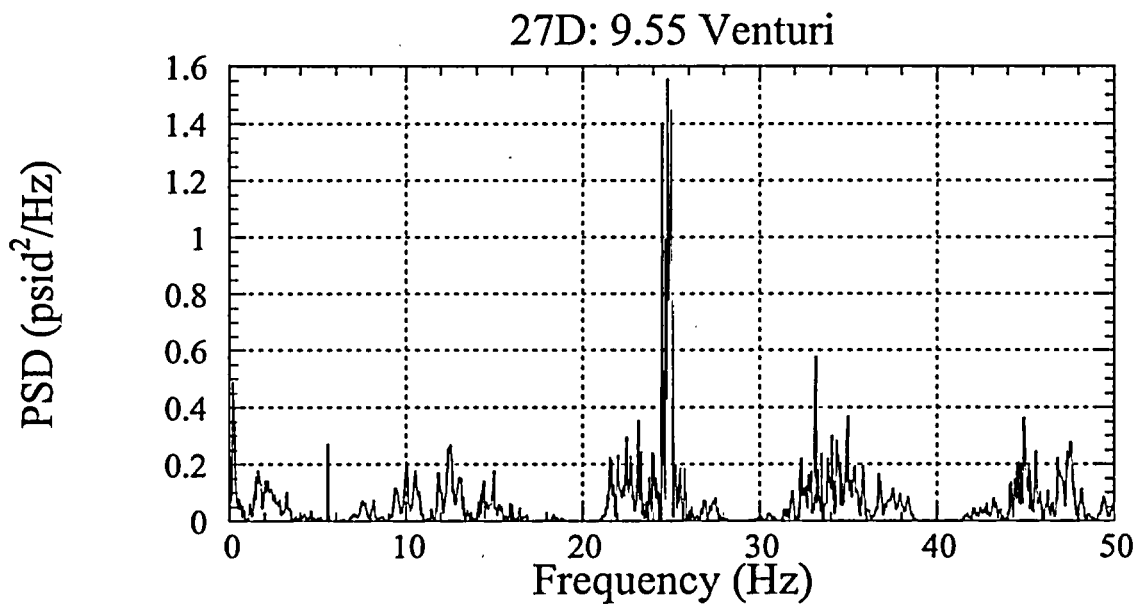
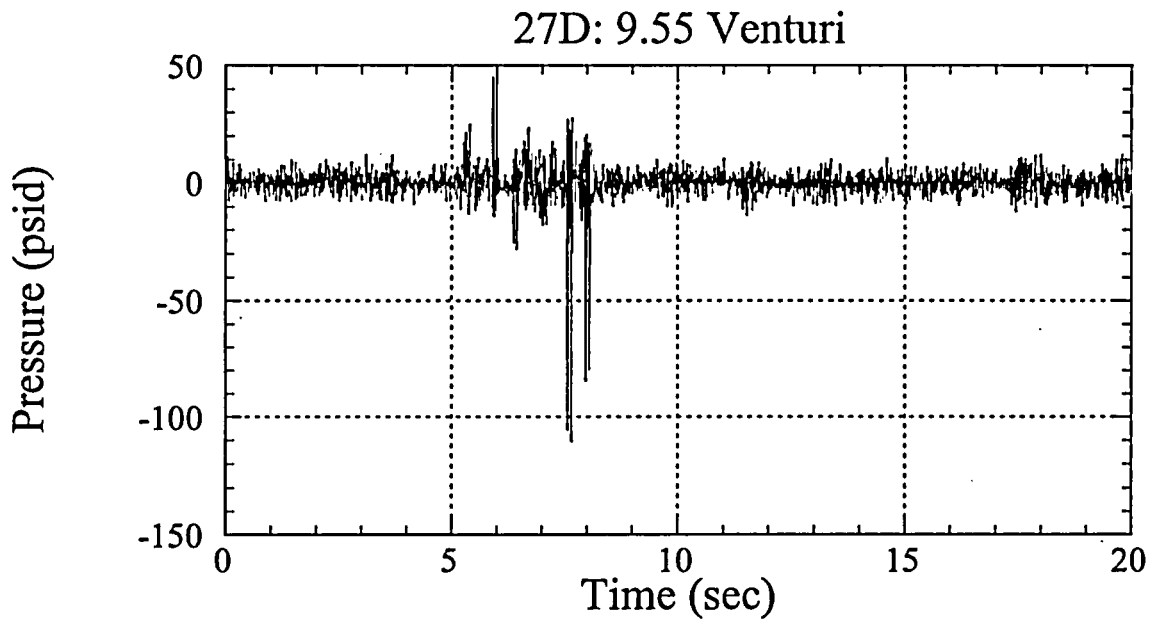


Figure 8-d

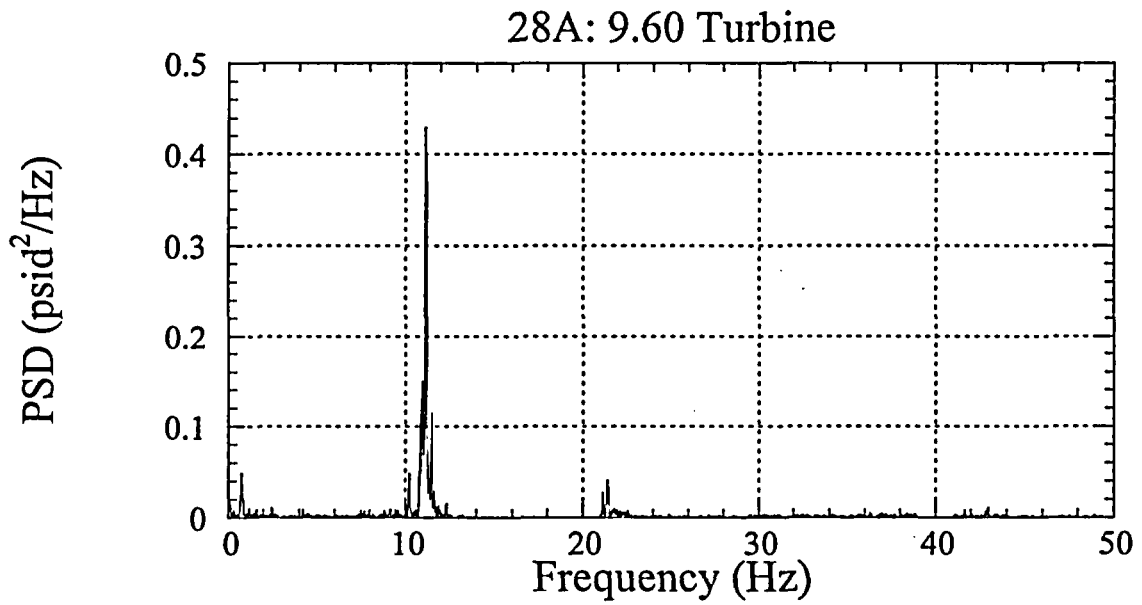
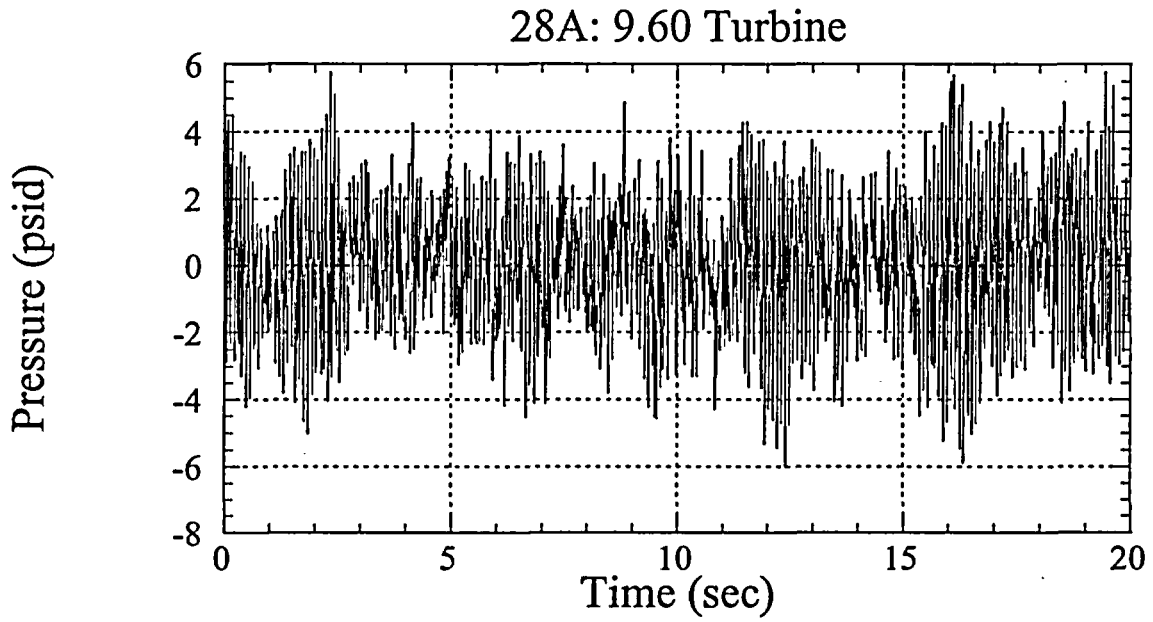


Figure 9-a

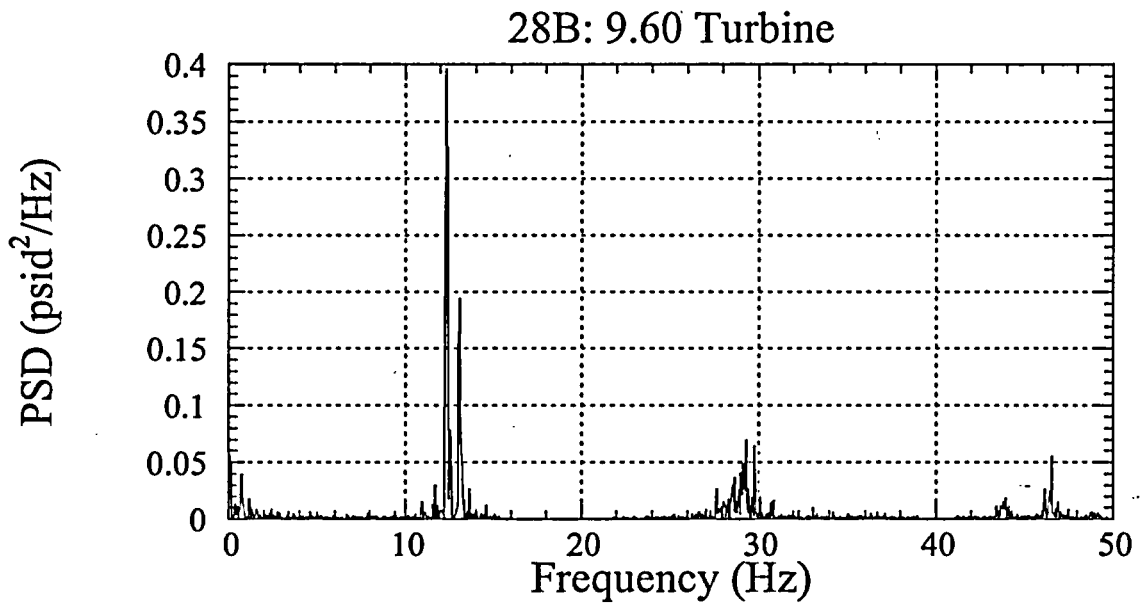
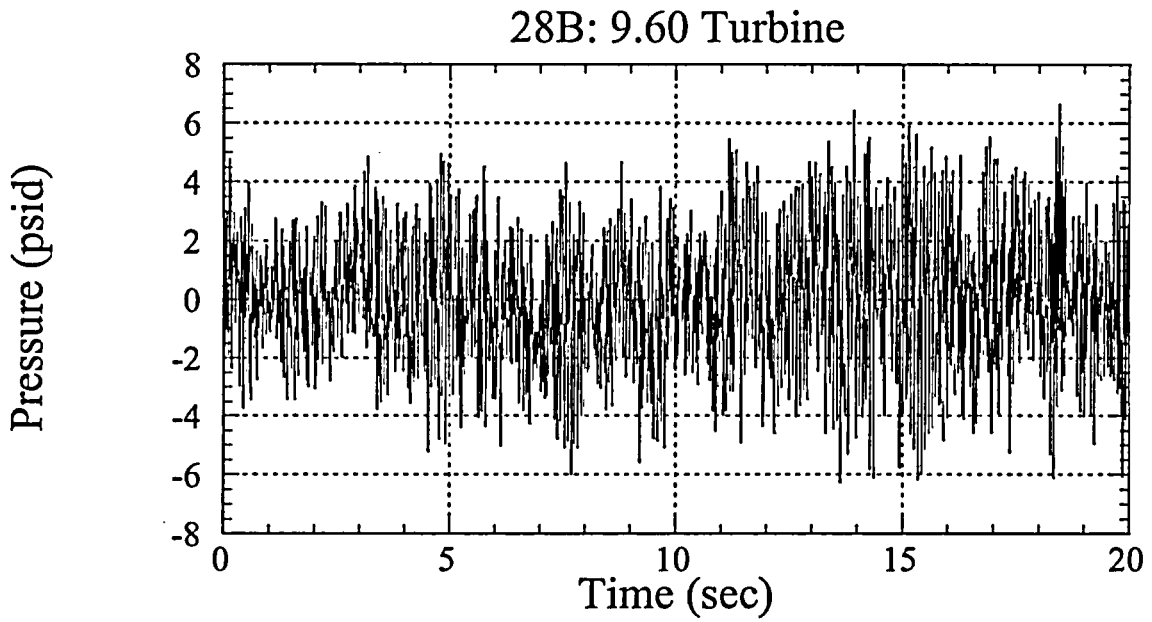


Figure 9-b

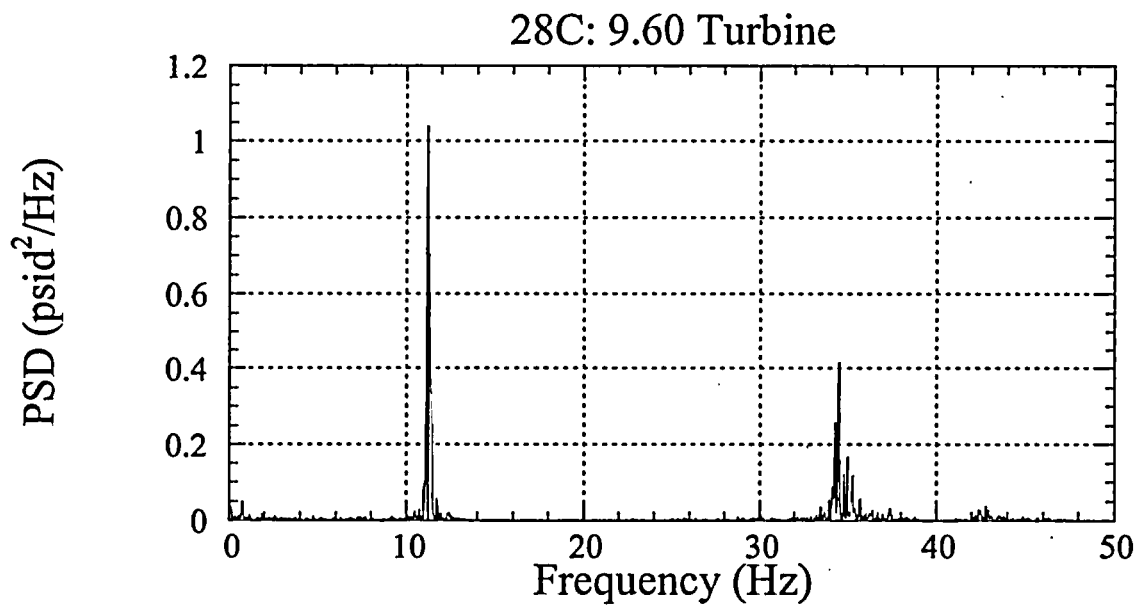
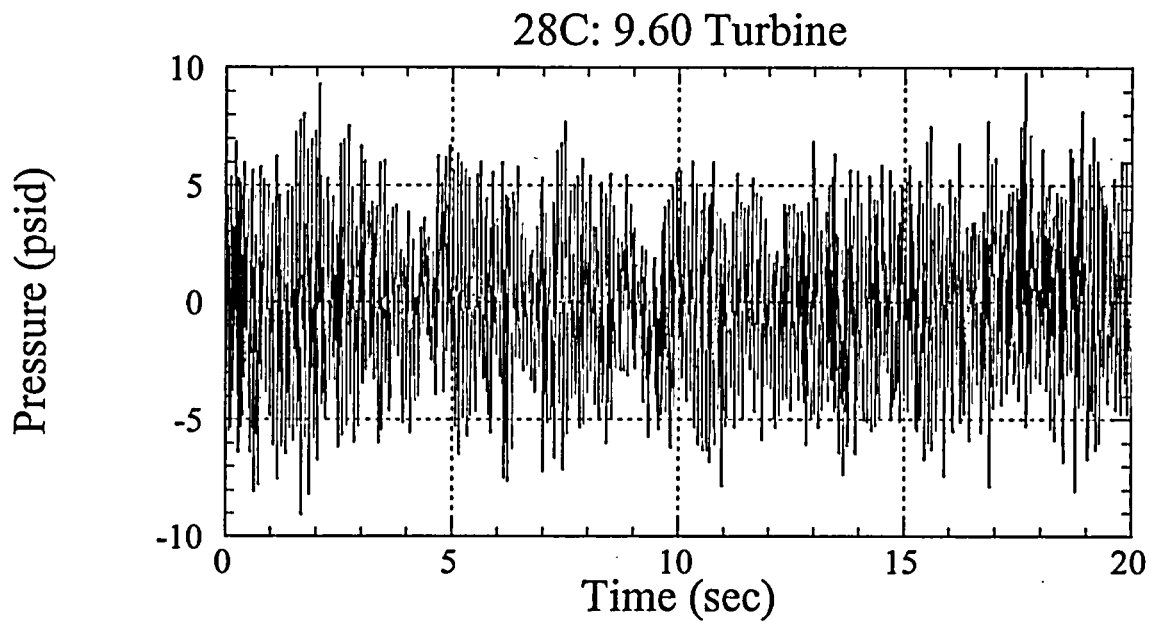


Figure 9-c

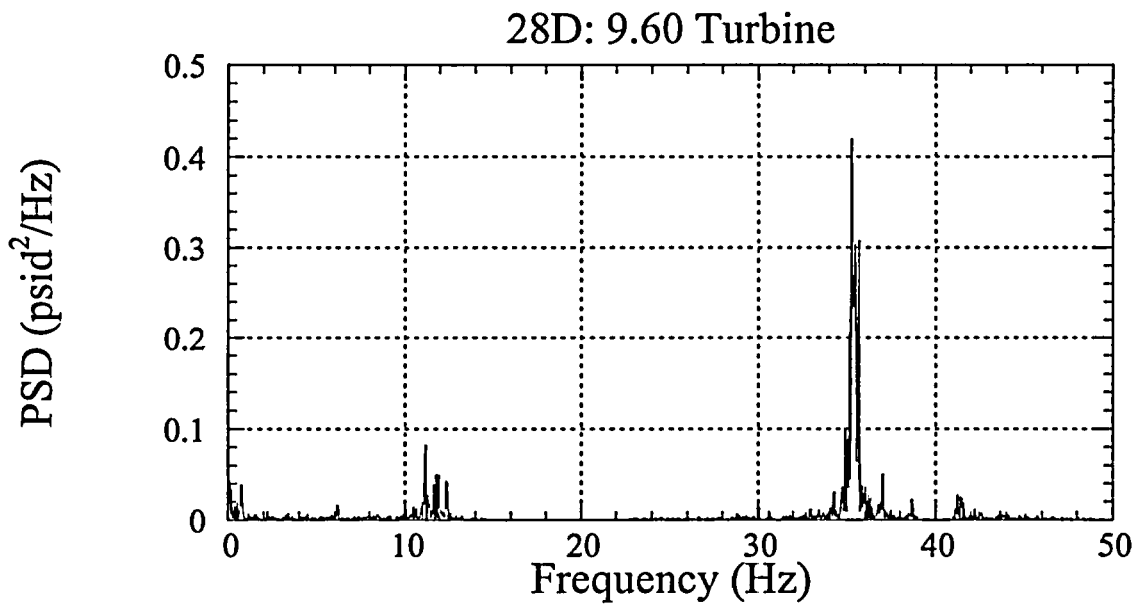
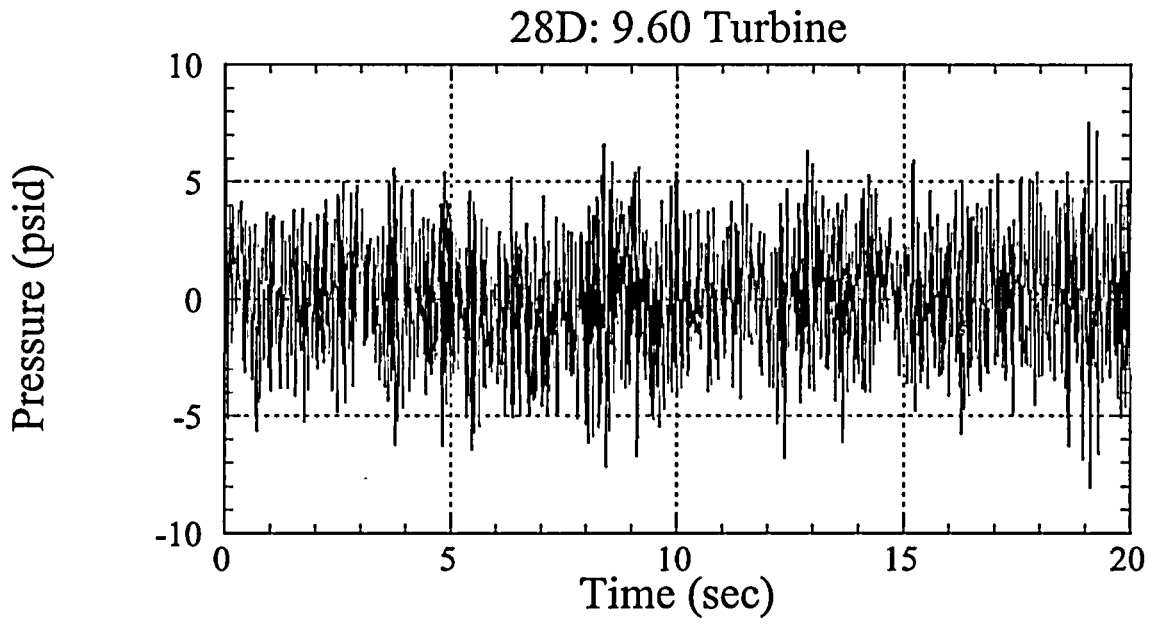


Figure 9-d

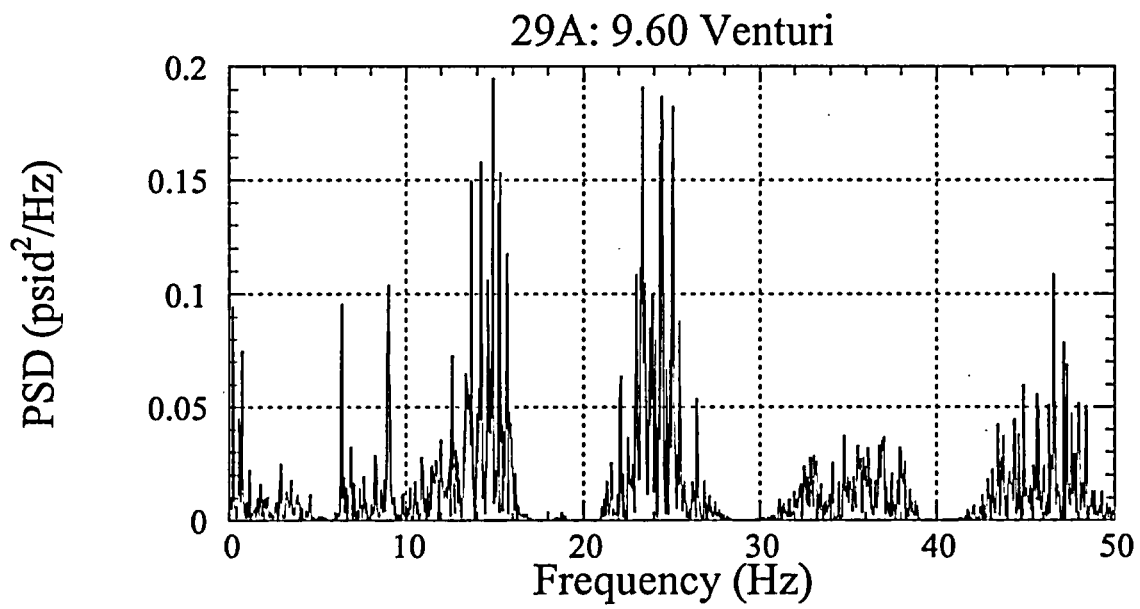
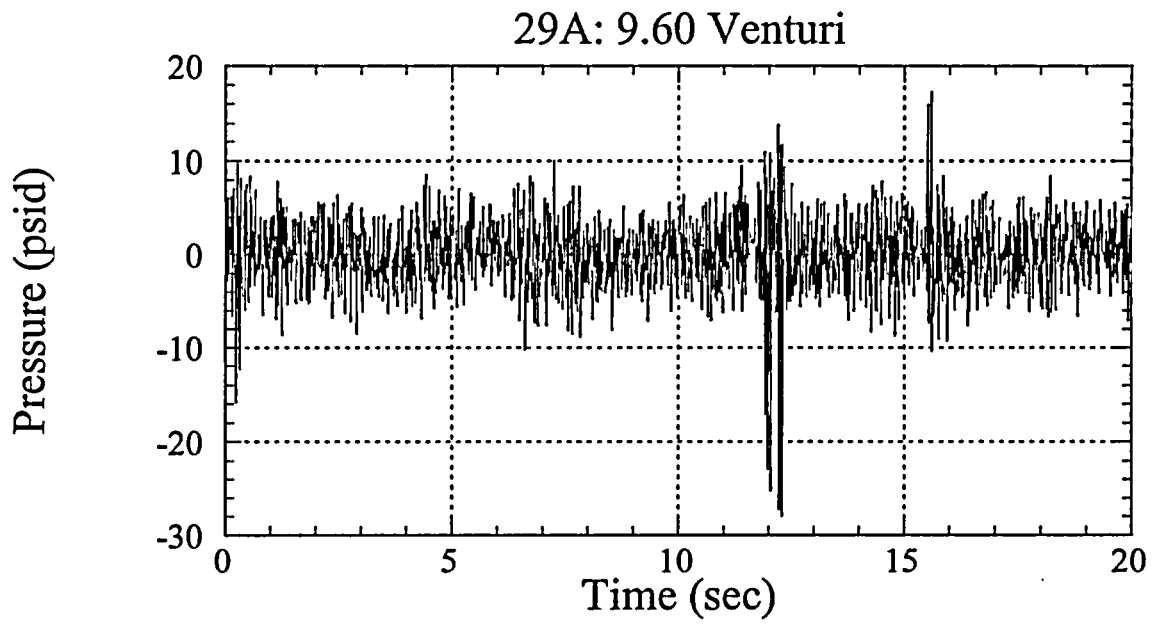


Figure 10-a

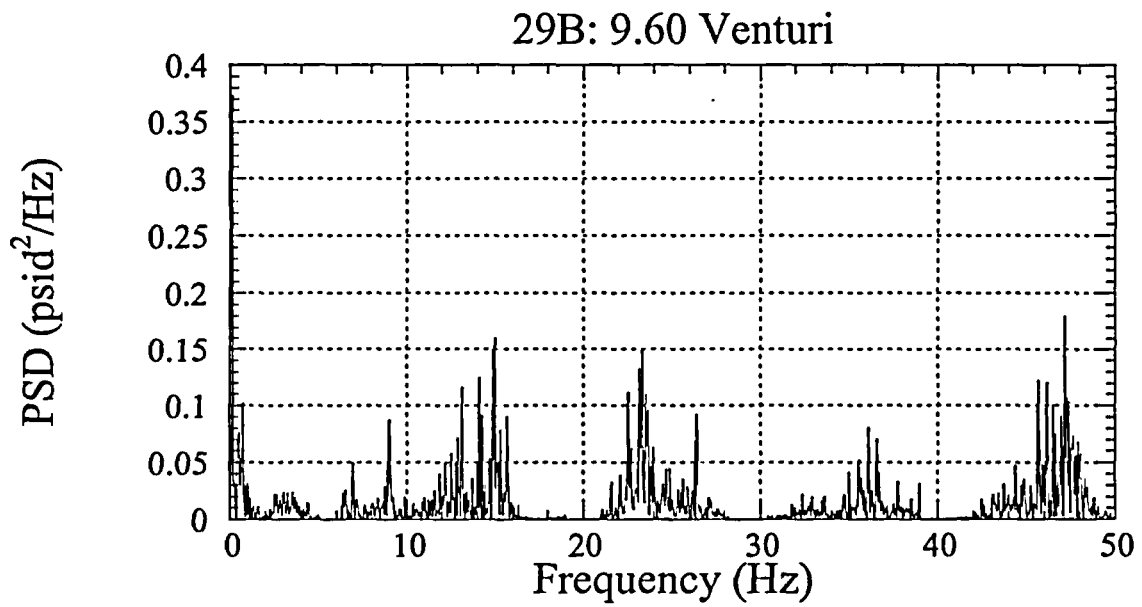
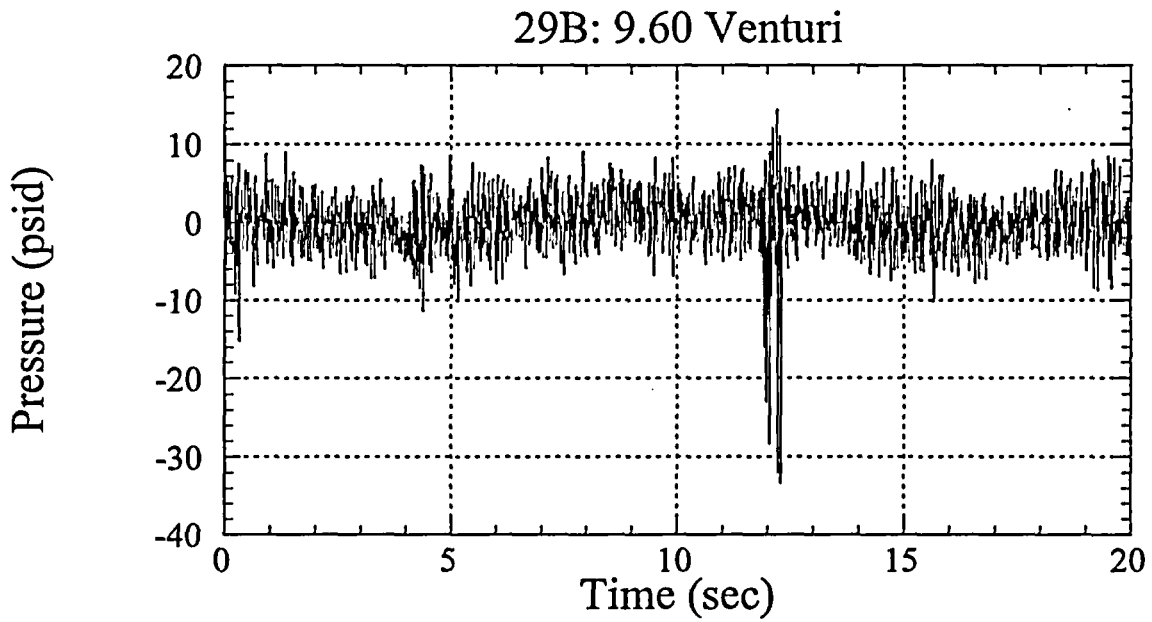


Figure 10-b

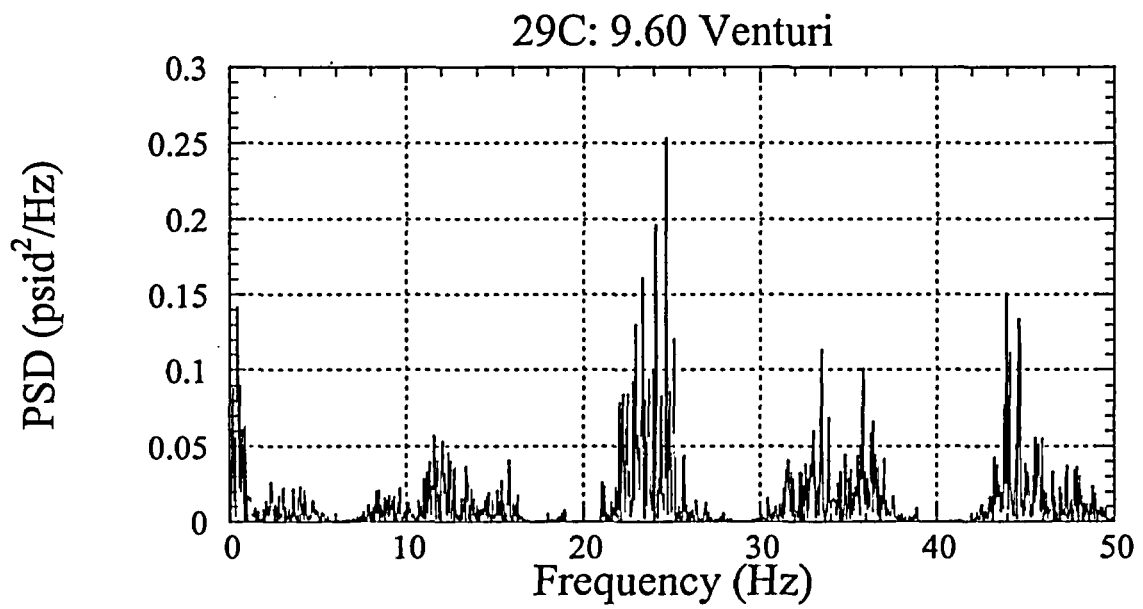
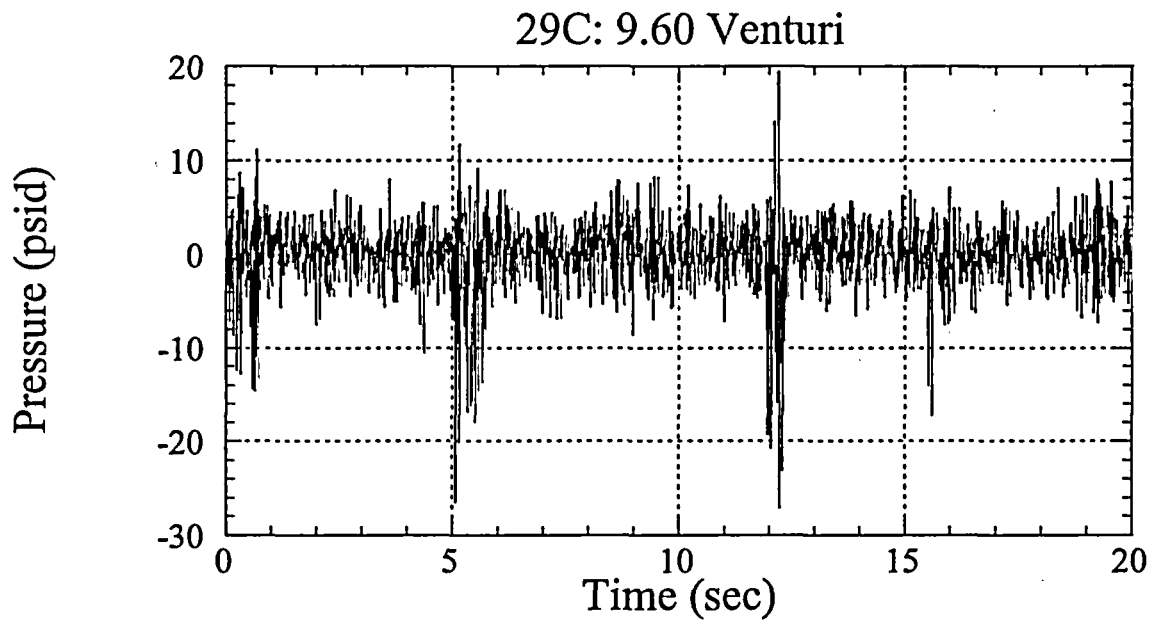


Figure 10-c

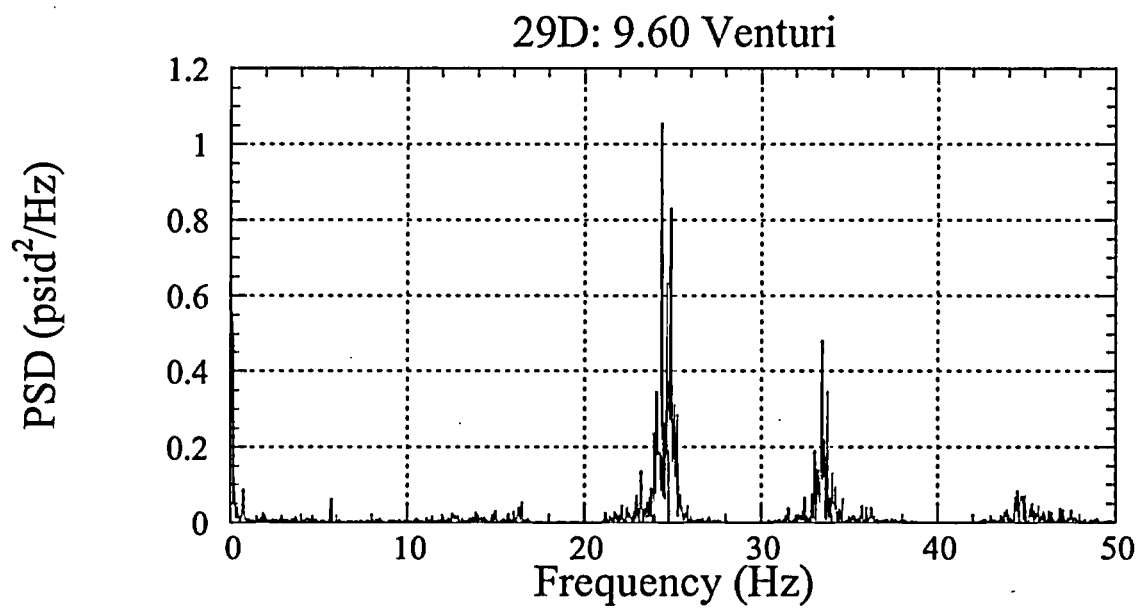
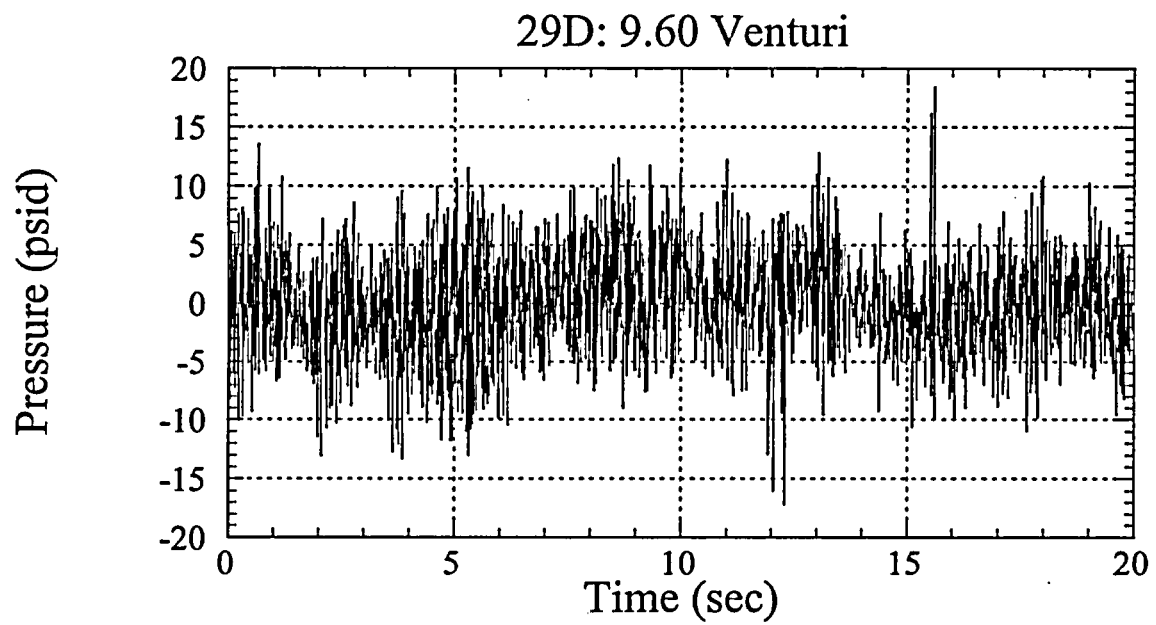


Figure 10-d

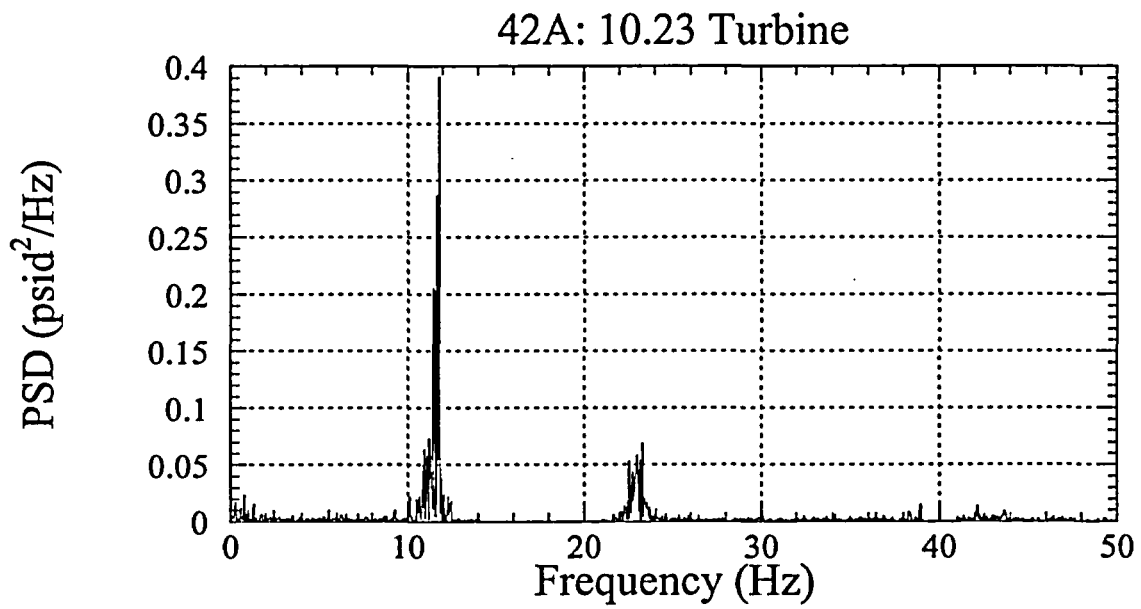
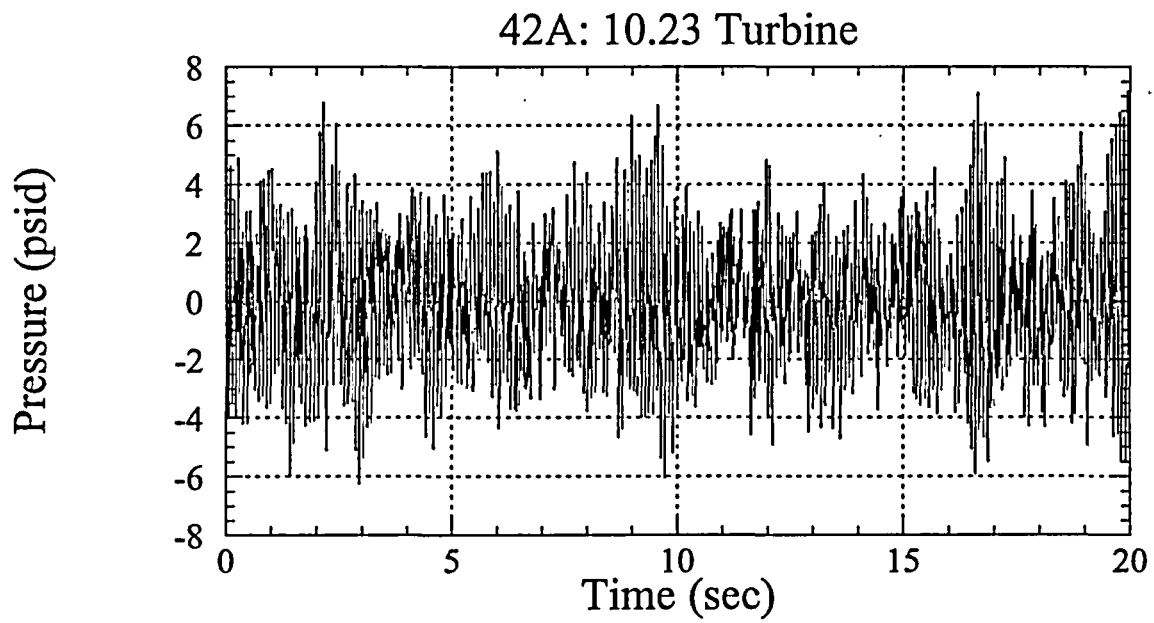


Figure 11-a

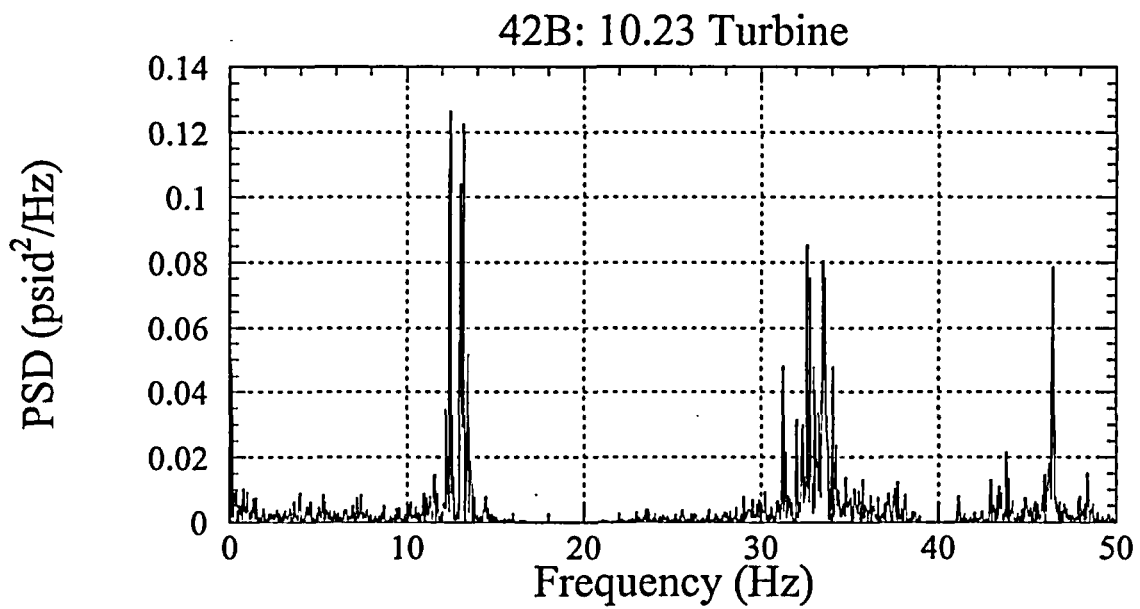
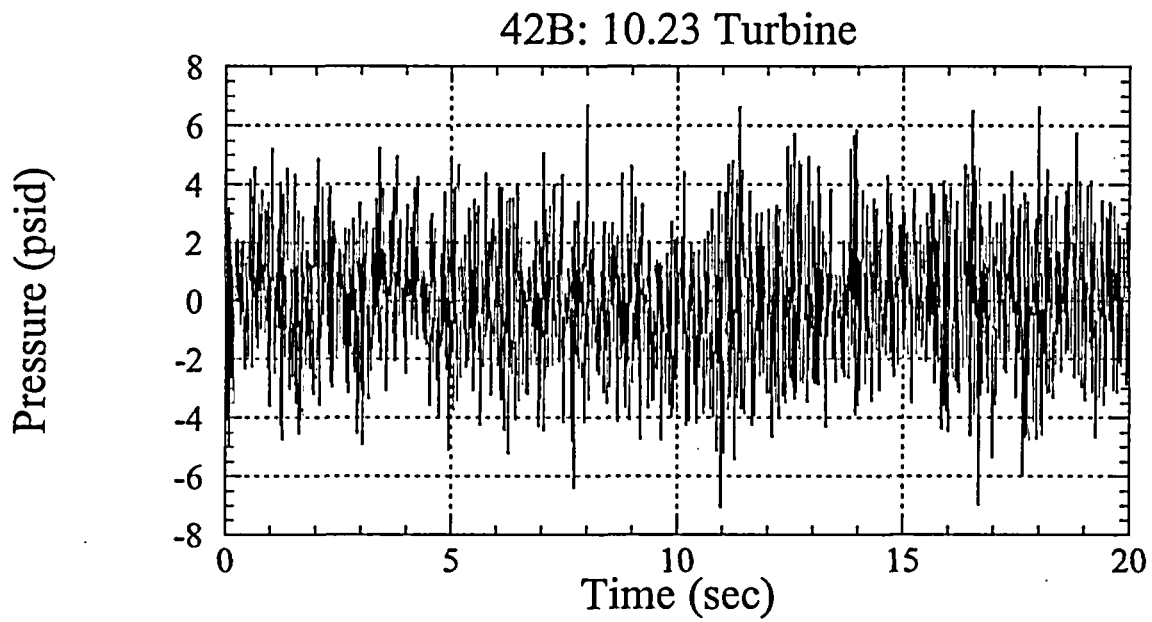


Figure 11-b

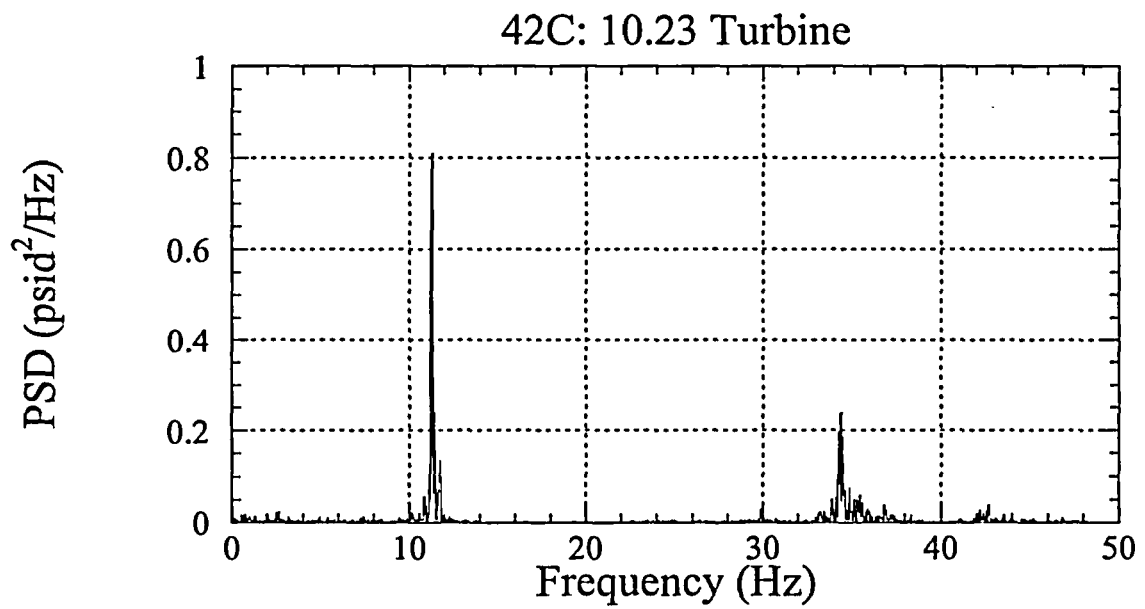
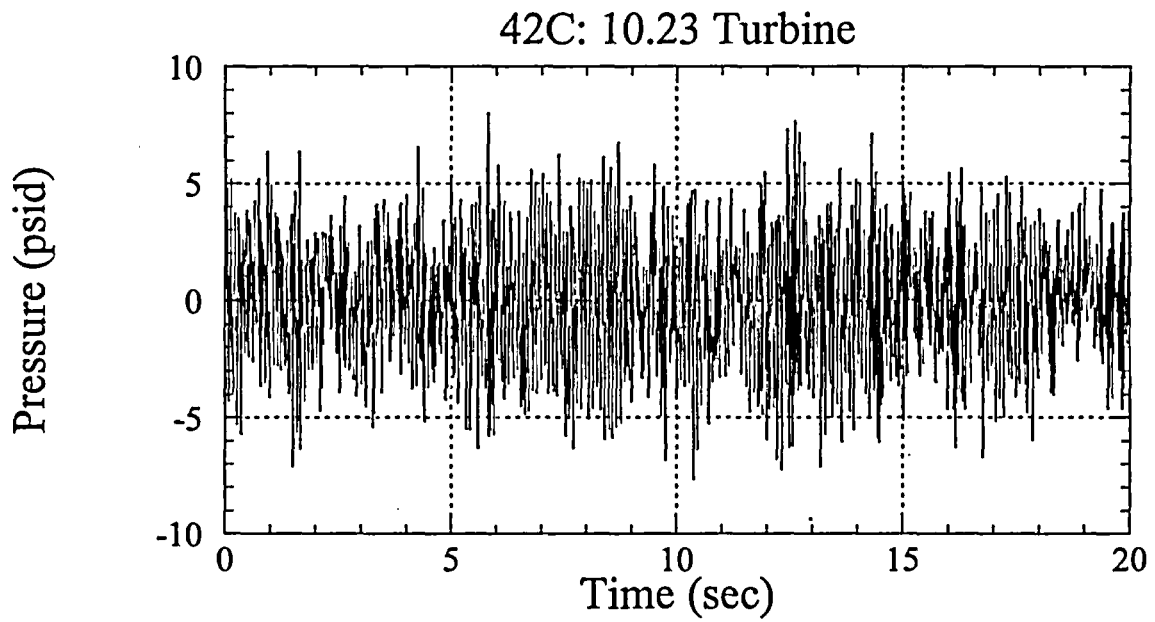


Figure 11-c

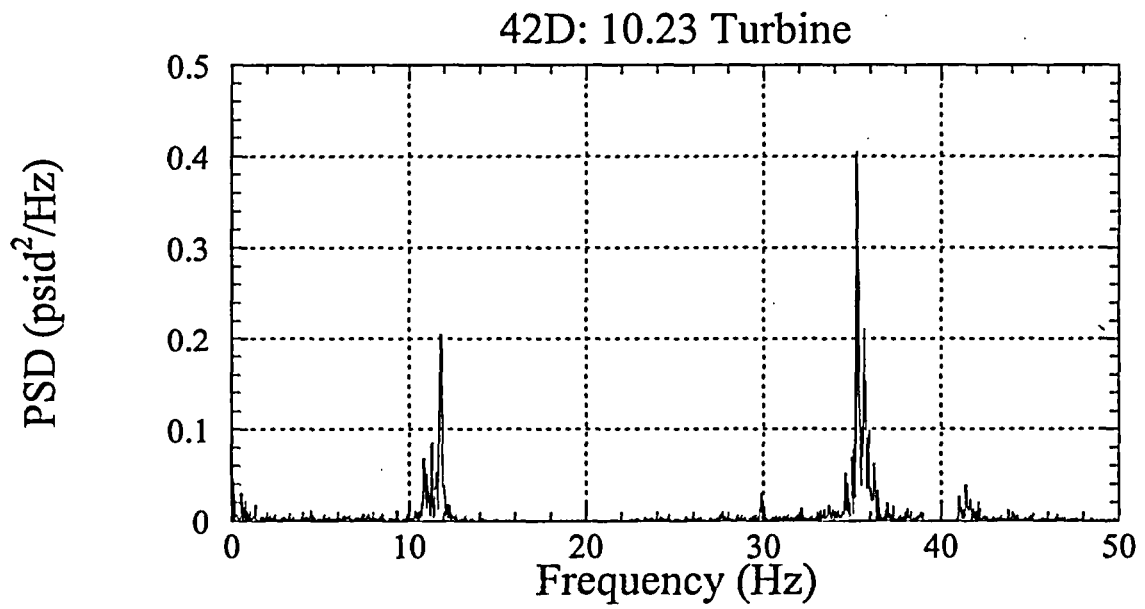
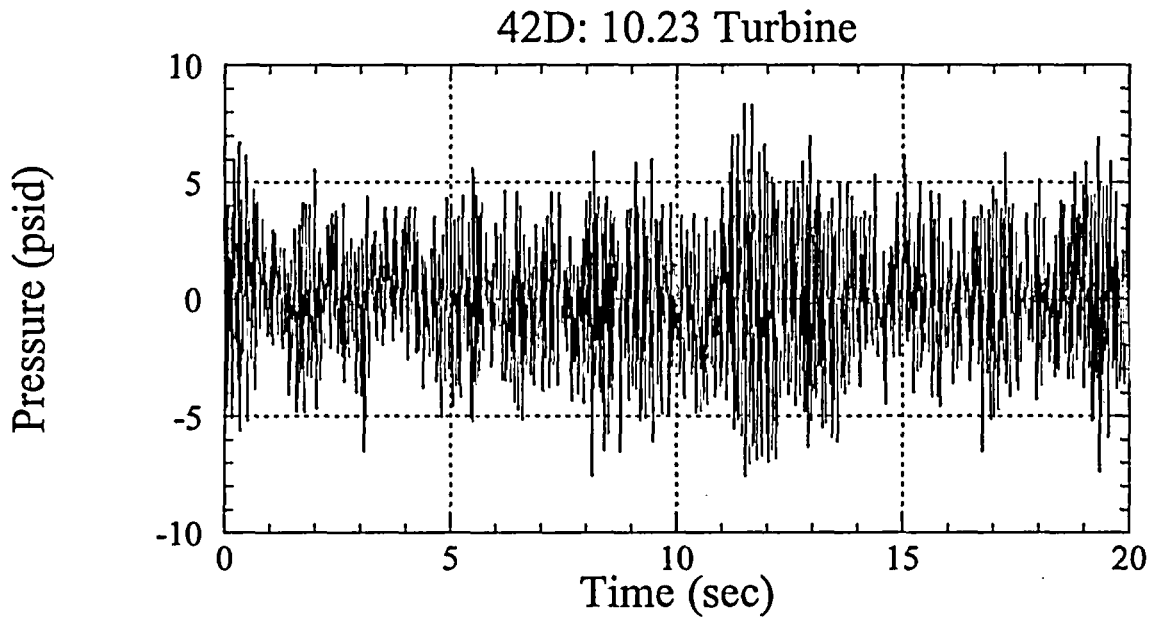


Figure 11-d

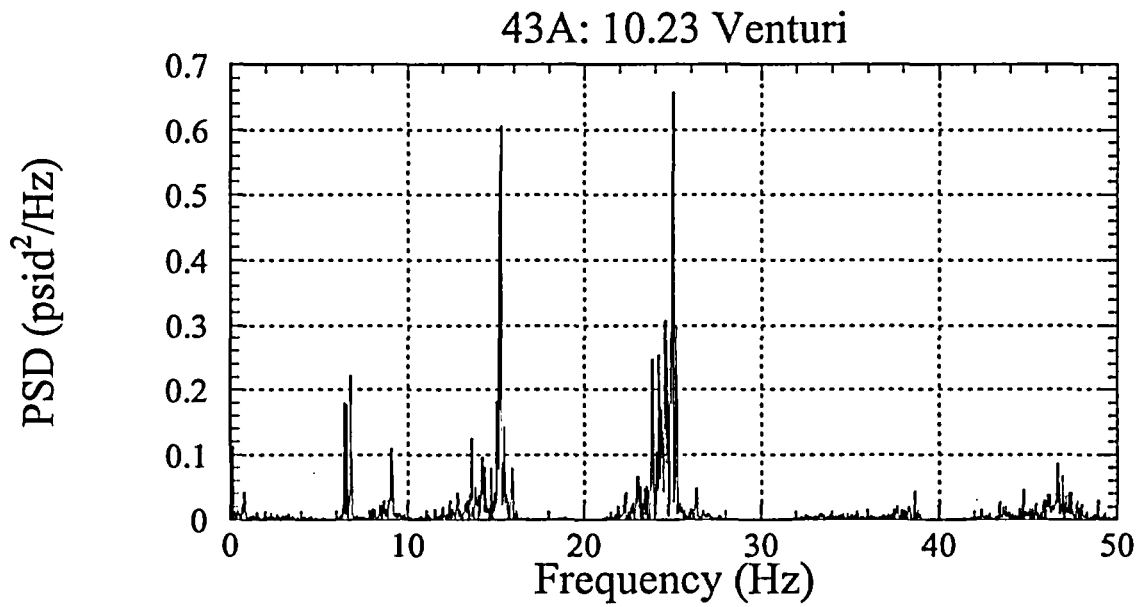
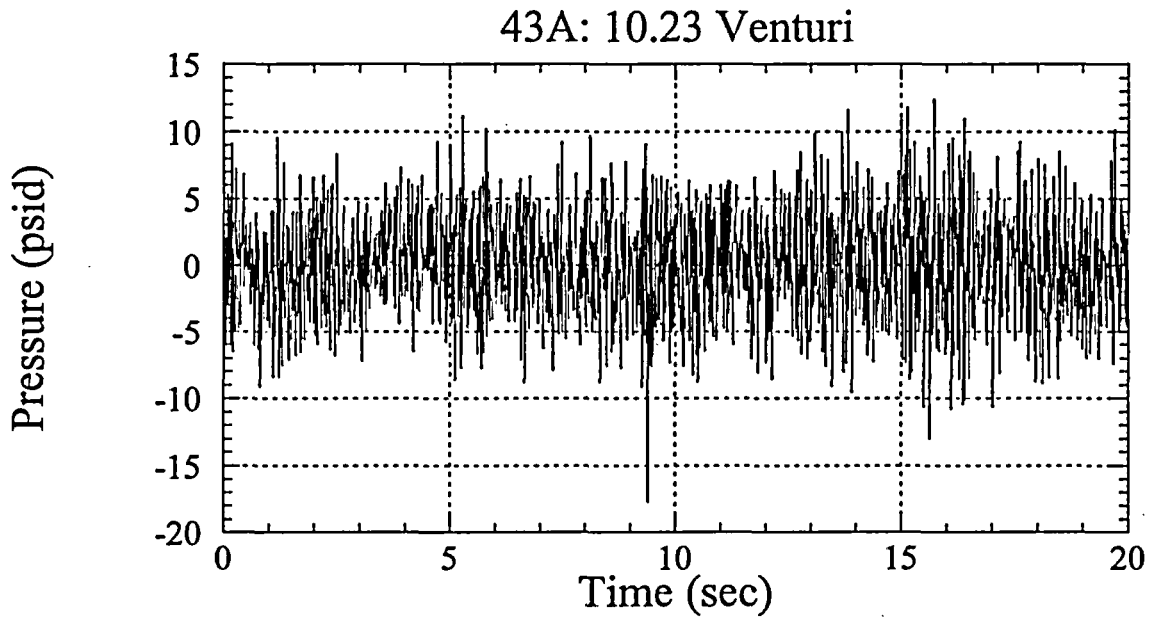


Figure 12-a

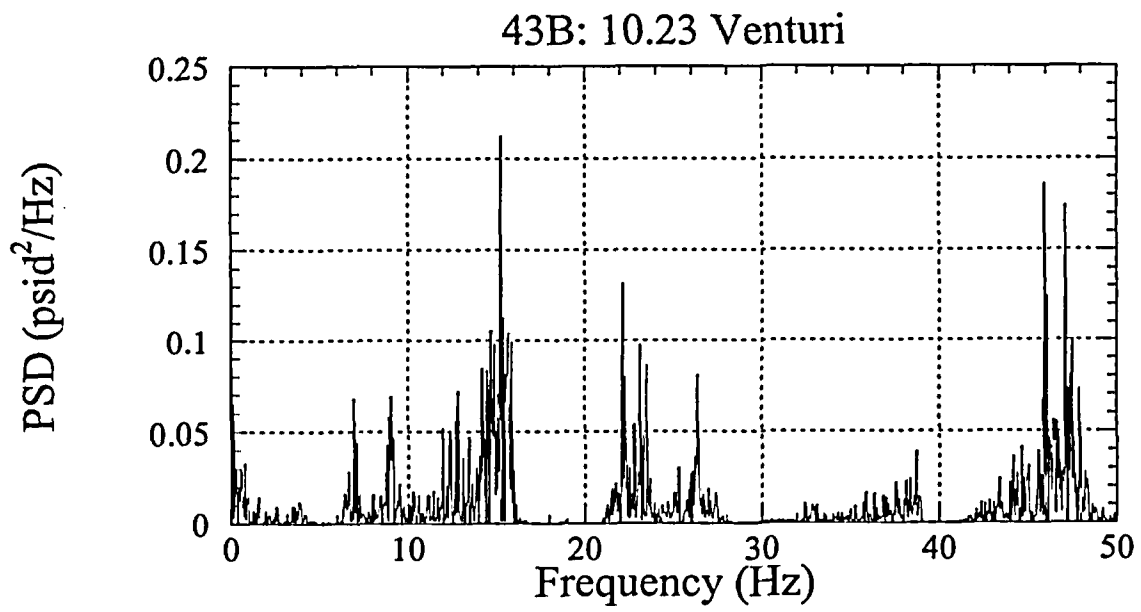
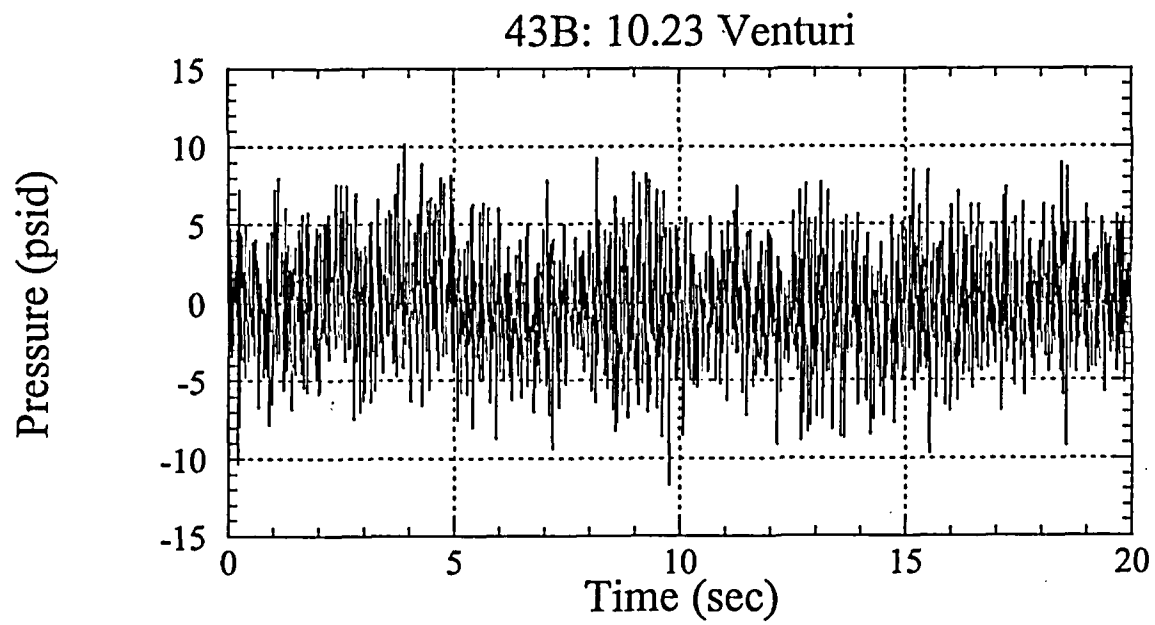


Figure 12-b

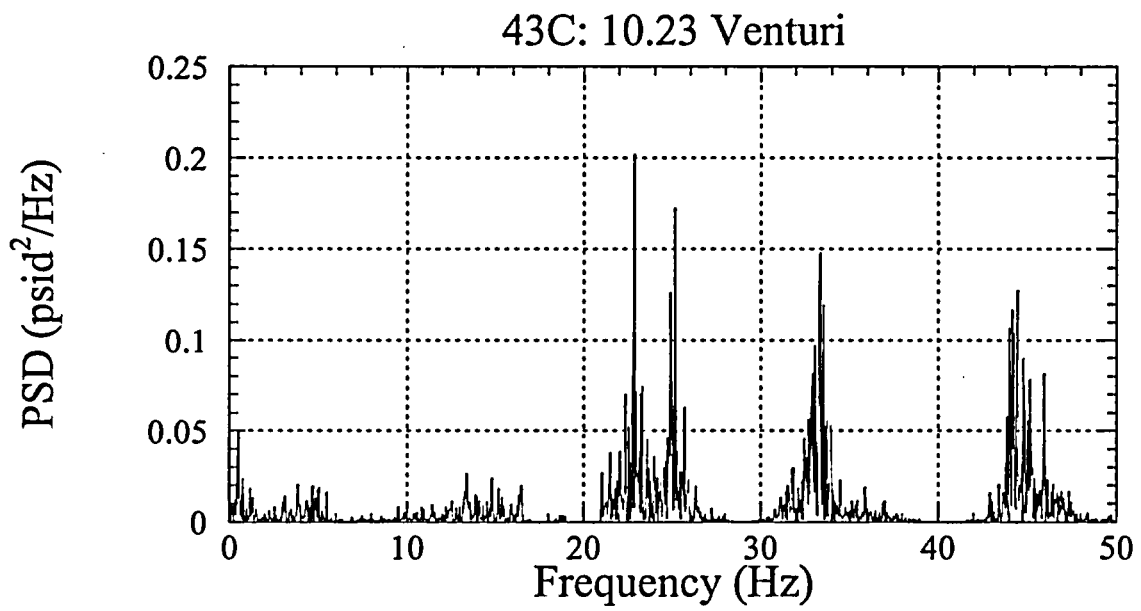
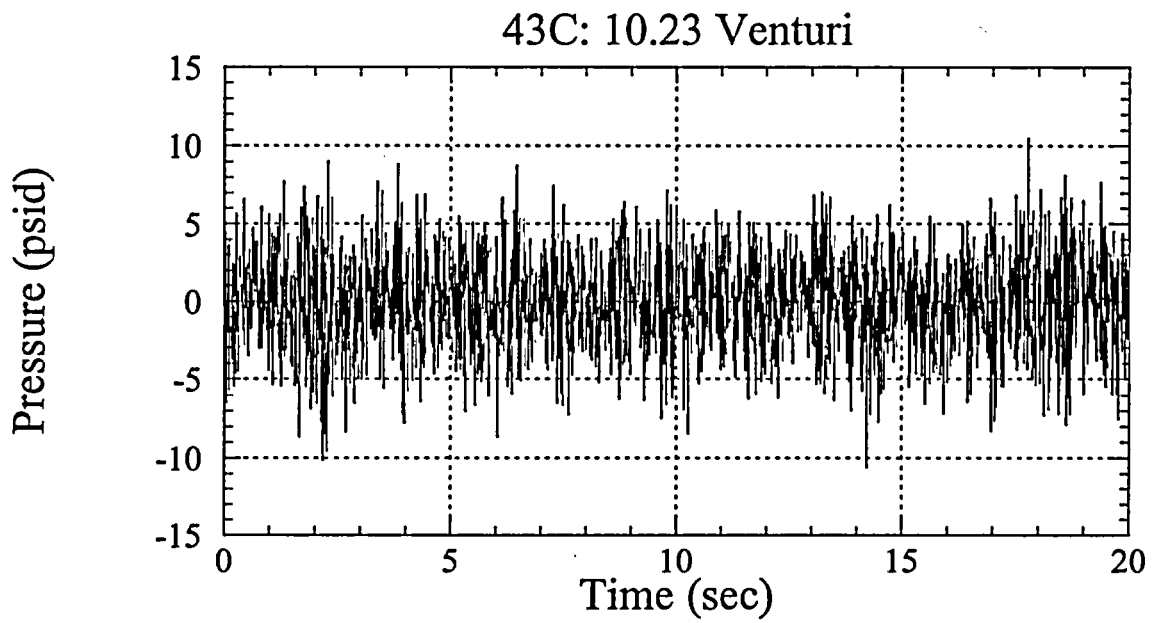


Figure 12-c

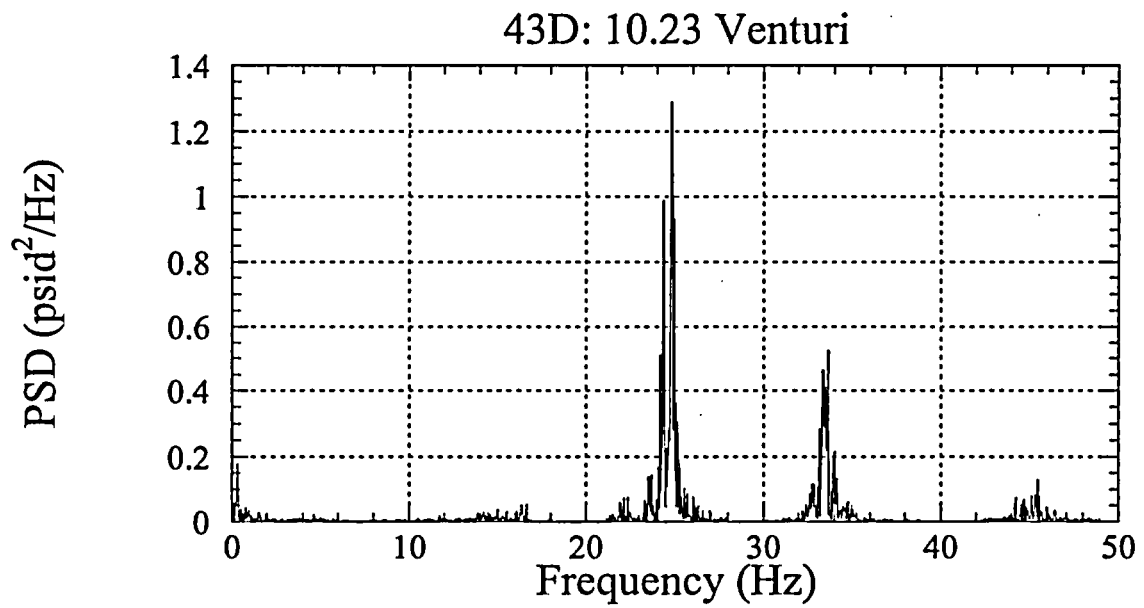
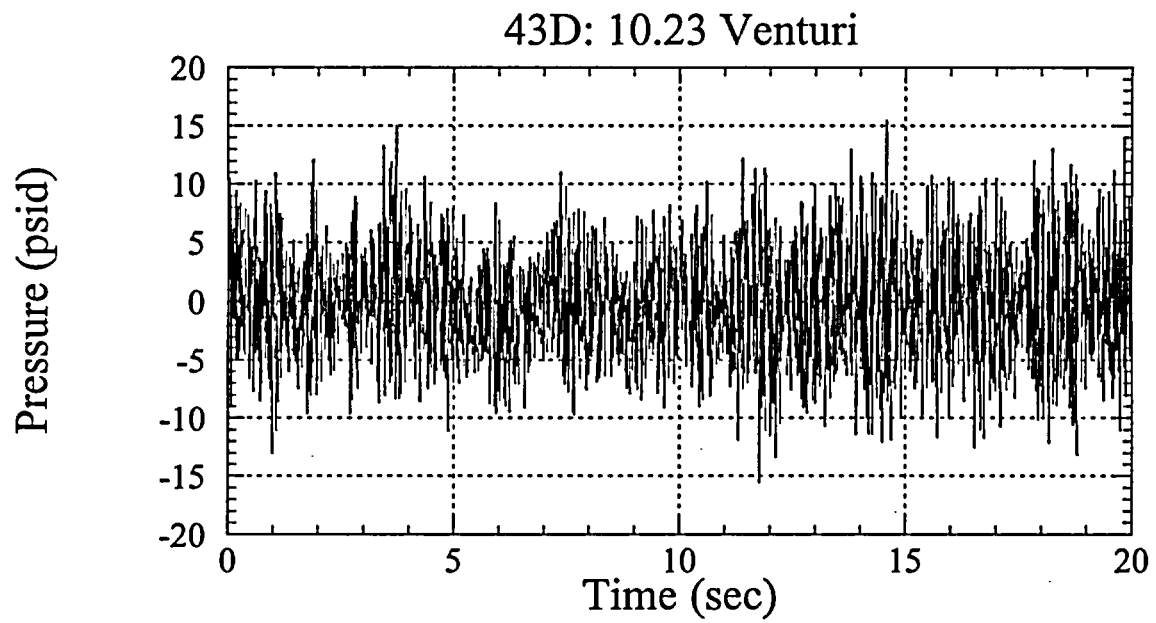


Figure 12-d

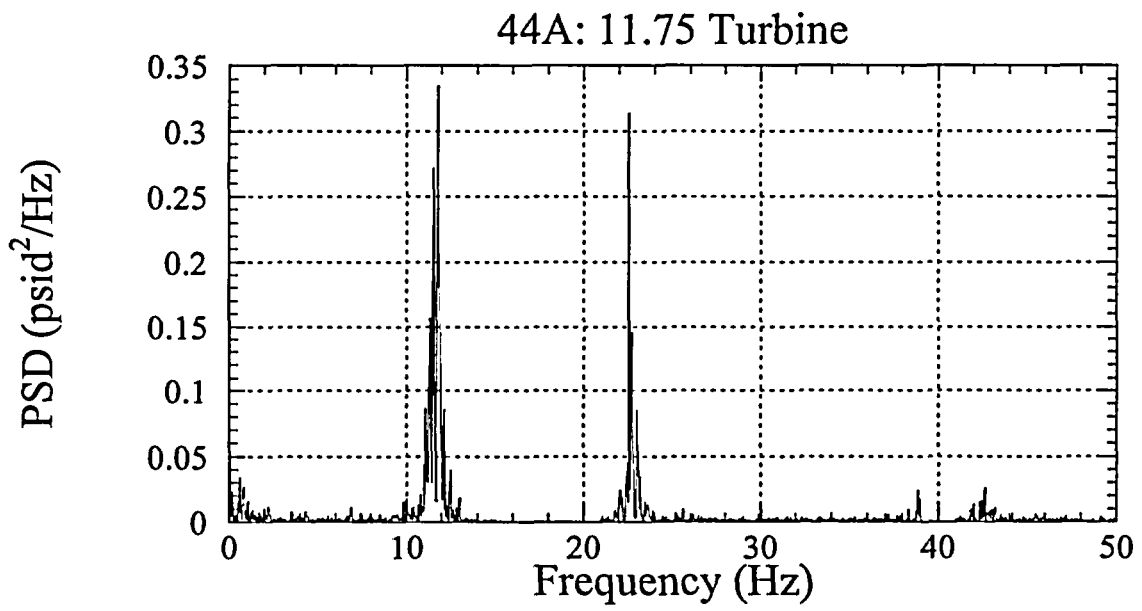
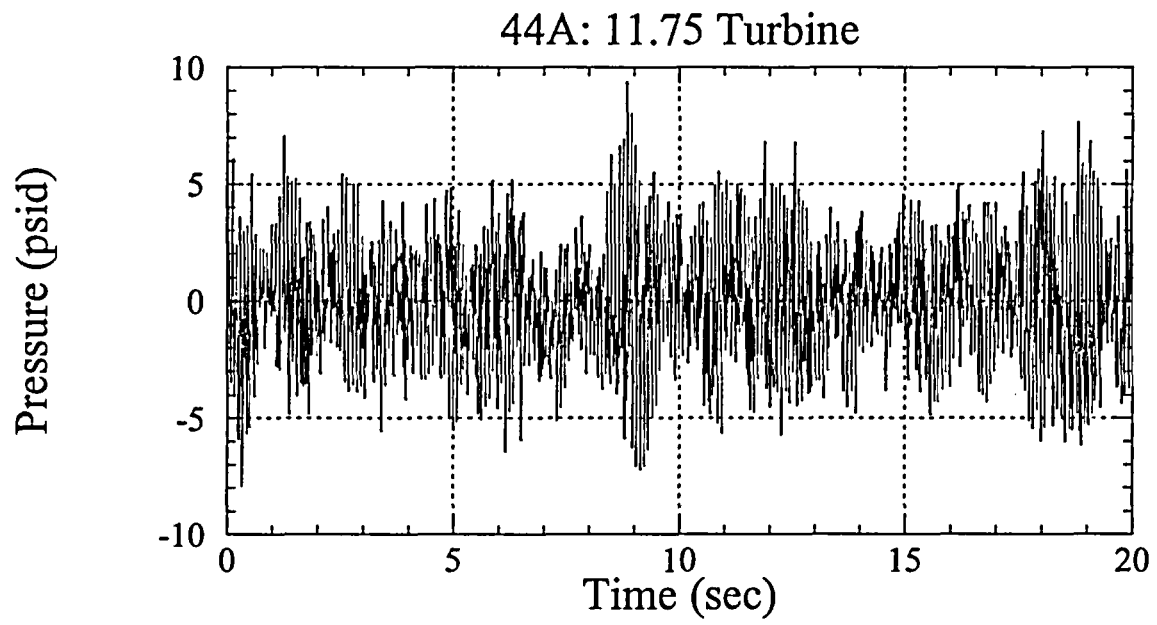


Figure 13-a

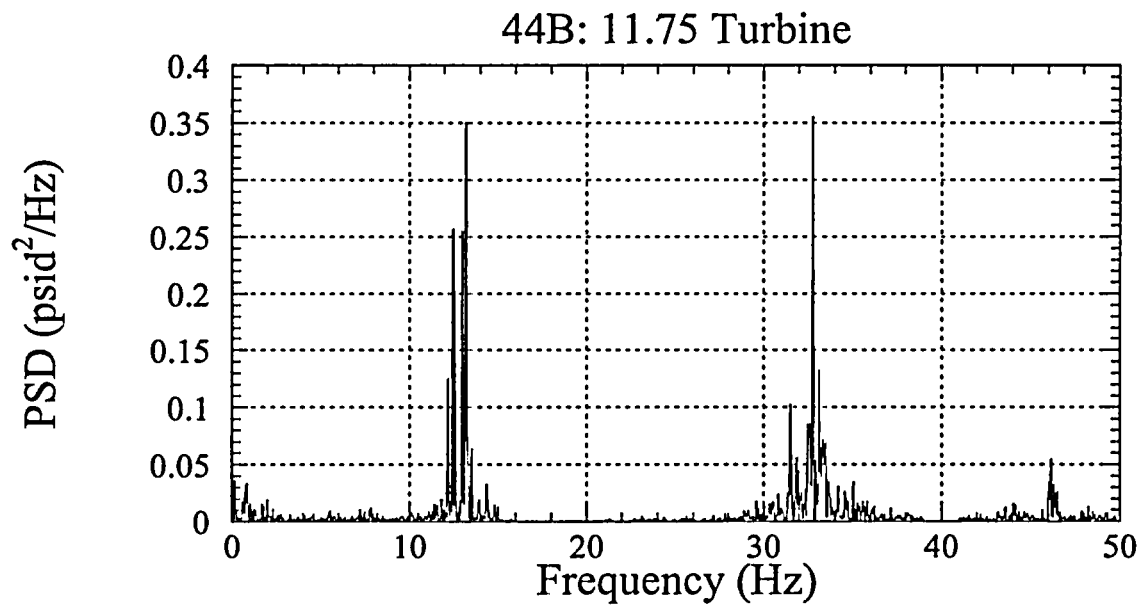
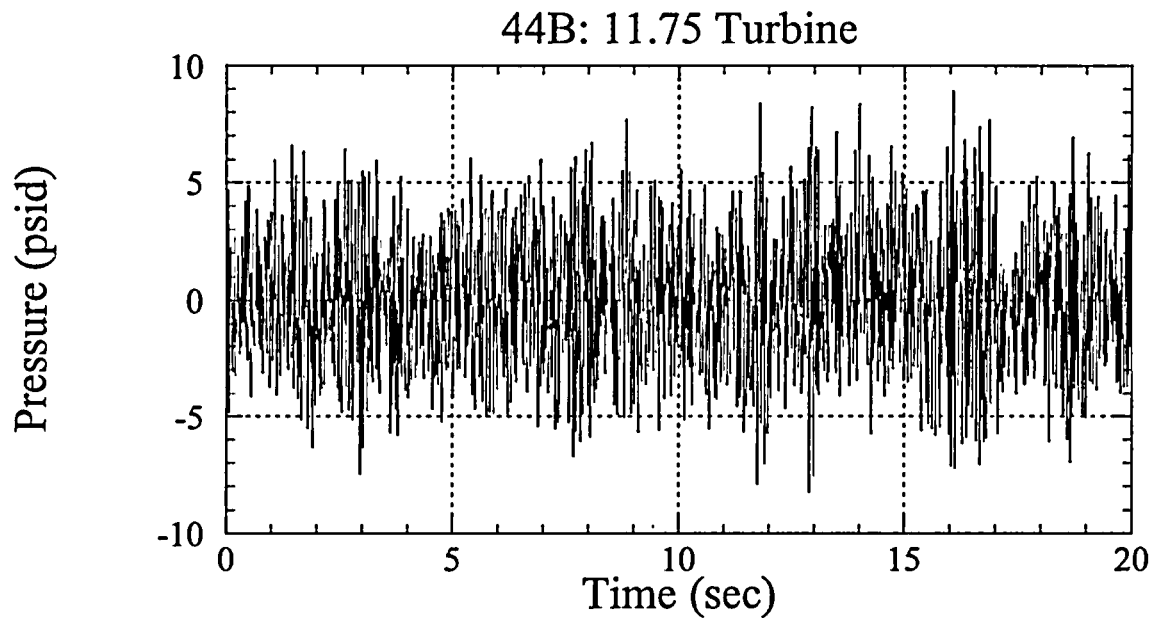


Figure 13-b

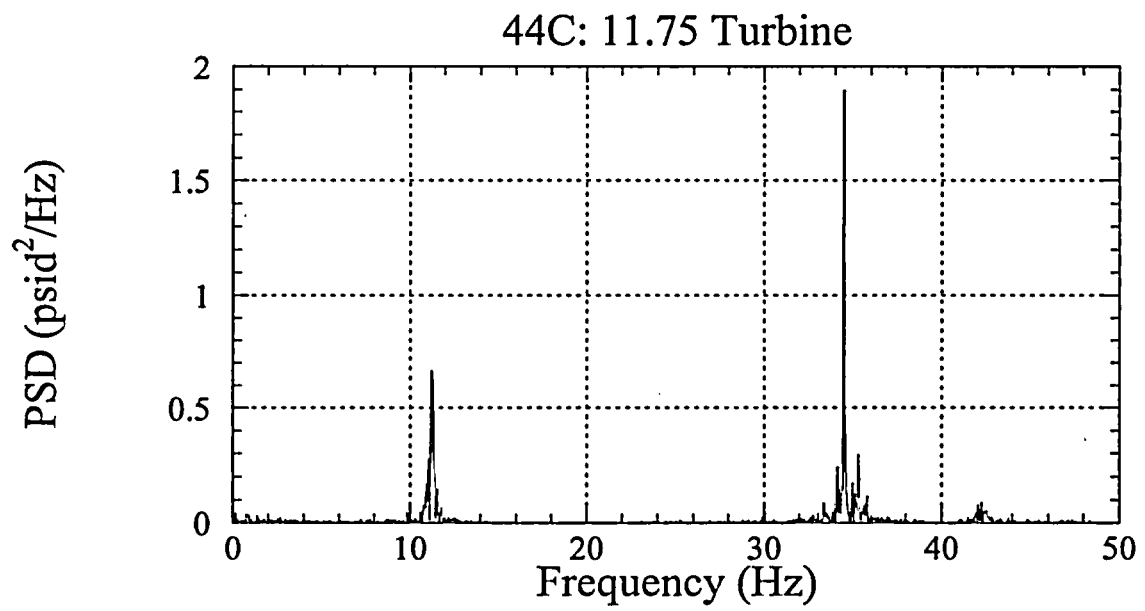
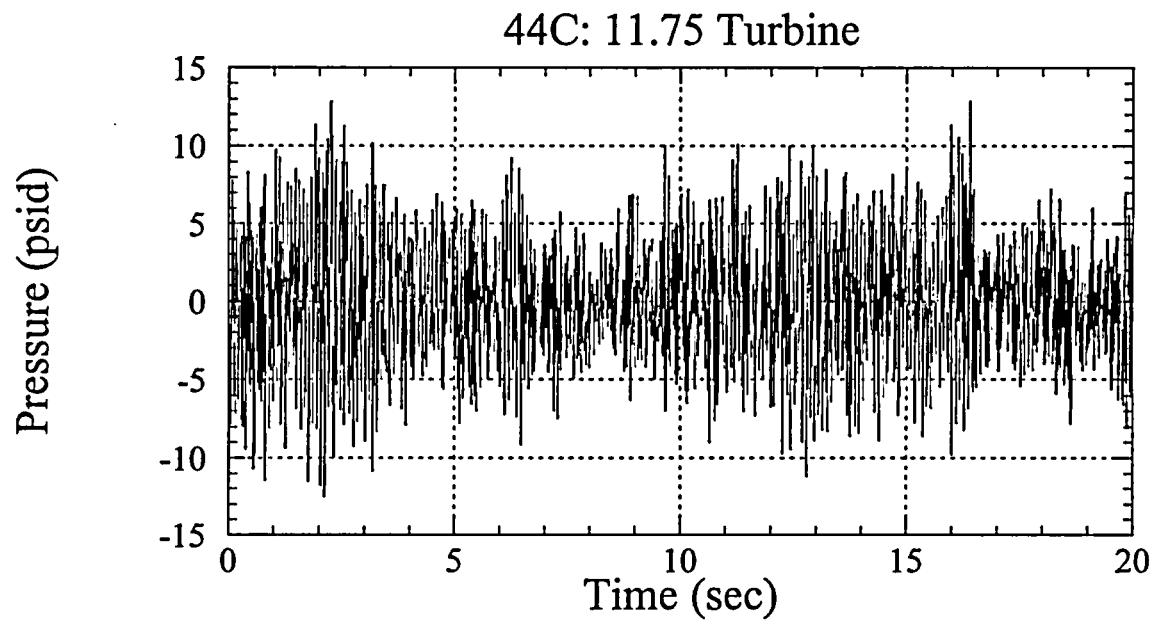


Figure 13-c

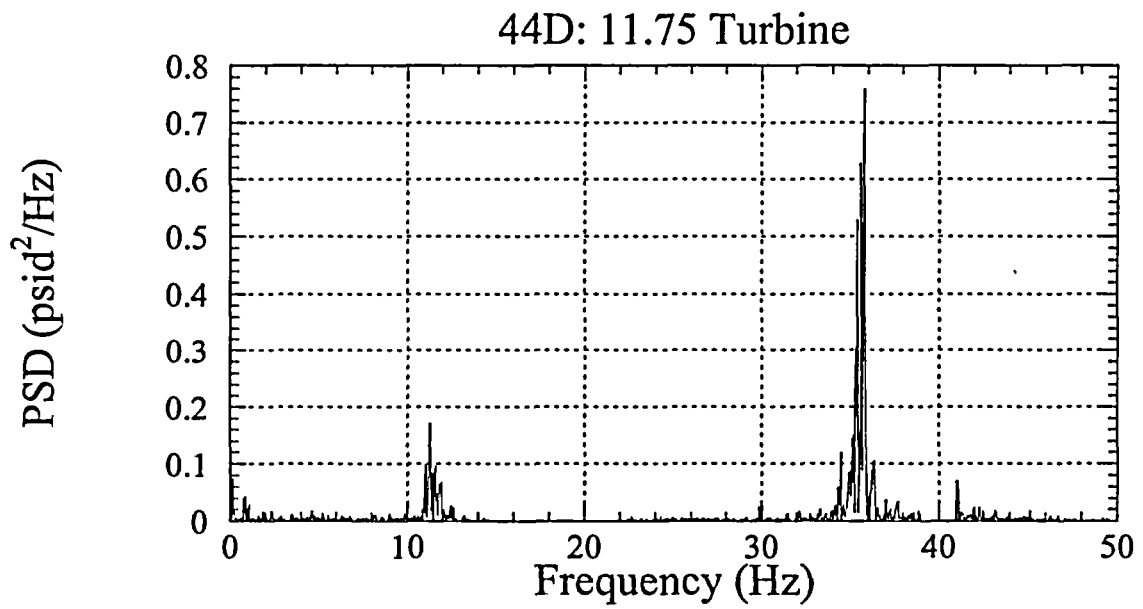
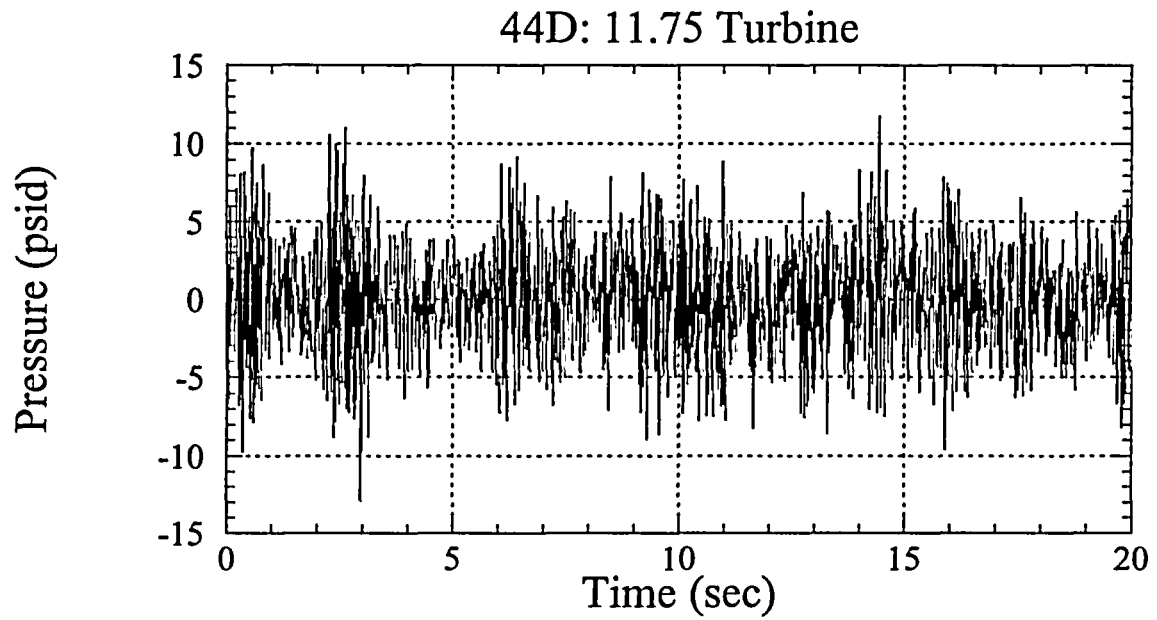


Figure 13-d

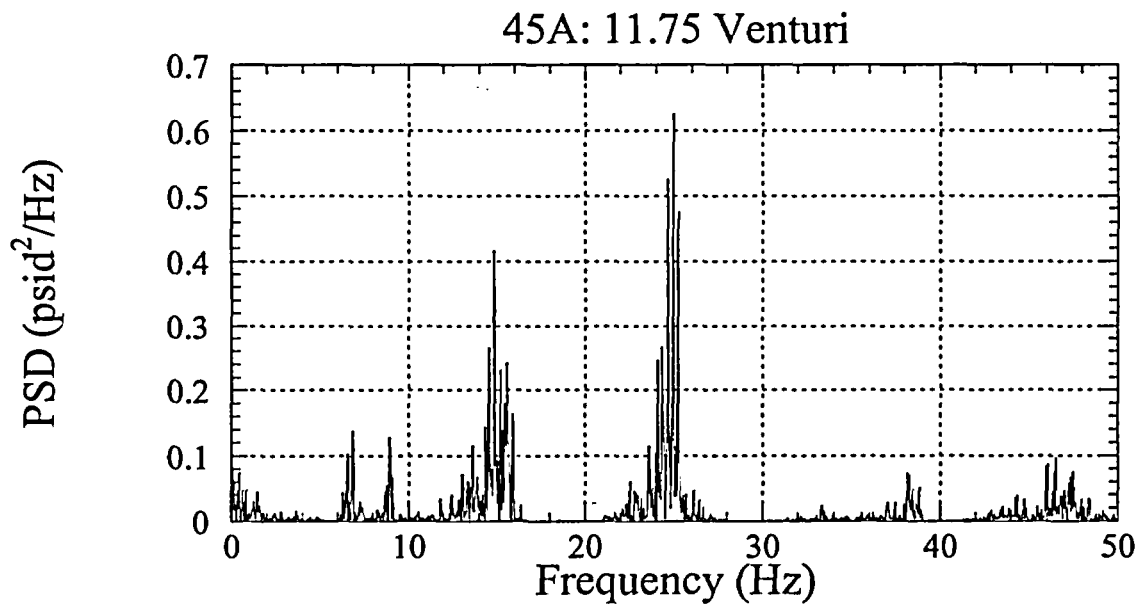
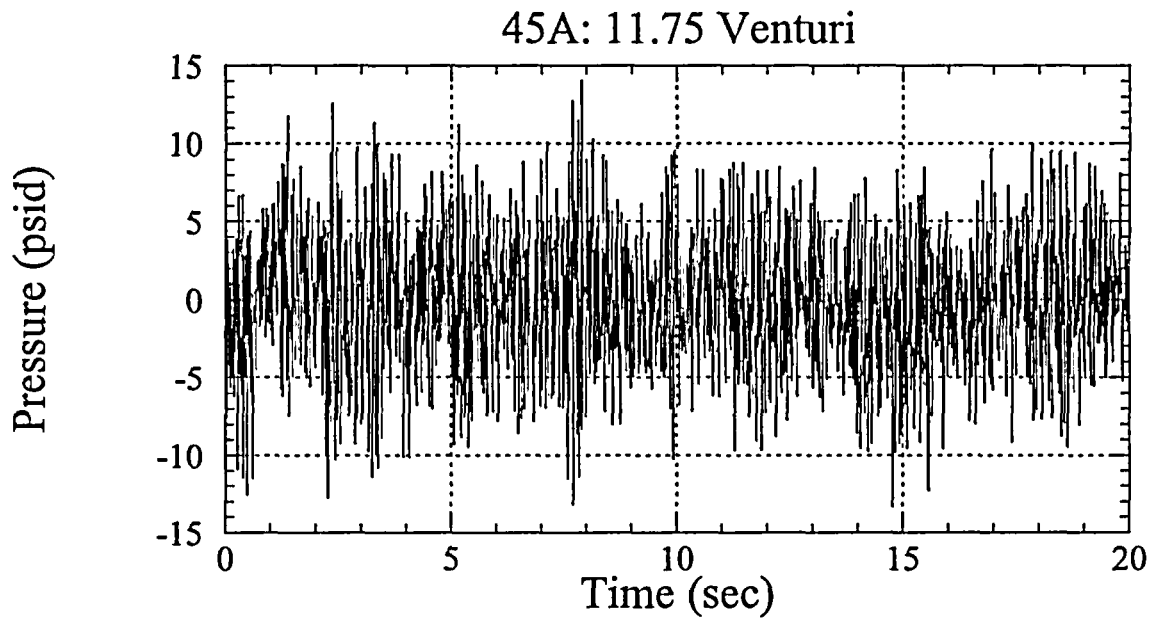


Figure 14-a

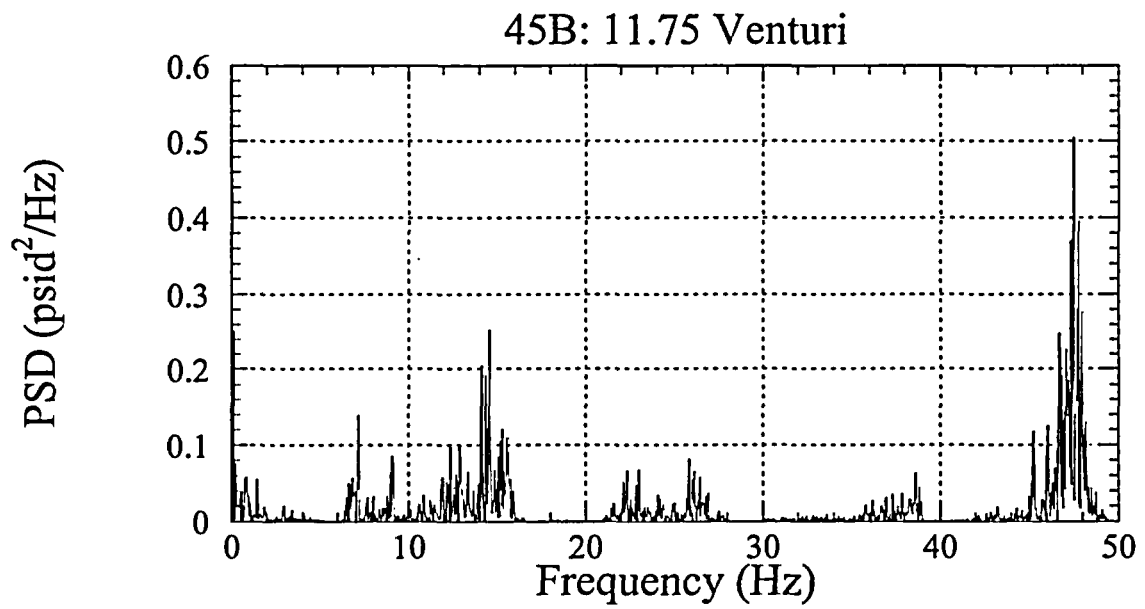
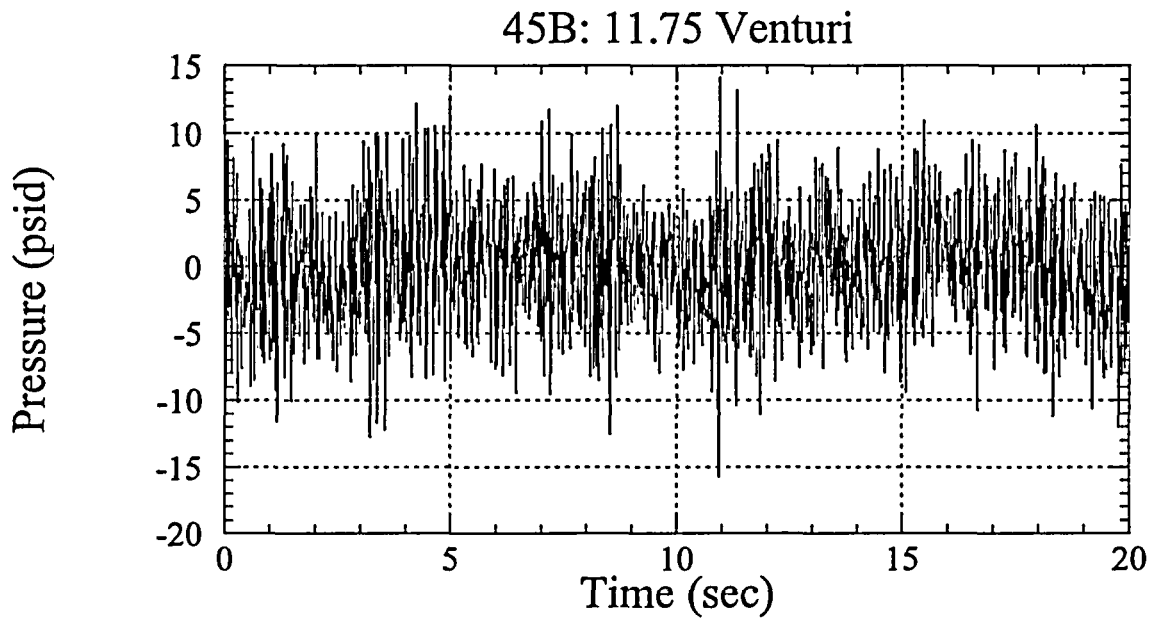


Figure 14-b

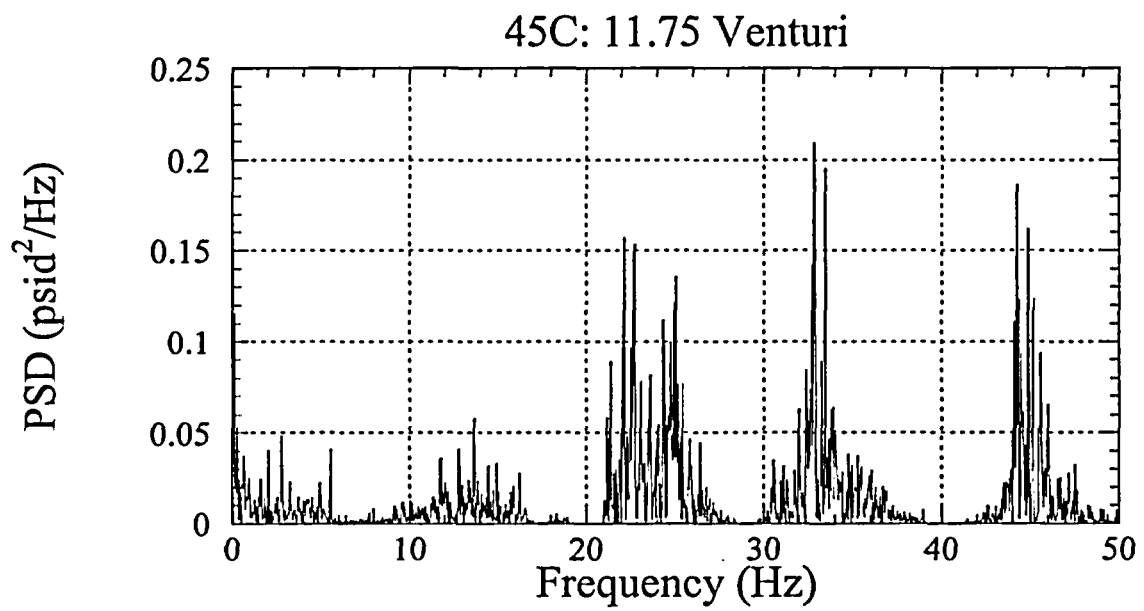
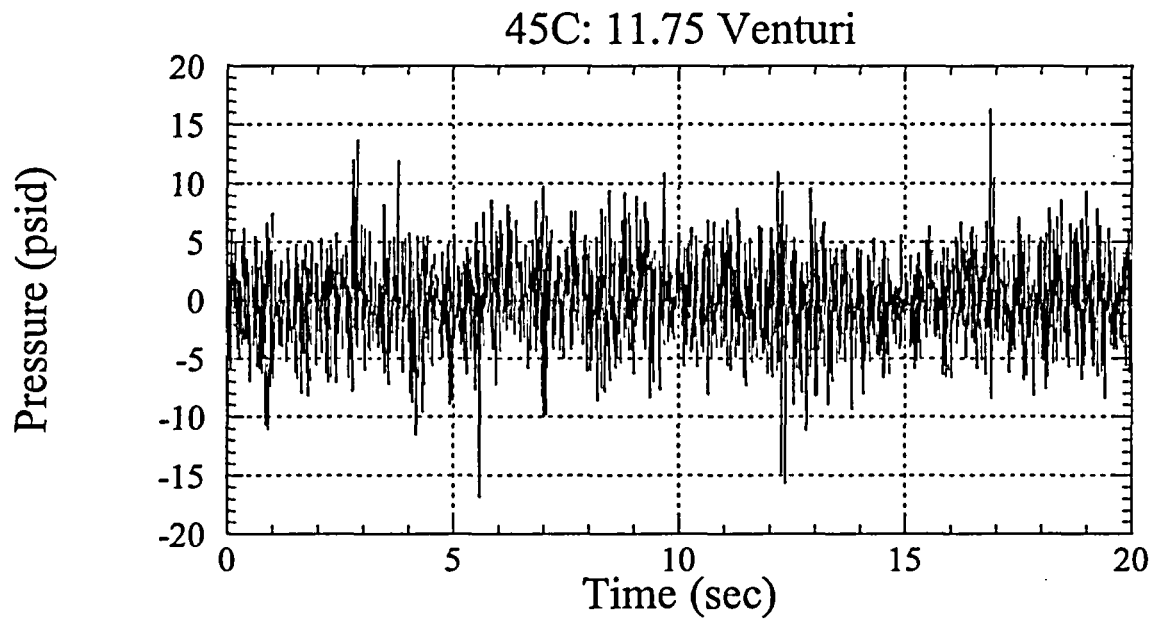


Figure 14-c

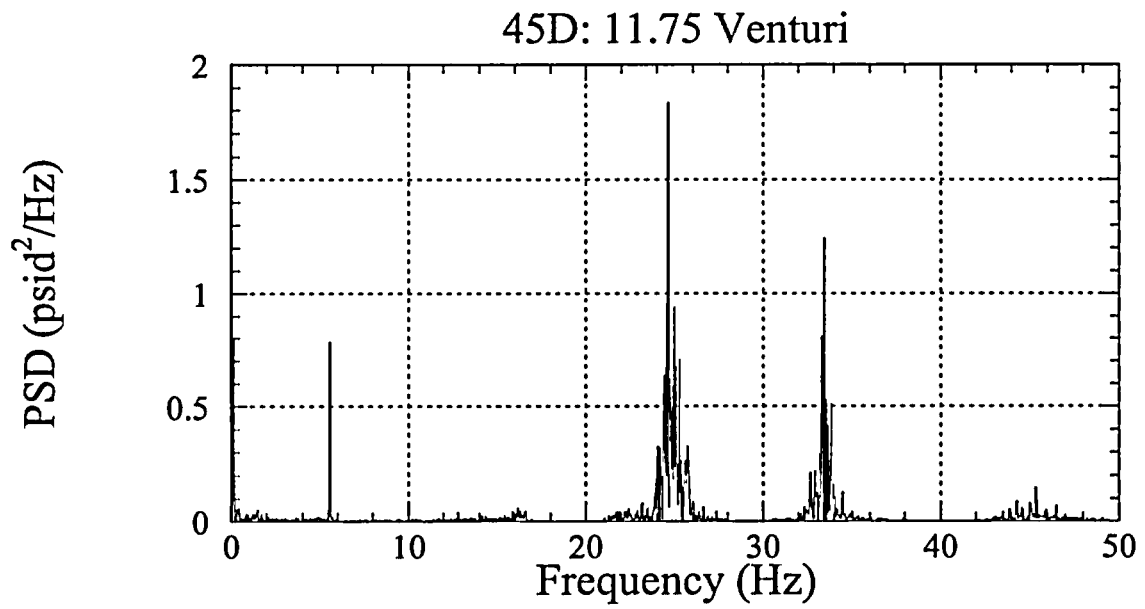
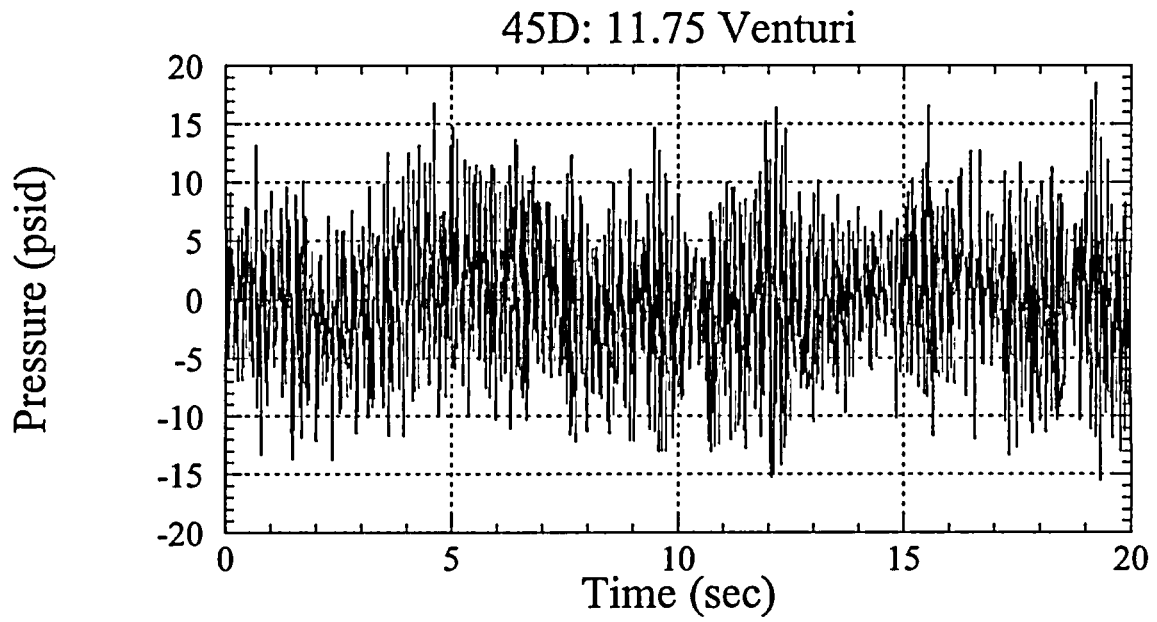


Figure 14-d

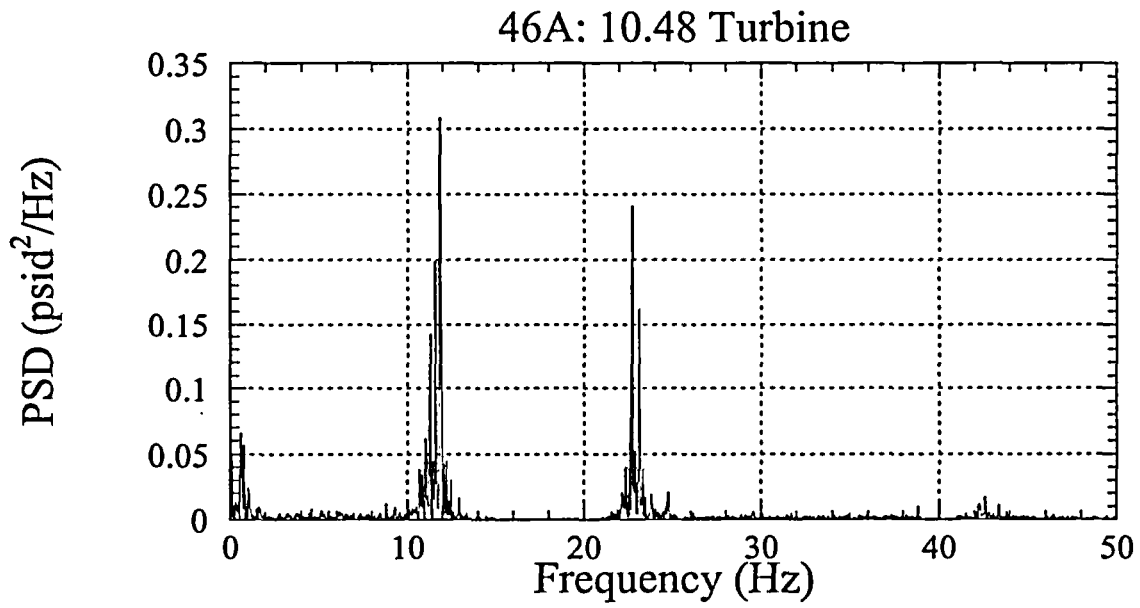
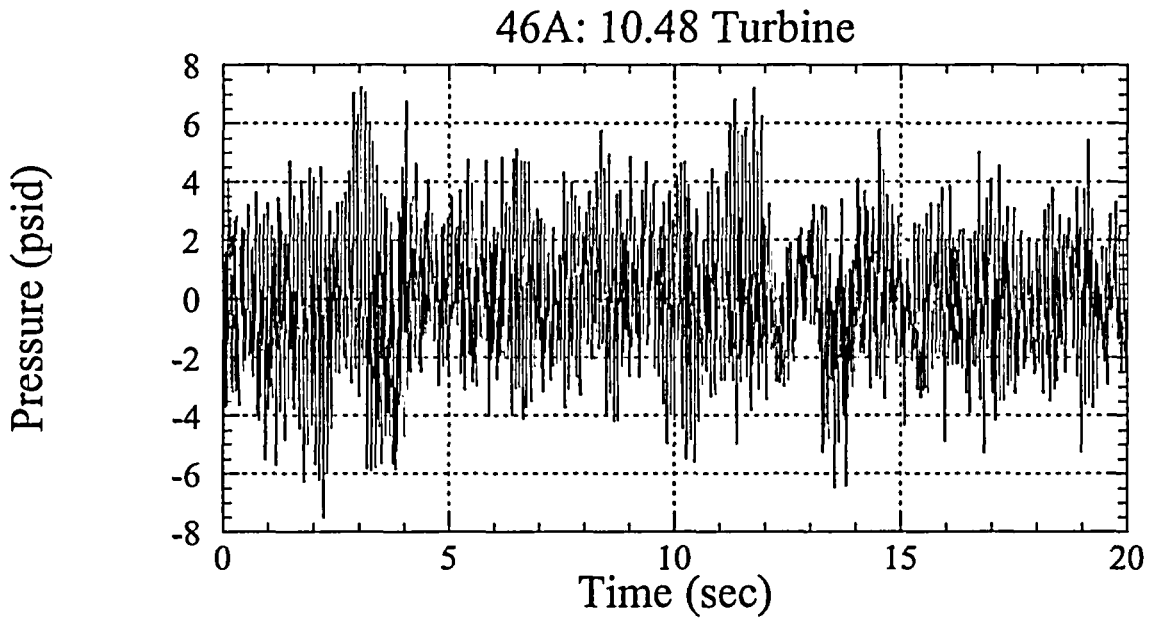


Figure 15-a

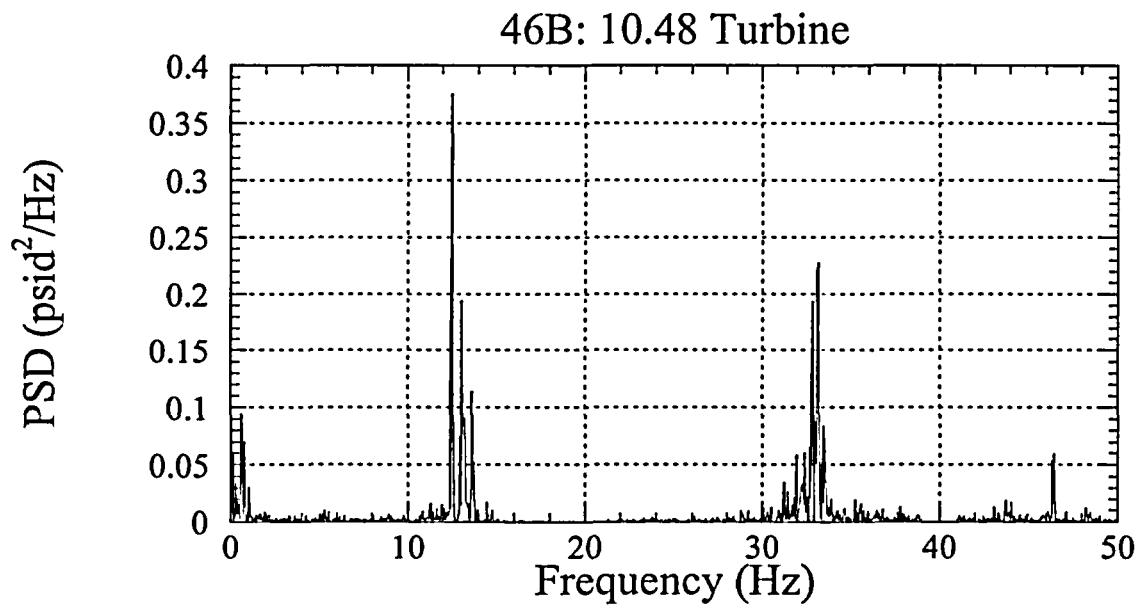
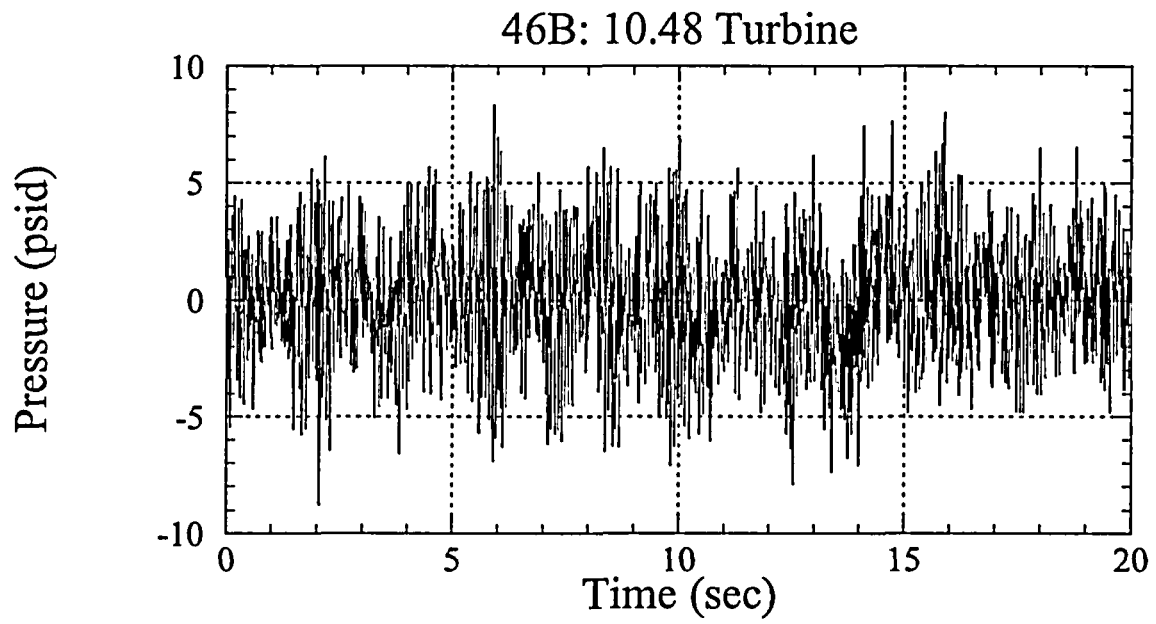


Figure 15-b

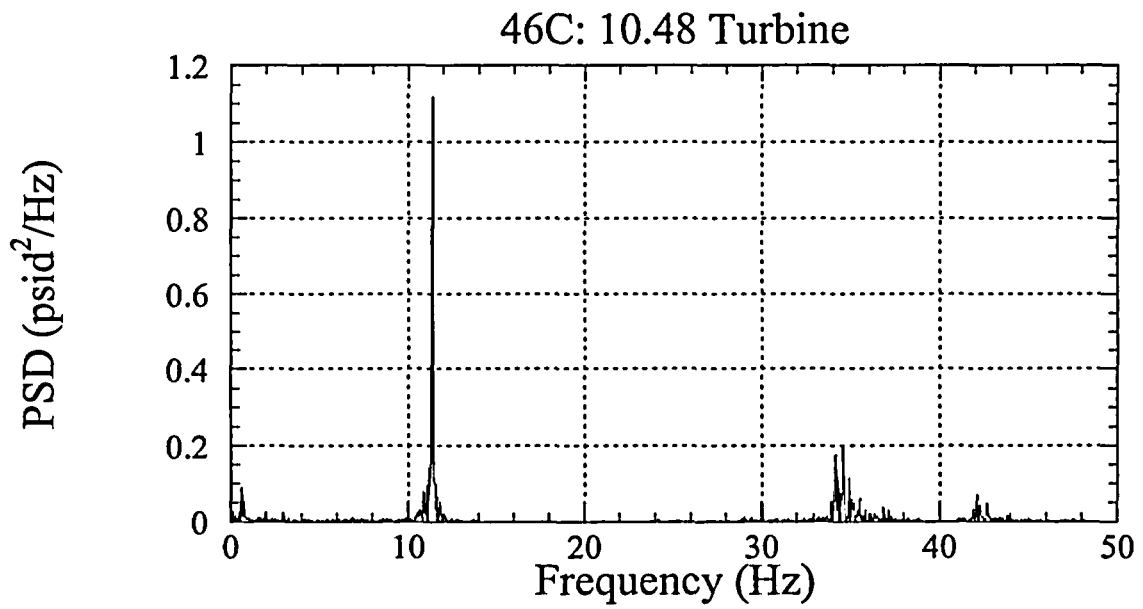
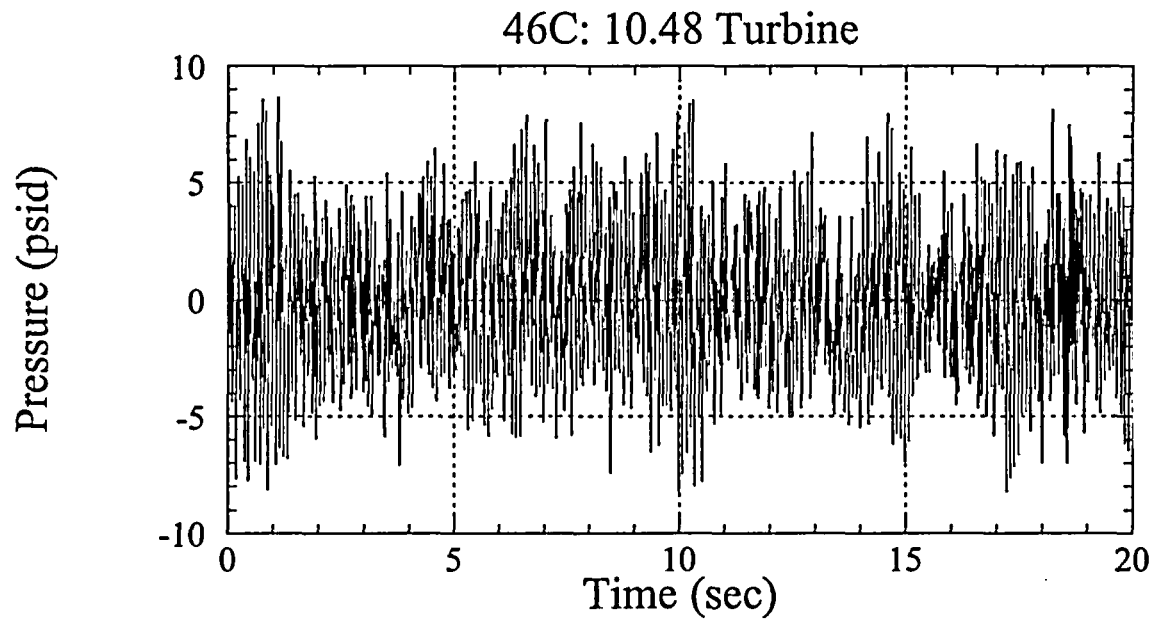


Figure 15-c

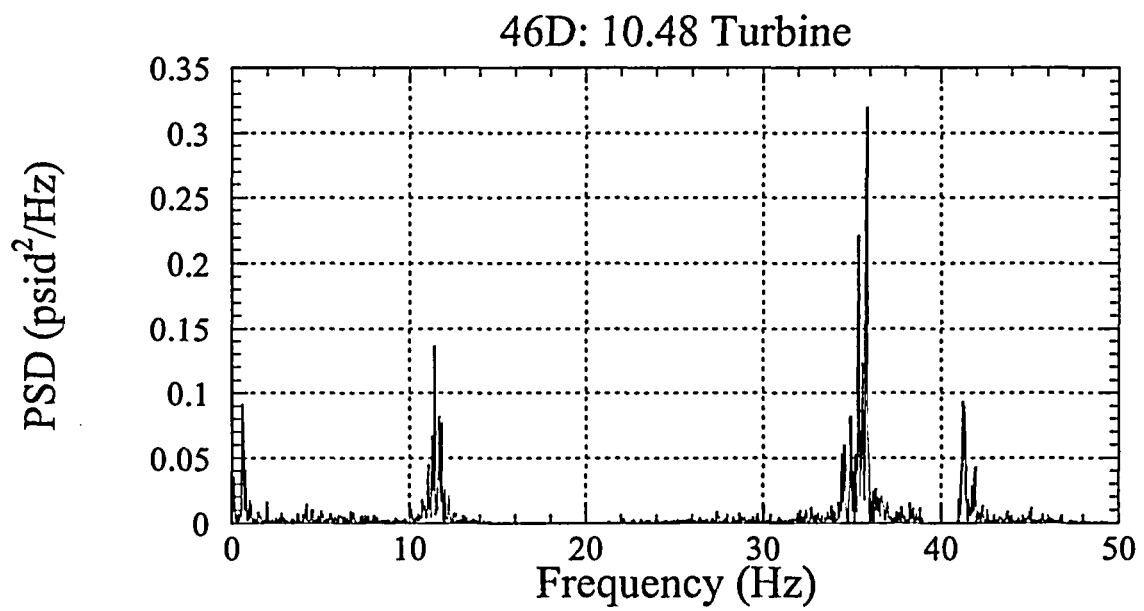
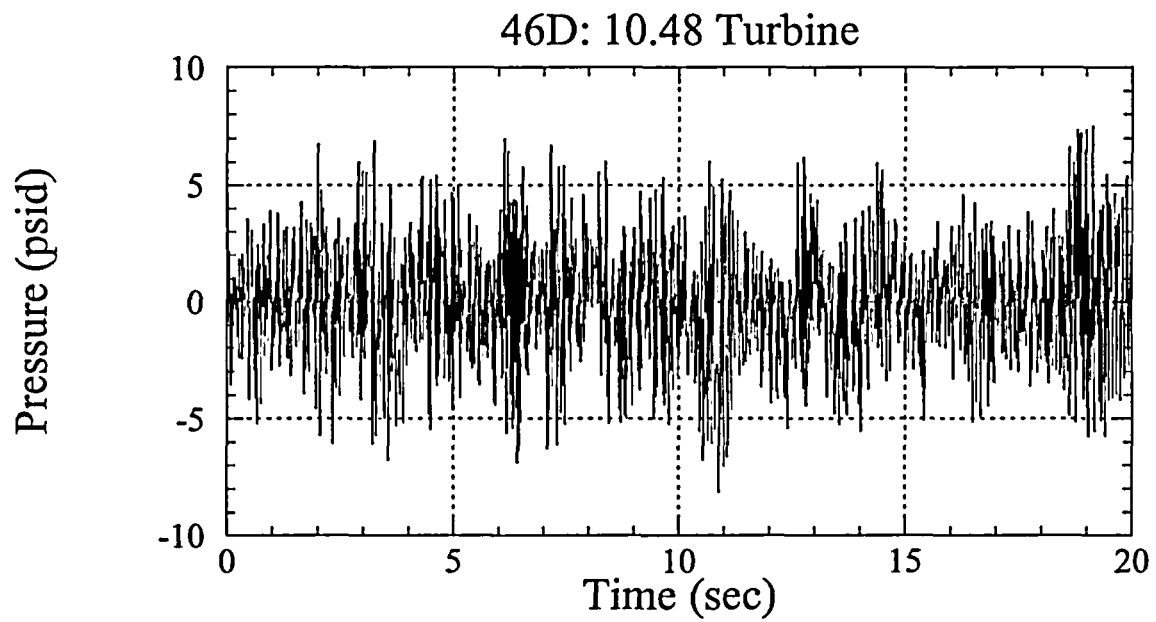


Figure 15-d

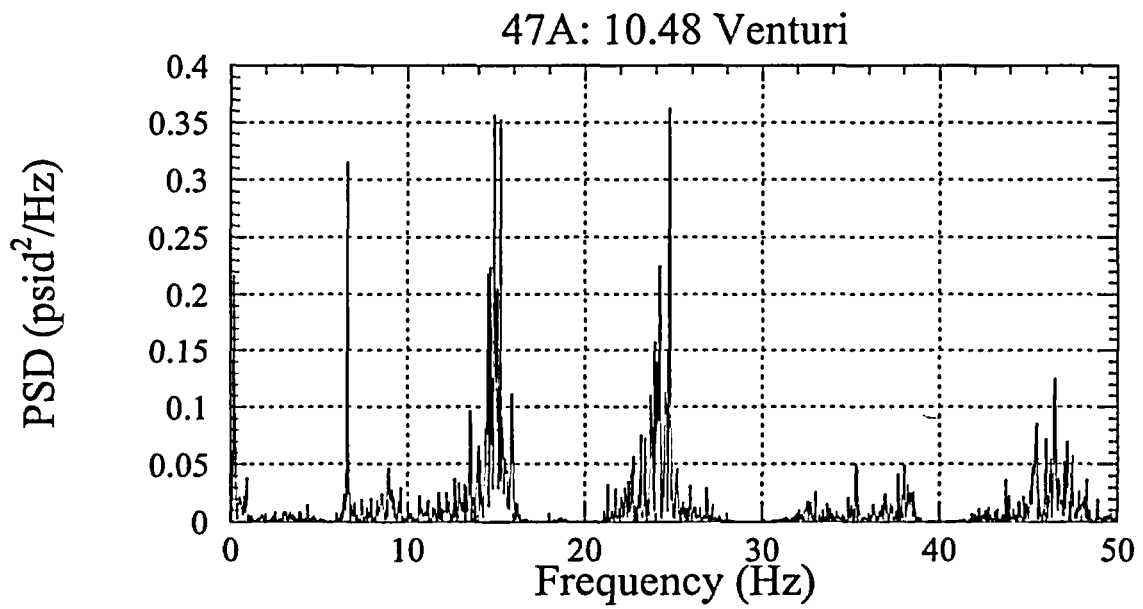
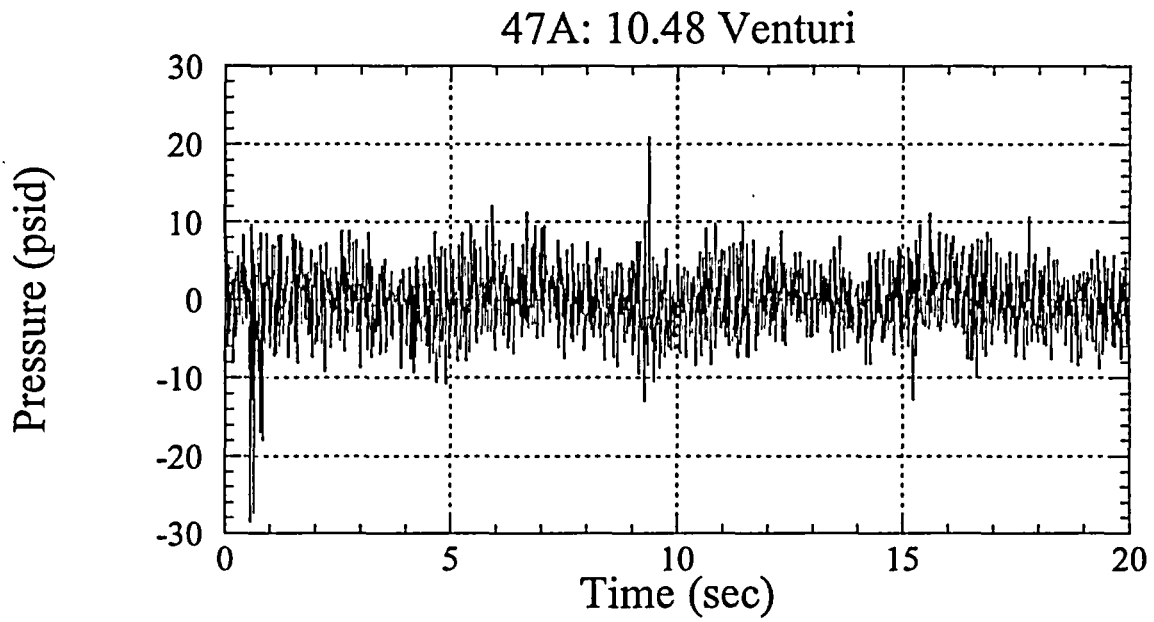


Figure 16-a

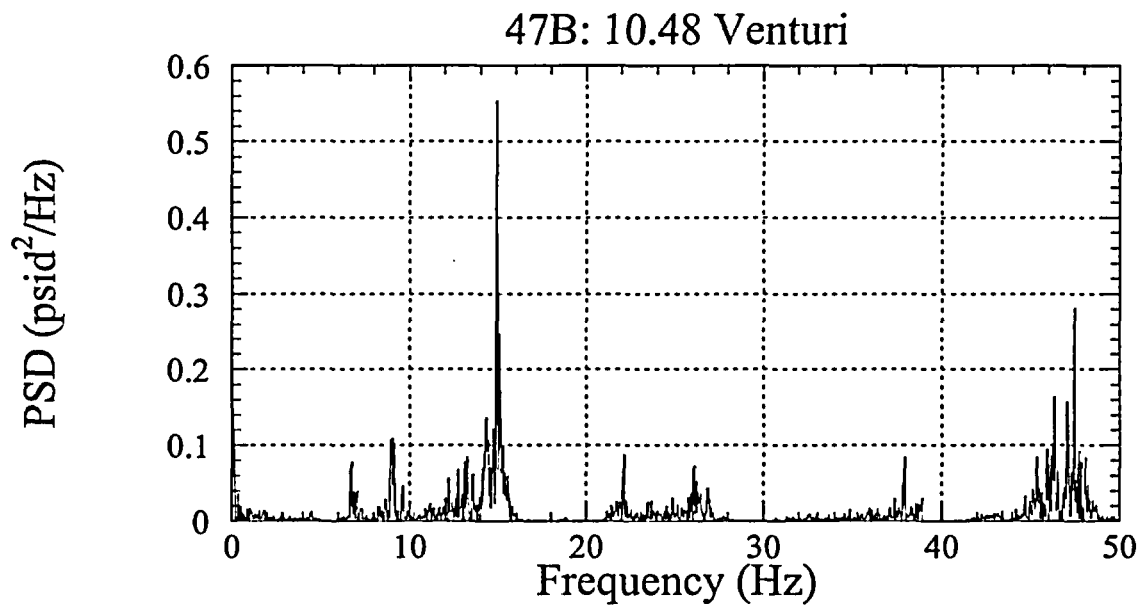
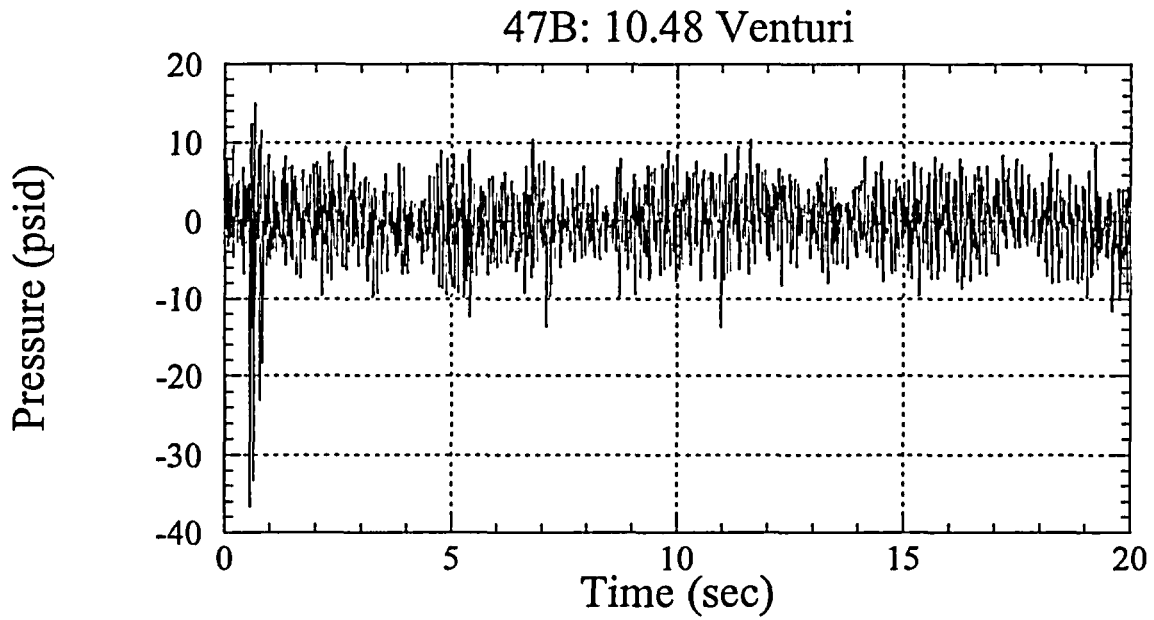


Figure 16-b

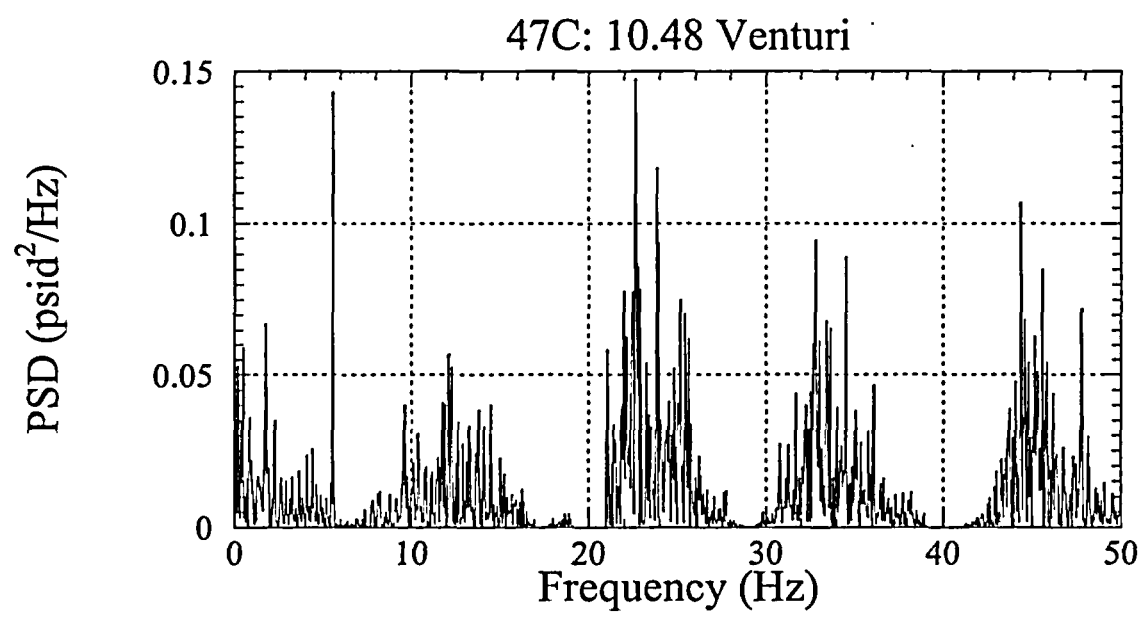
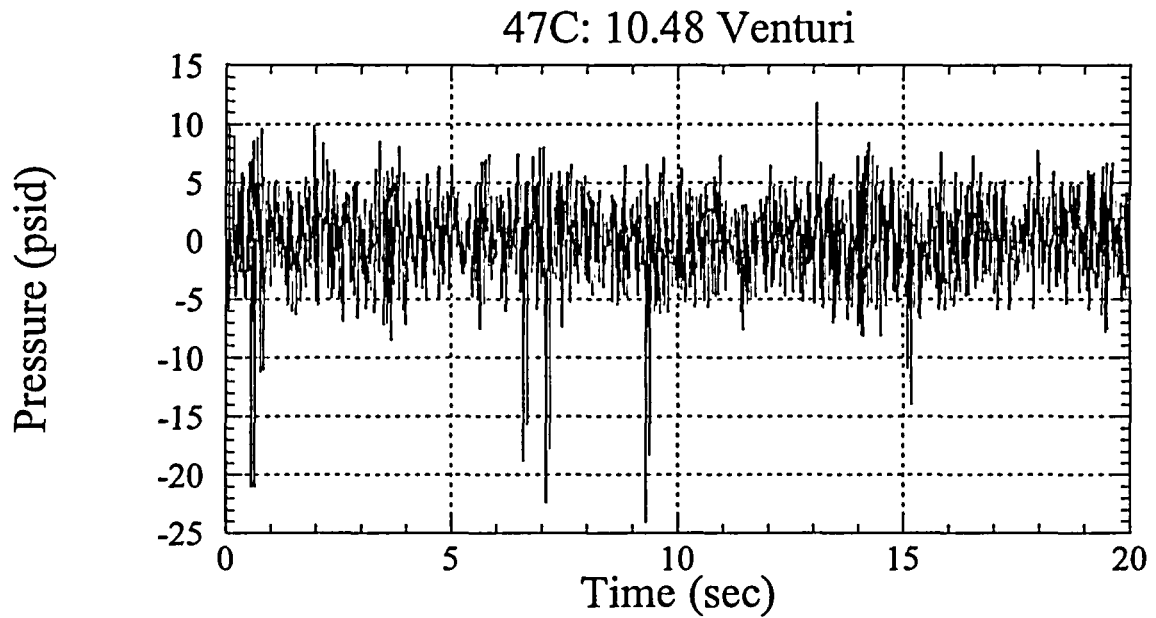


Figure 16-c

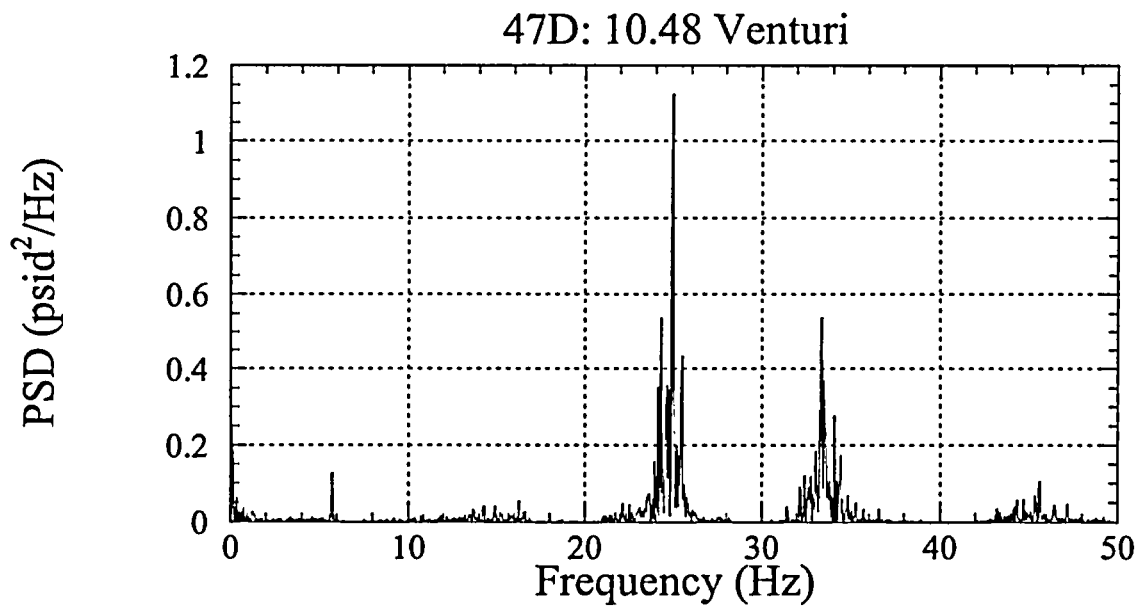
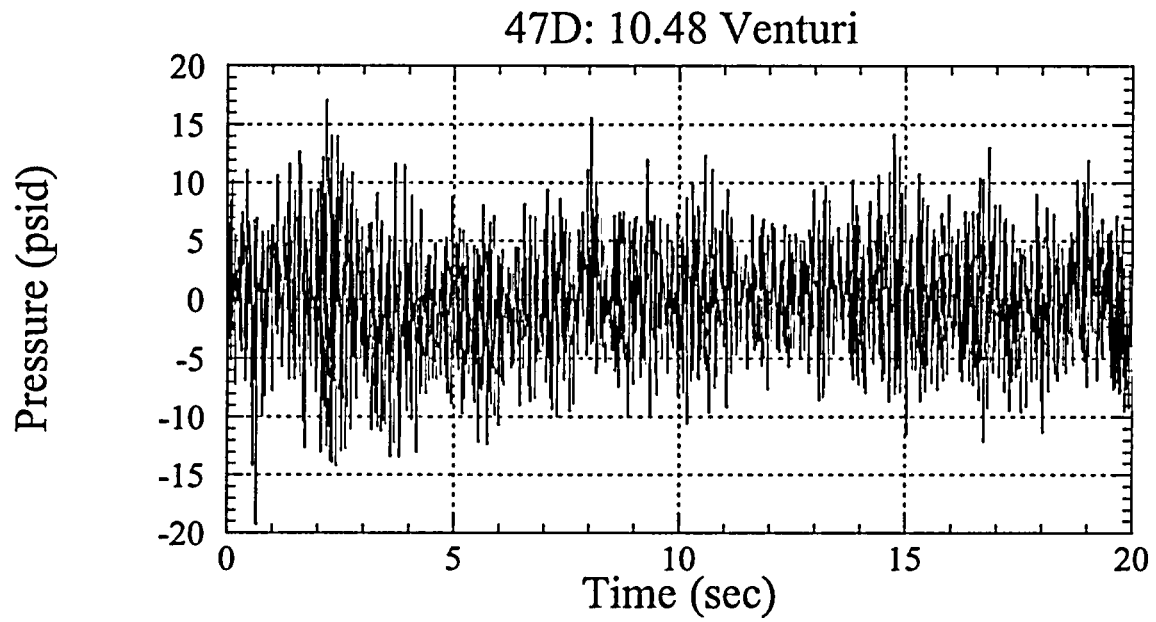


Figure 16-d

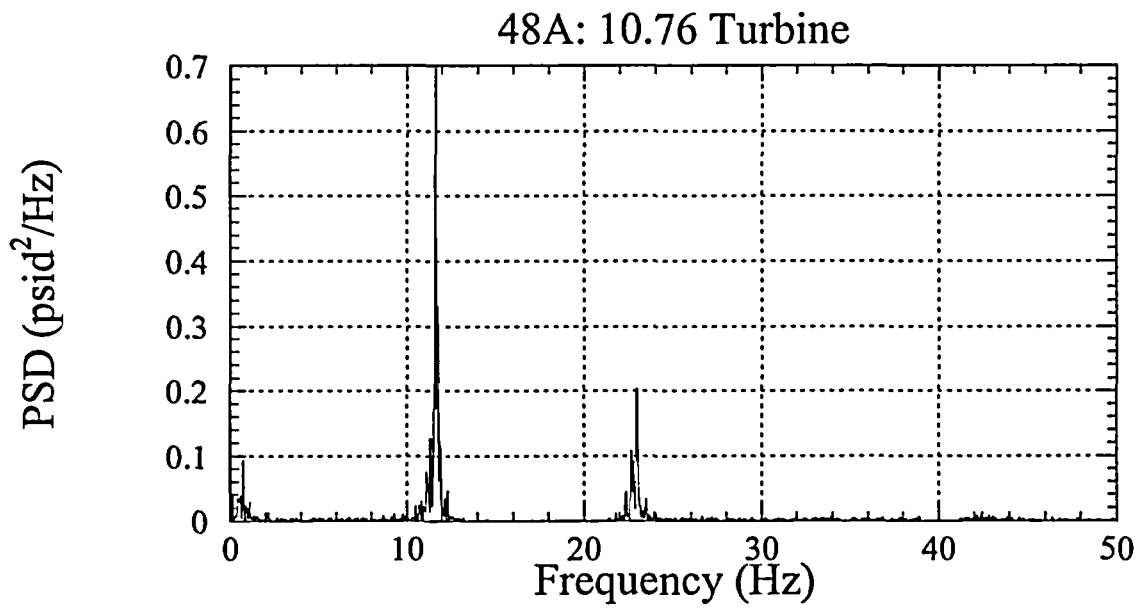
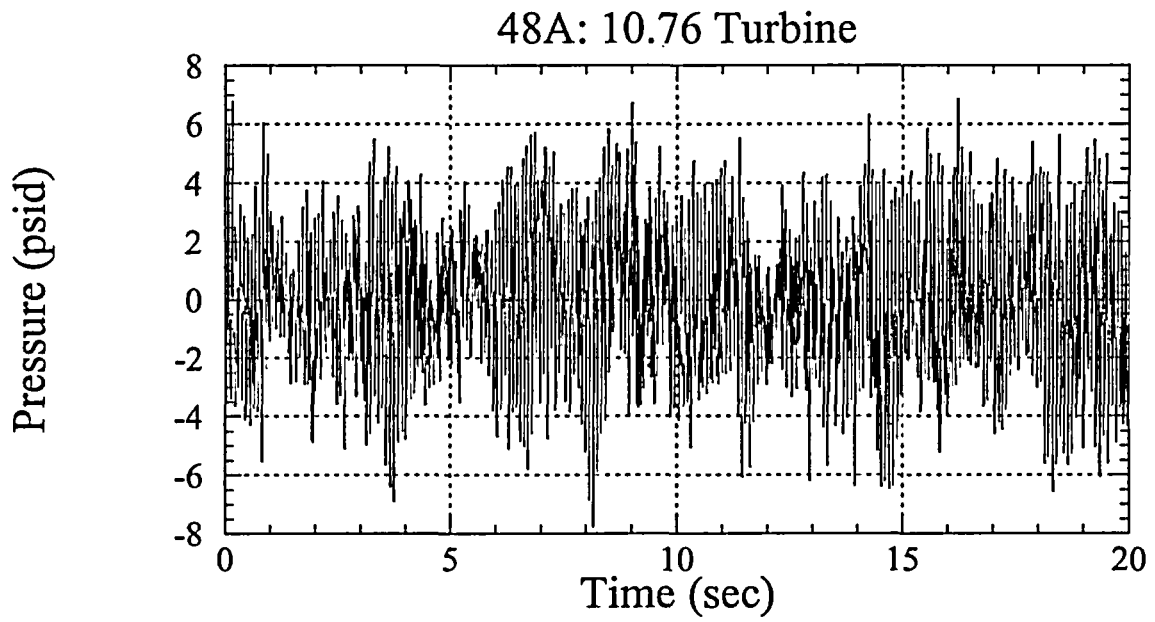


Figure 17-a

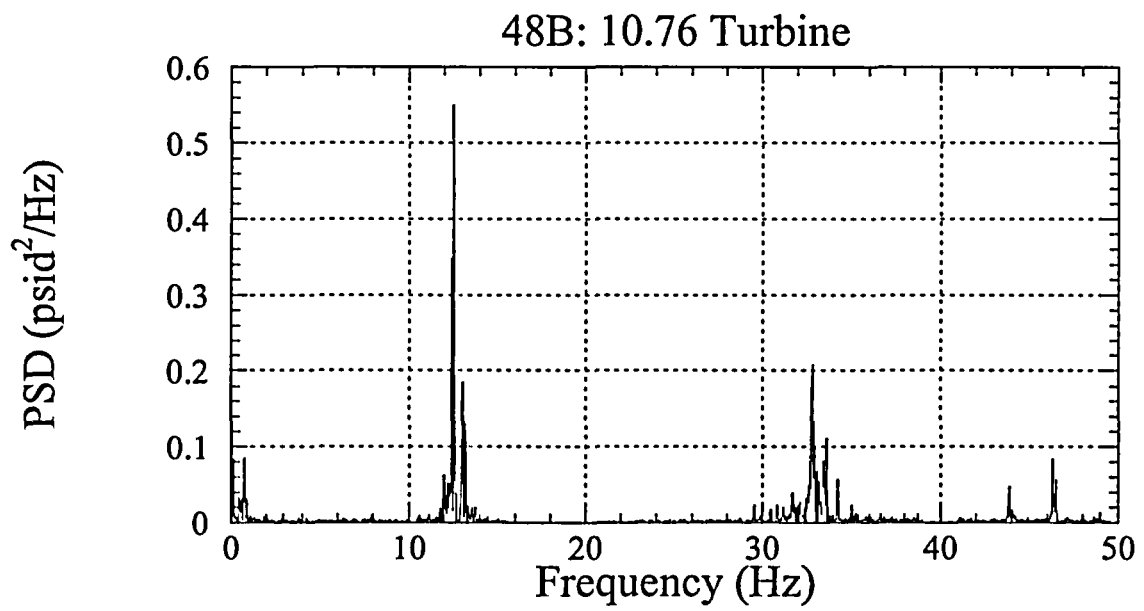
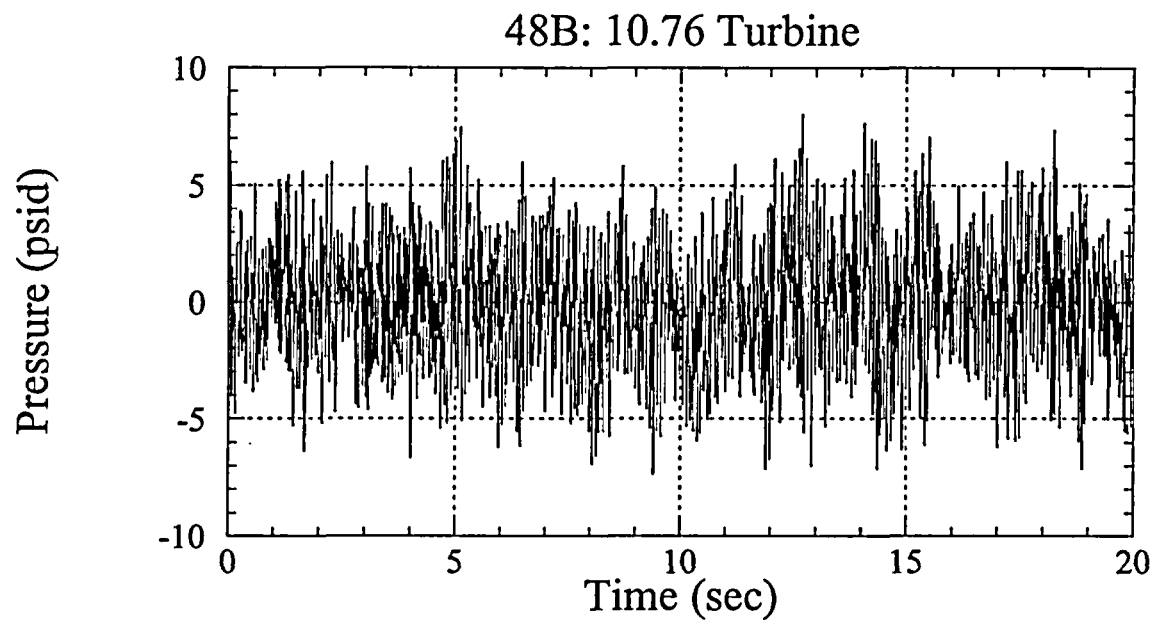


Figure 17-b

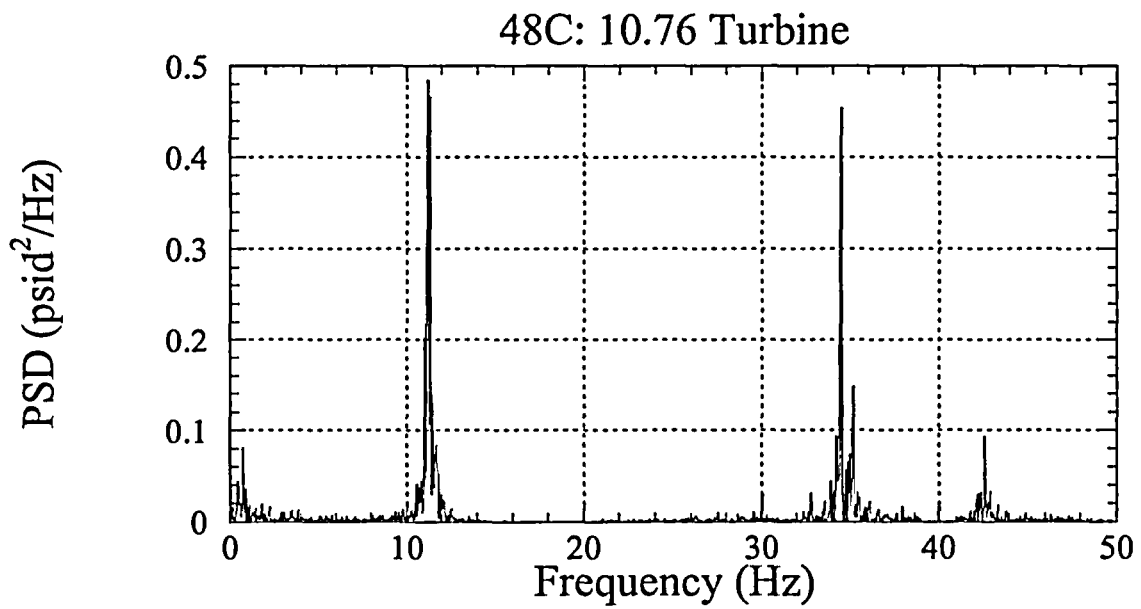
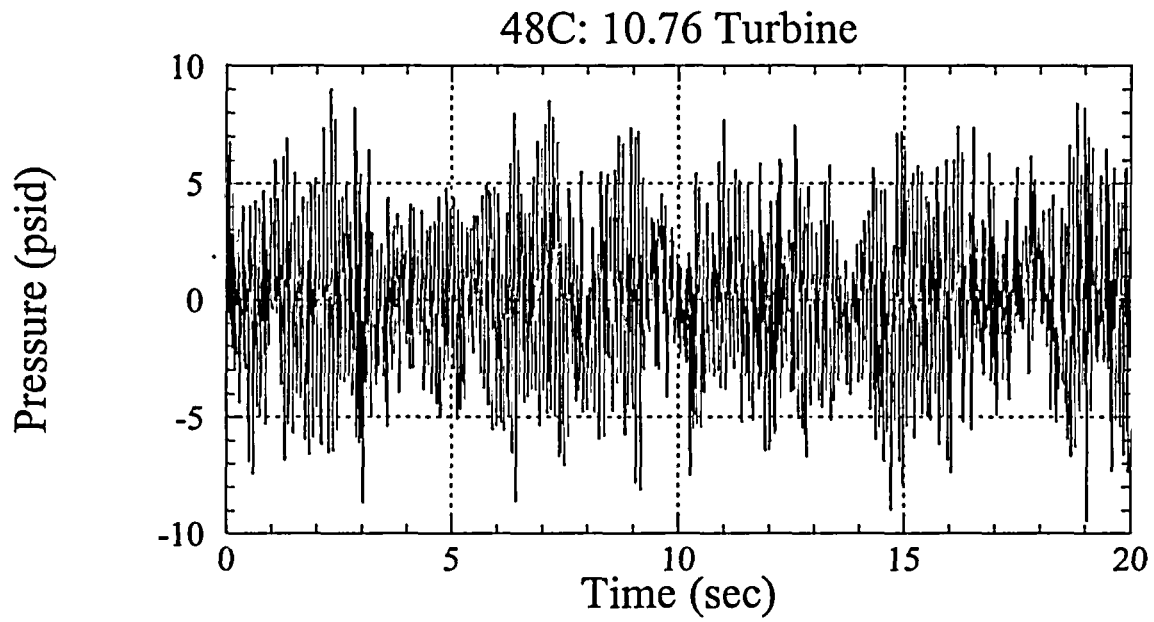


Figure 17-c

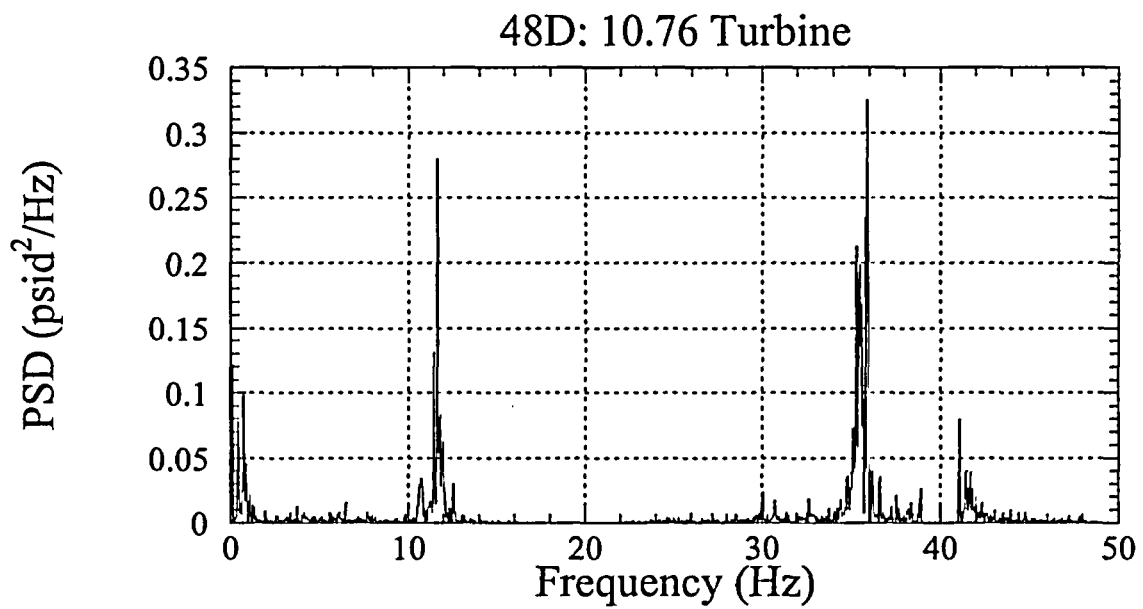
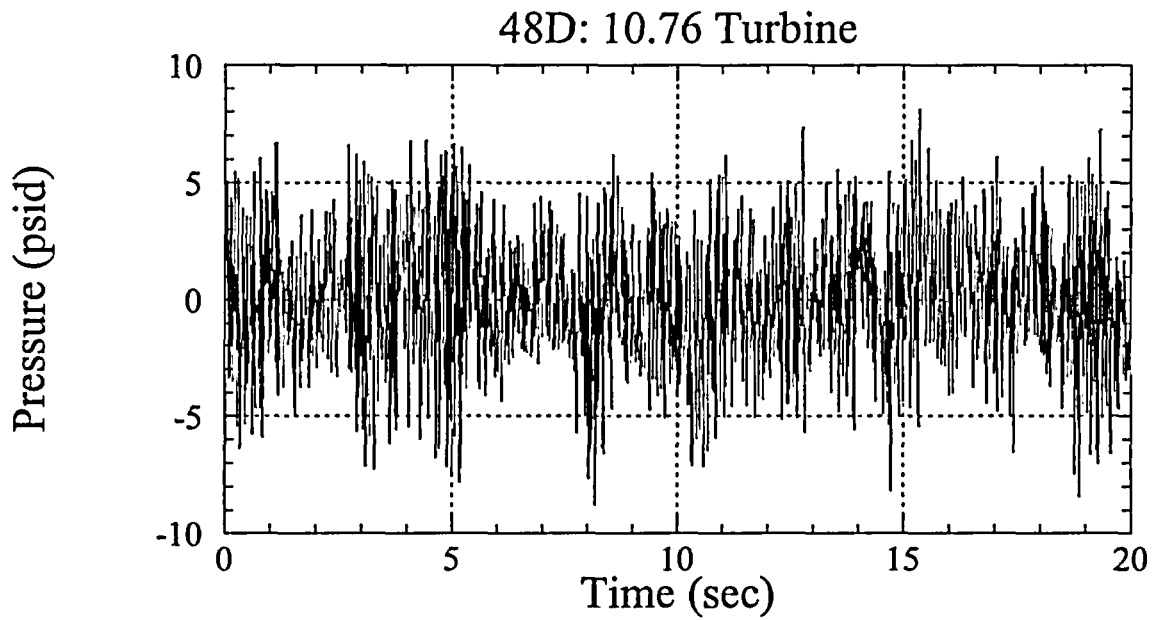


Figure 17-d

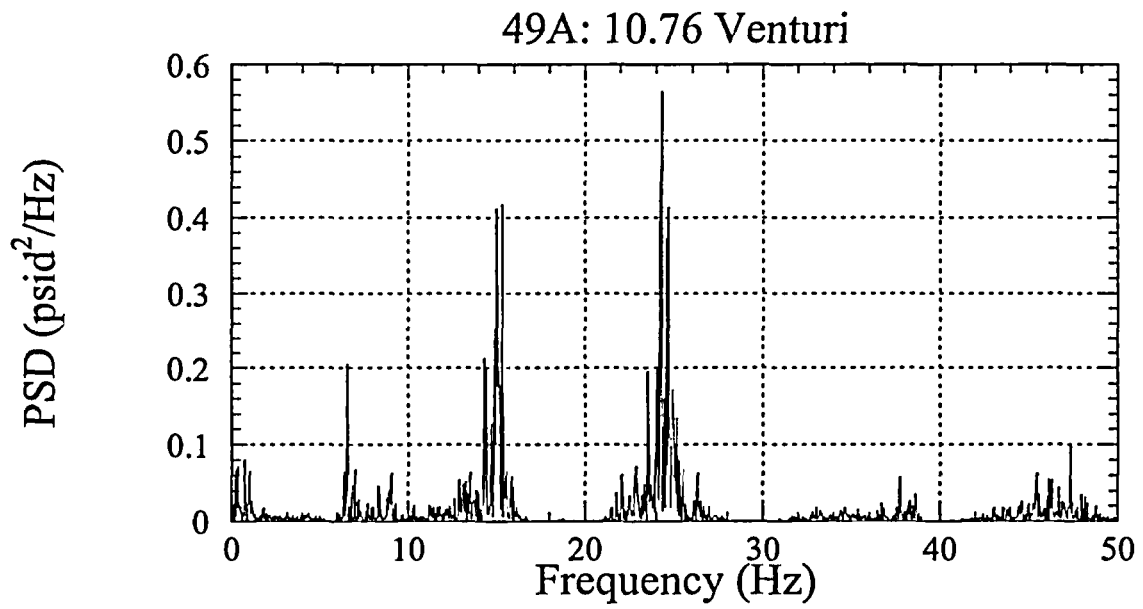
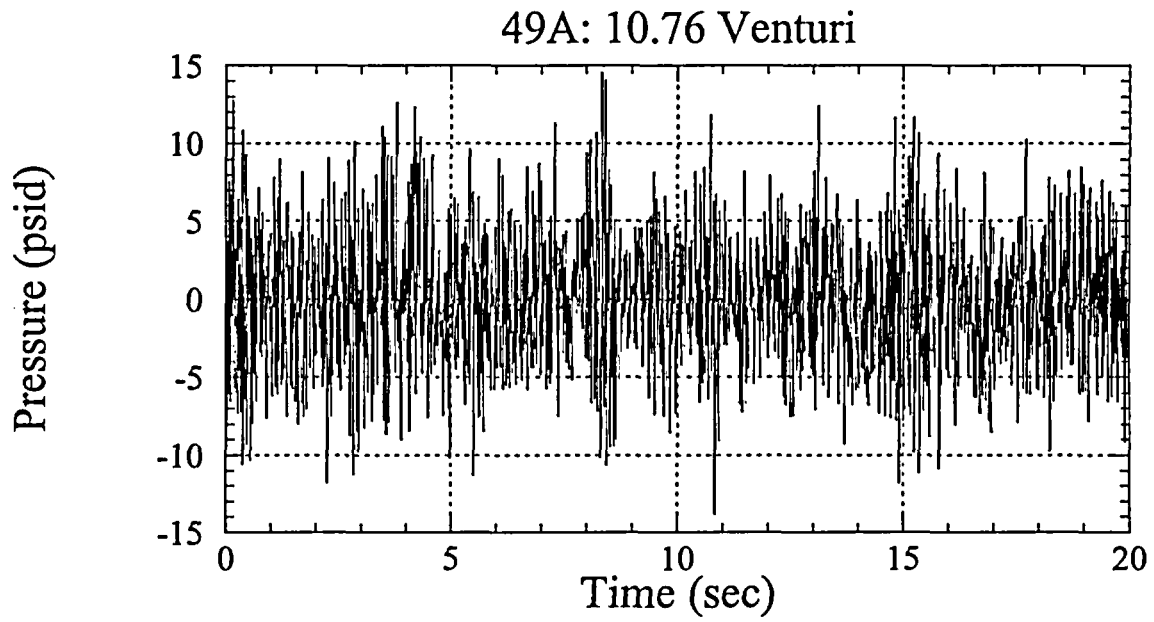
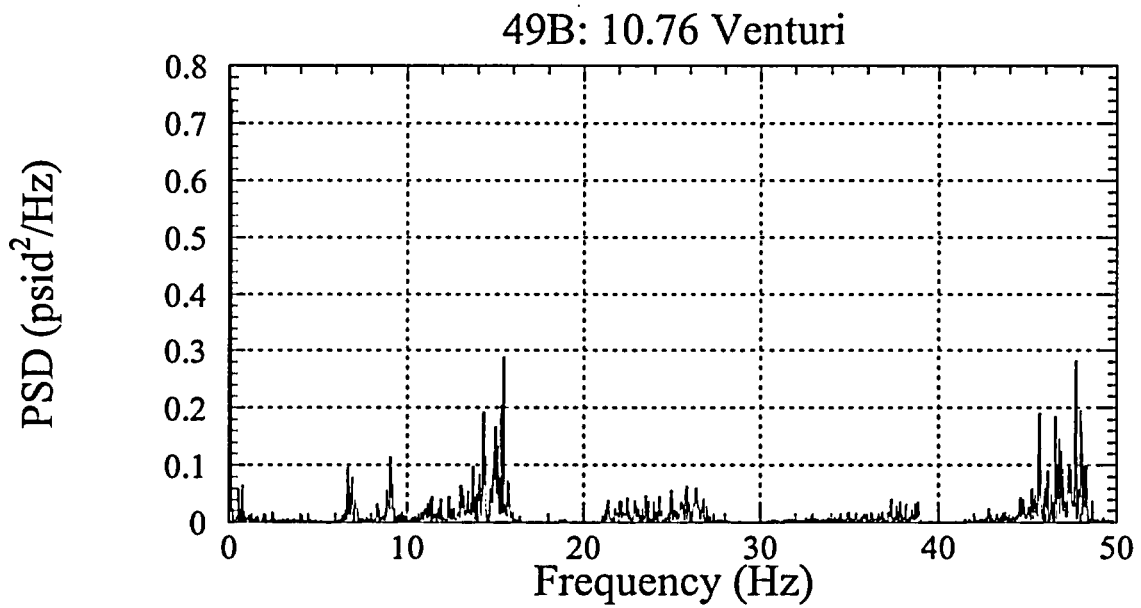
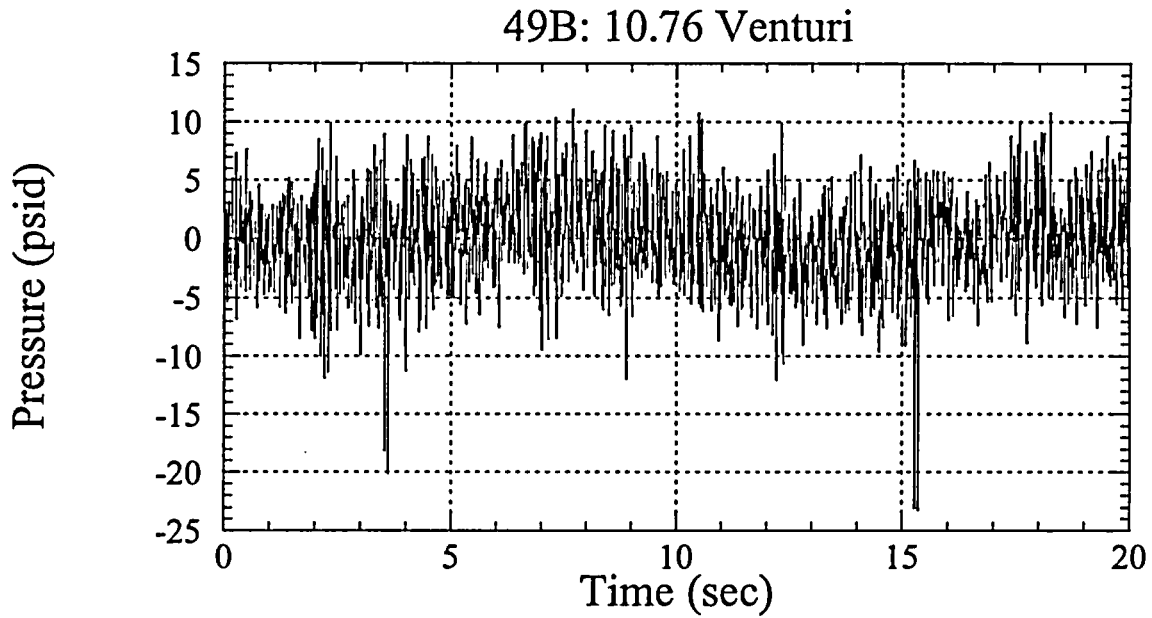


Figure 18-a



.Figure 18-b

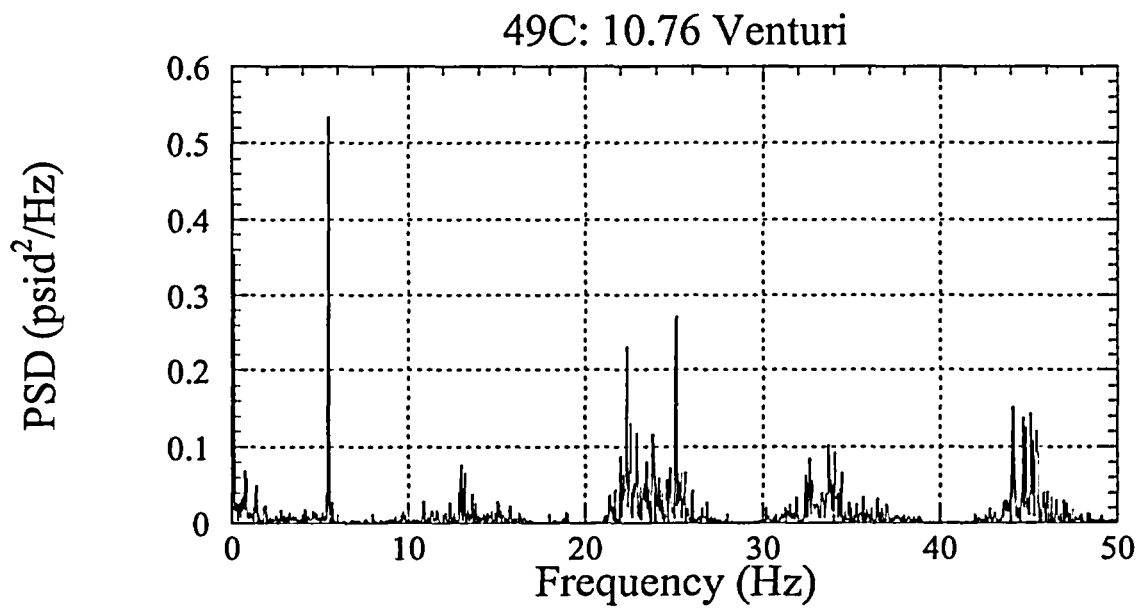
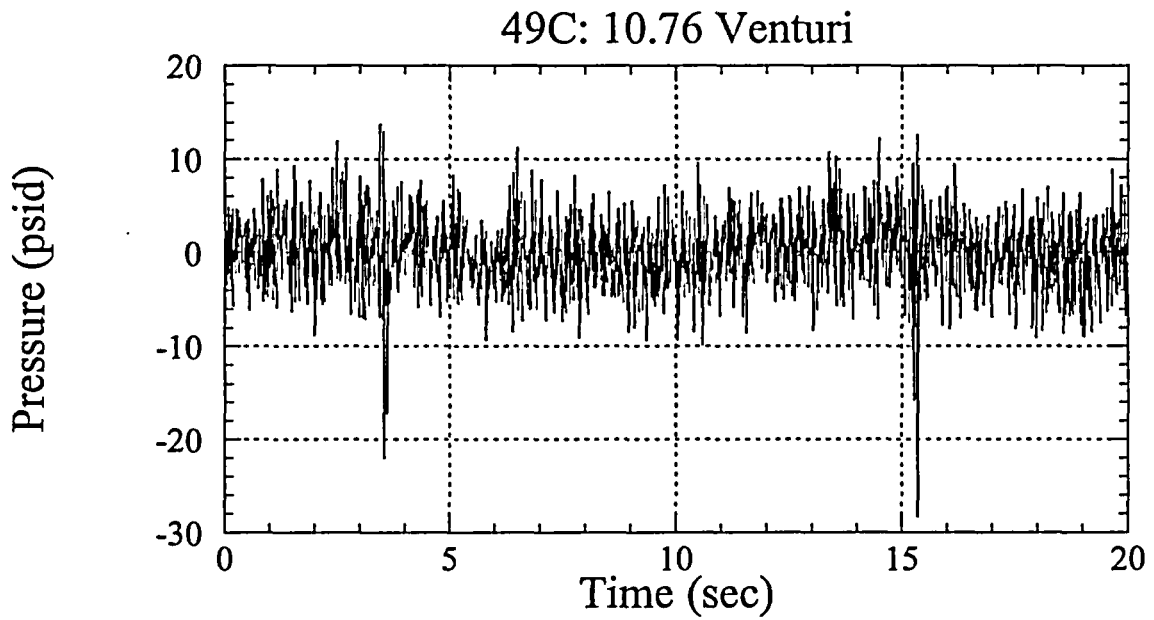


Figure 18-c

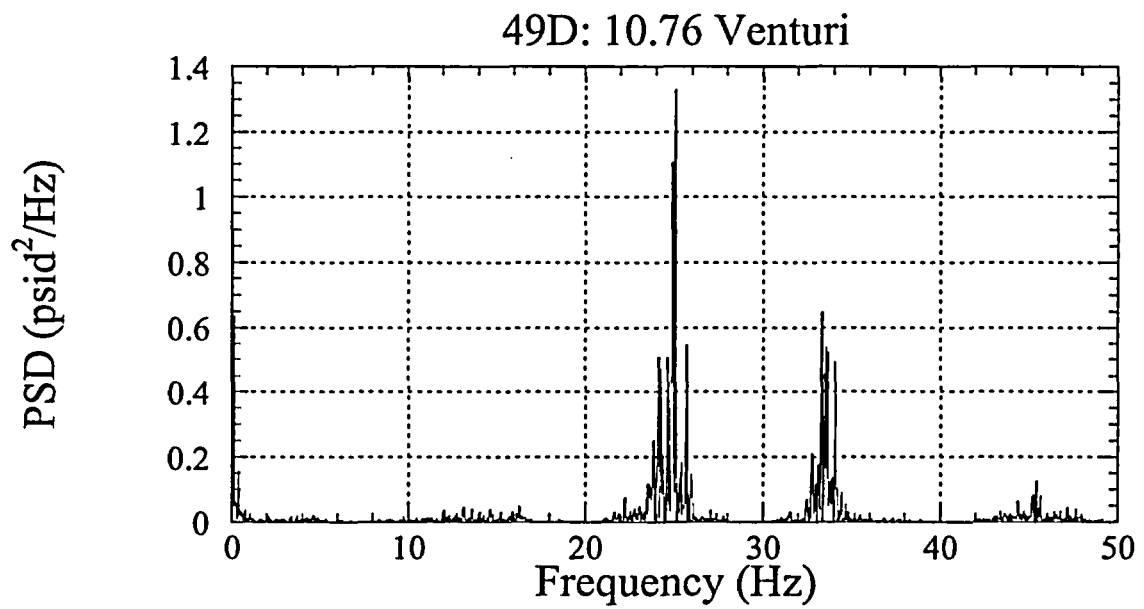
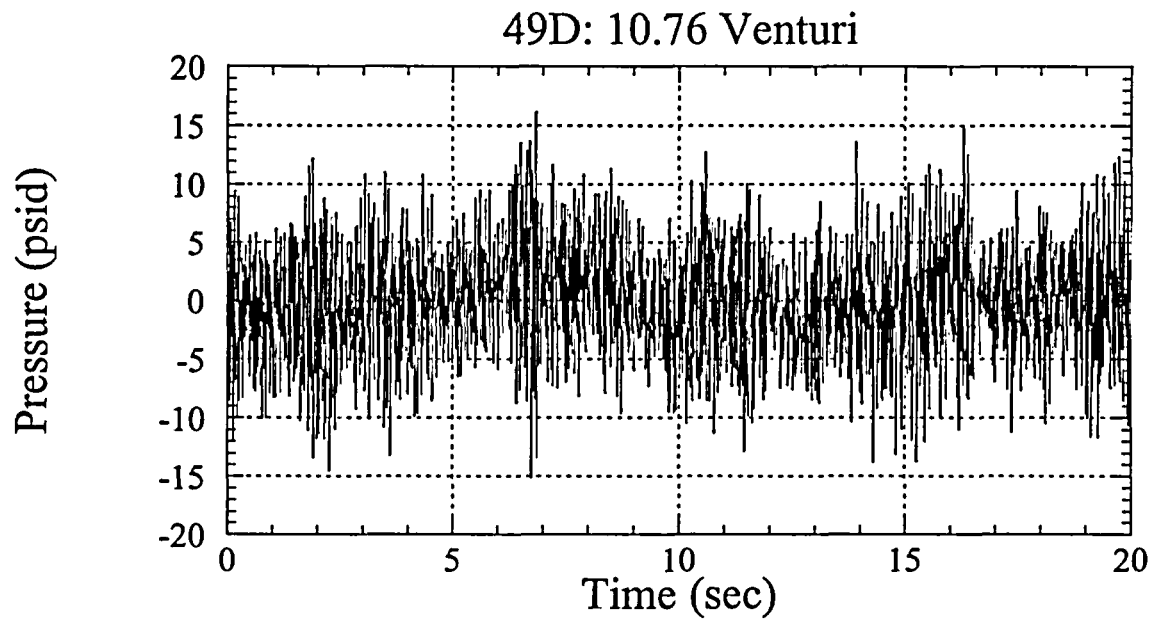


Figure 18-d

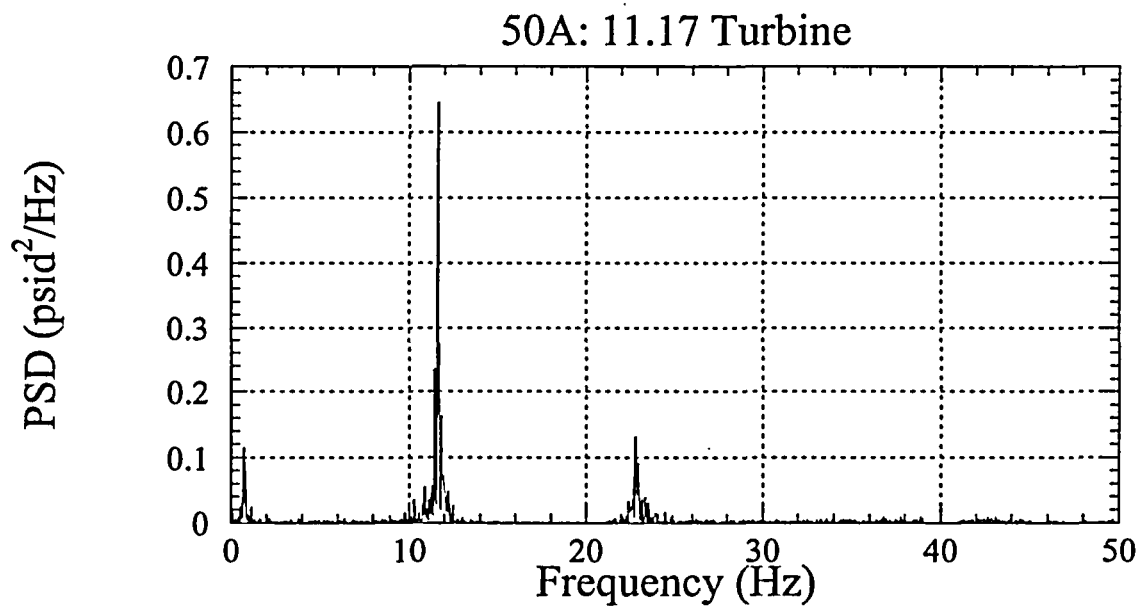
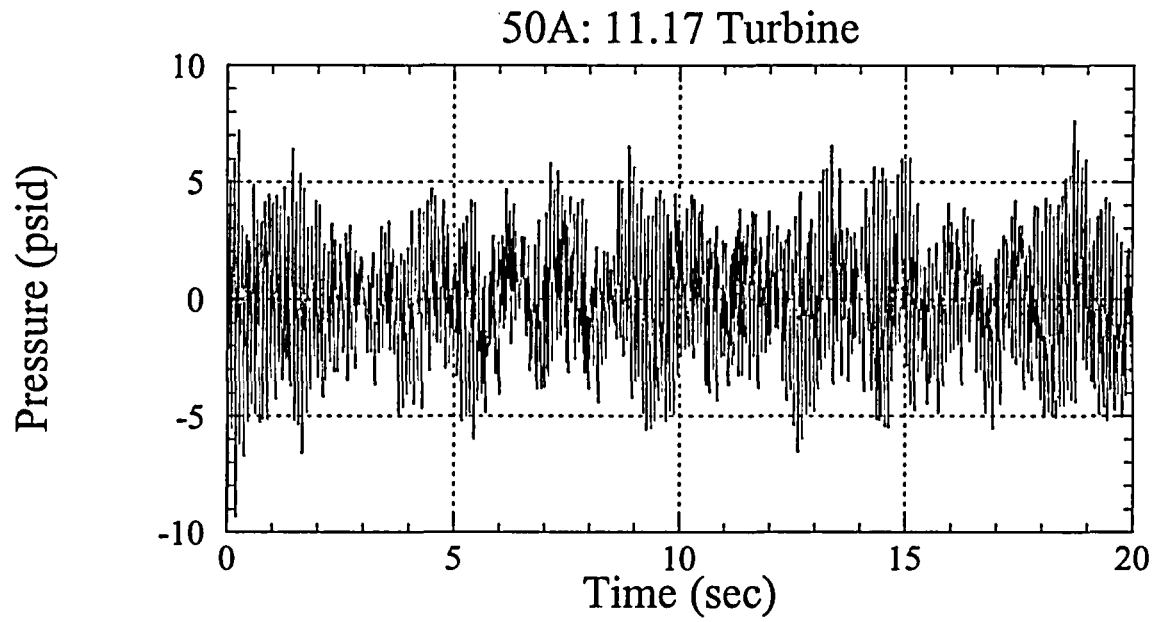


Figure 19-a

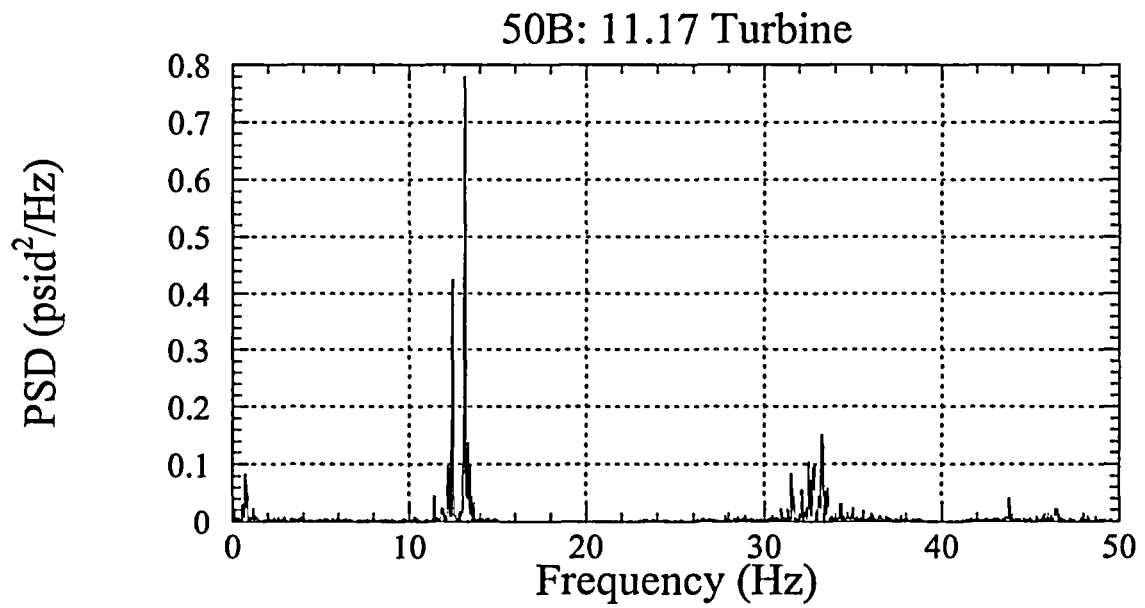
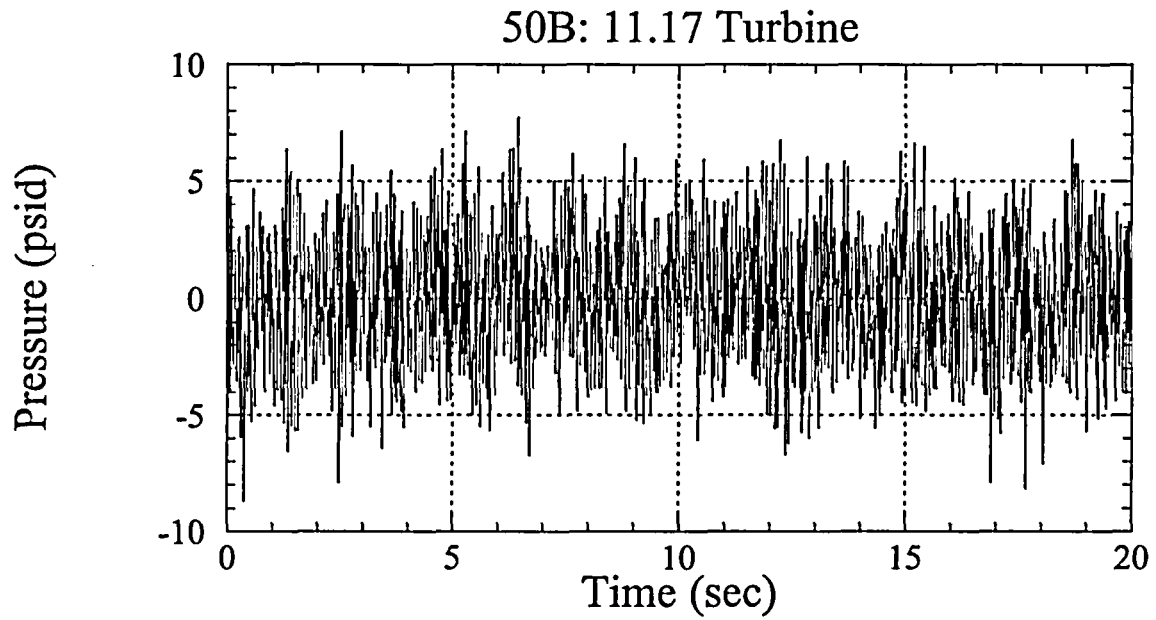


Figure 19-b

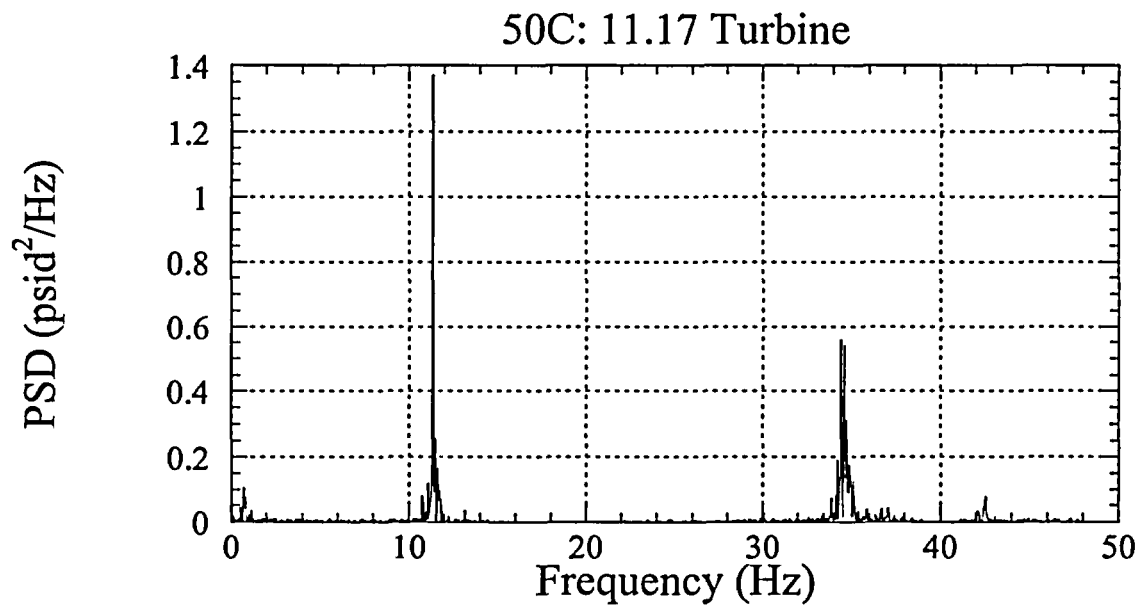
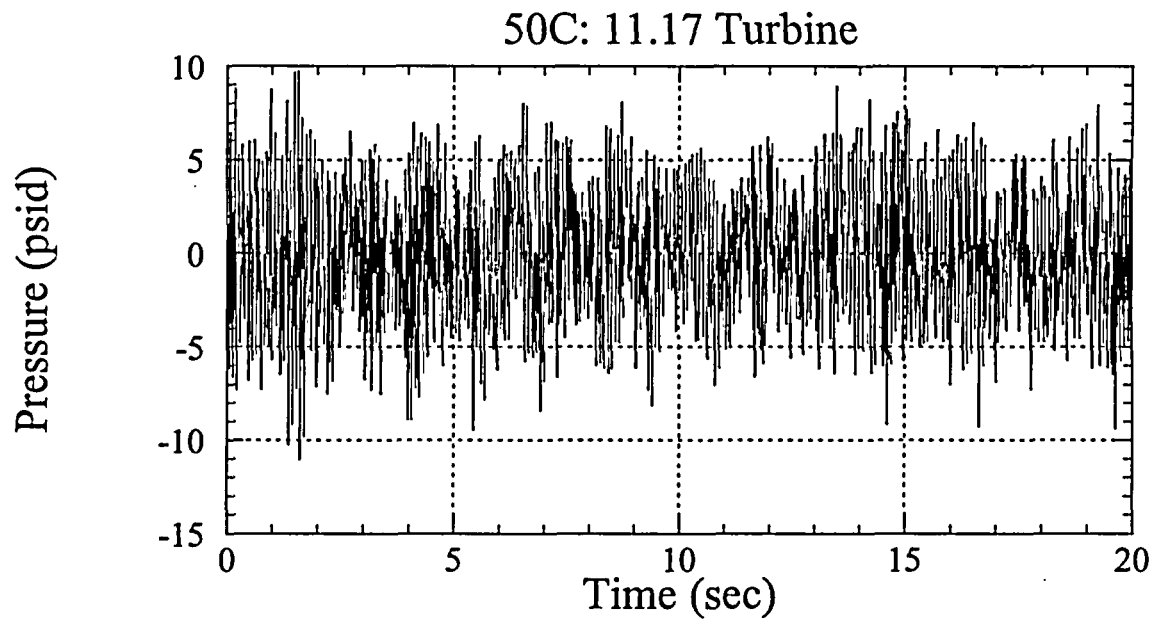


Figure 19-c

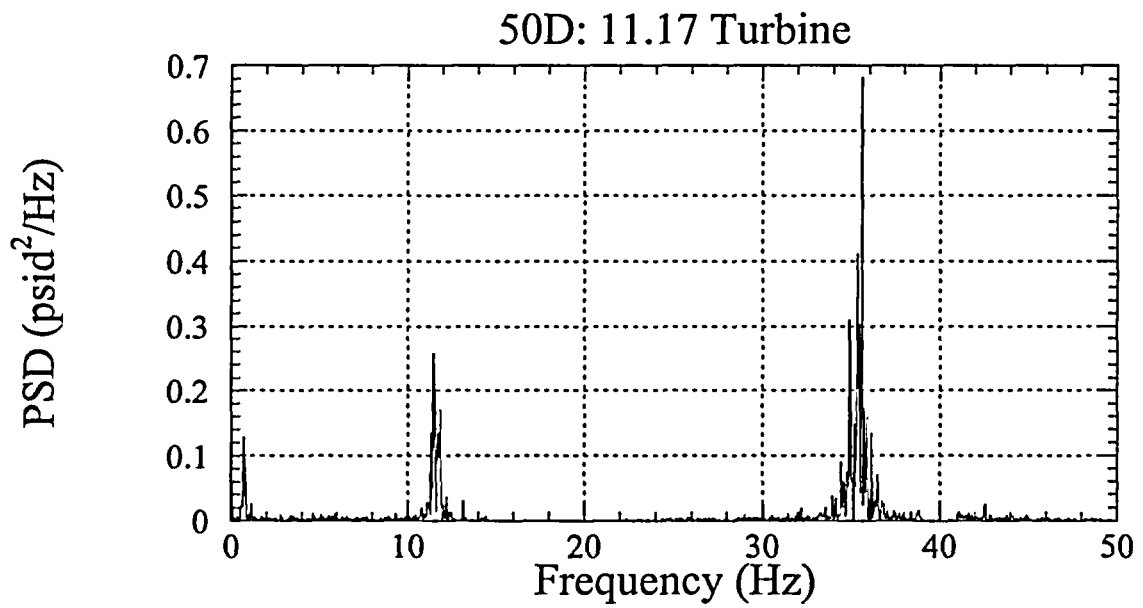
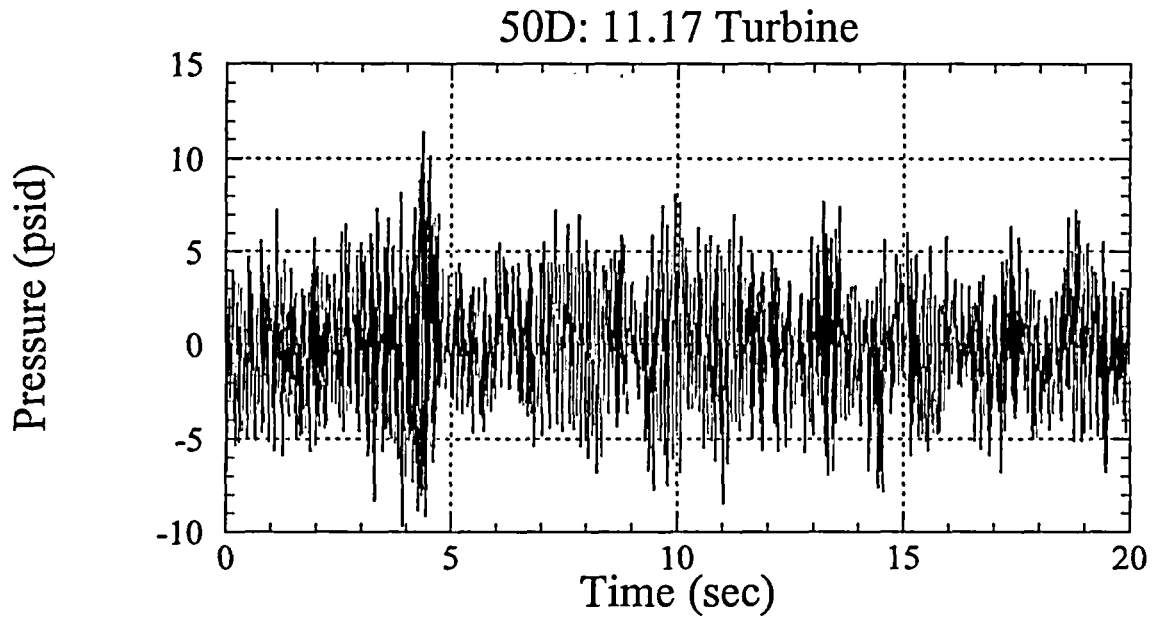


Figure 19-d

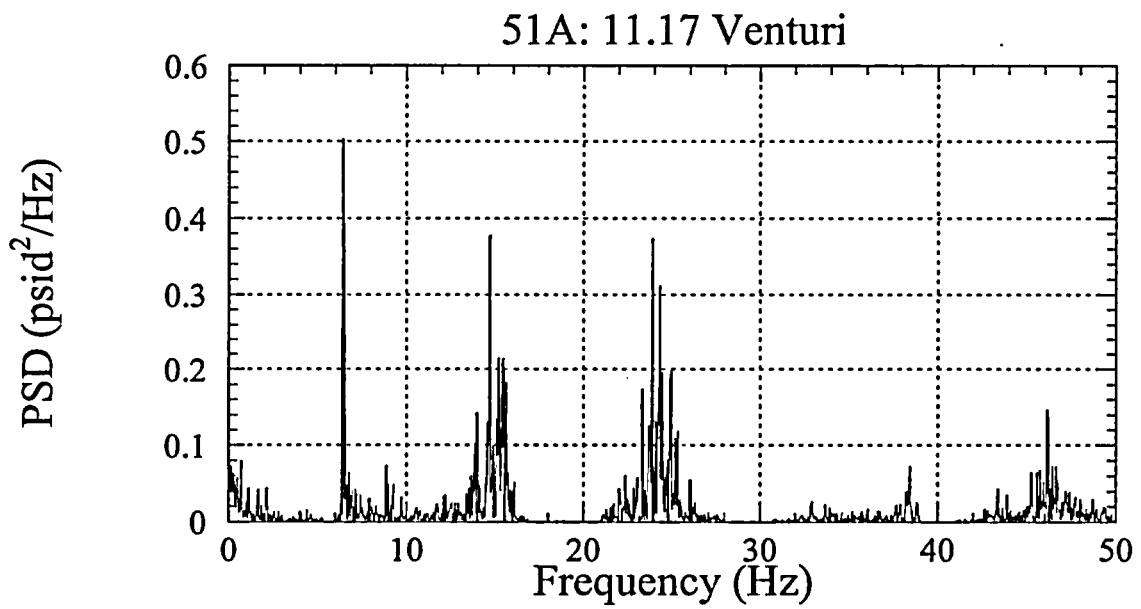
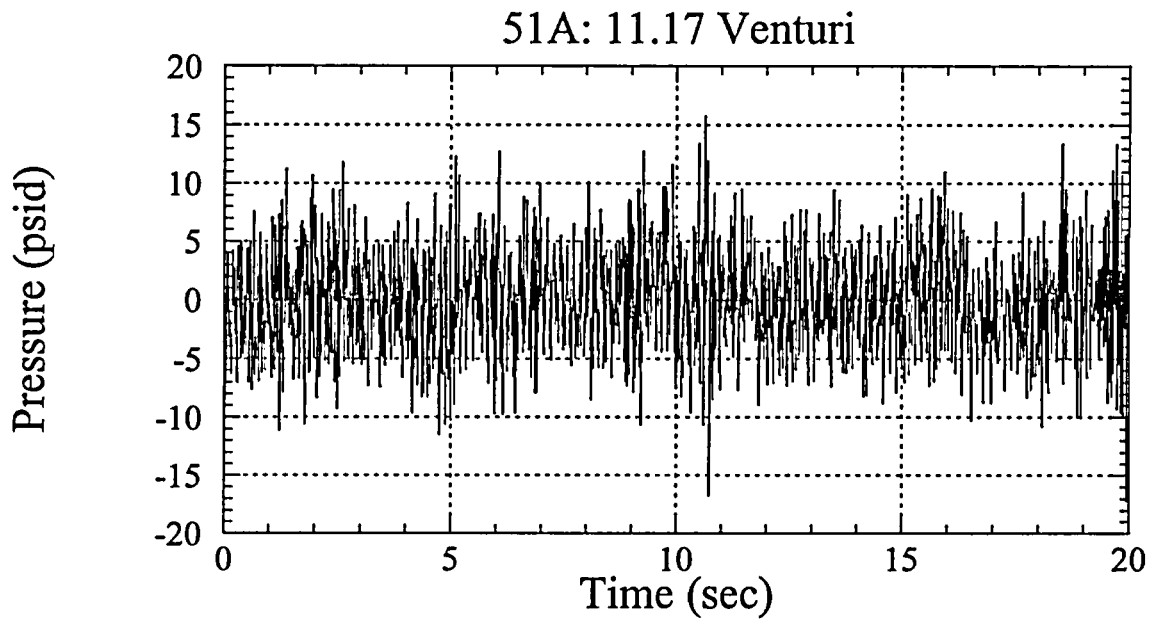


Figure 20-a

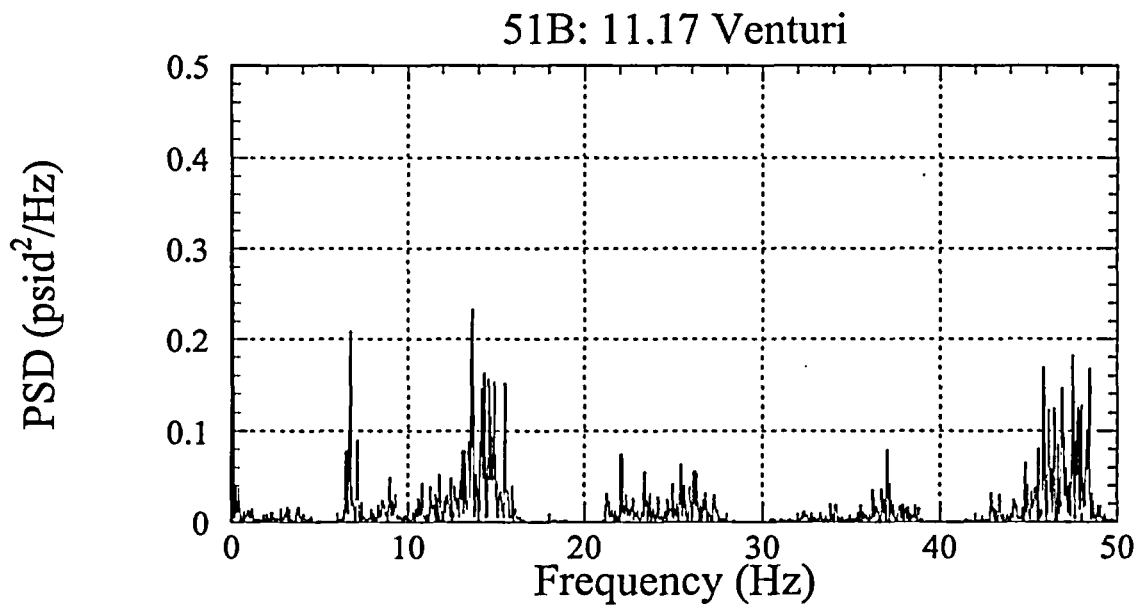
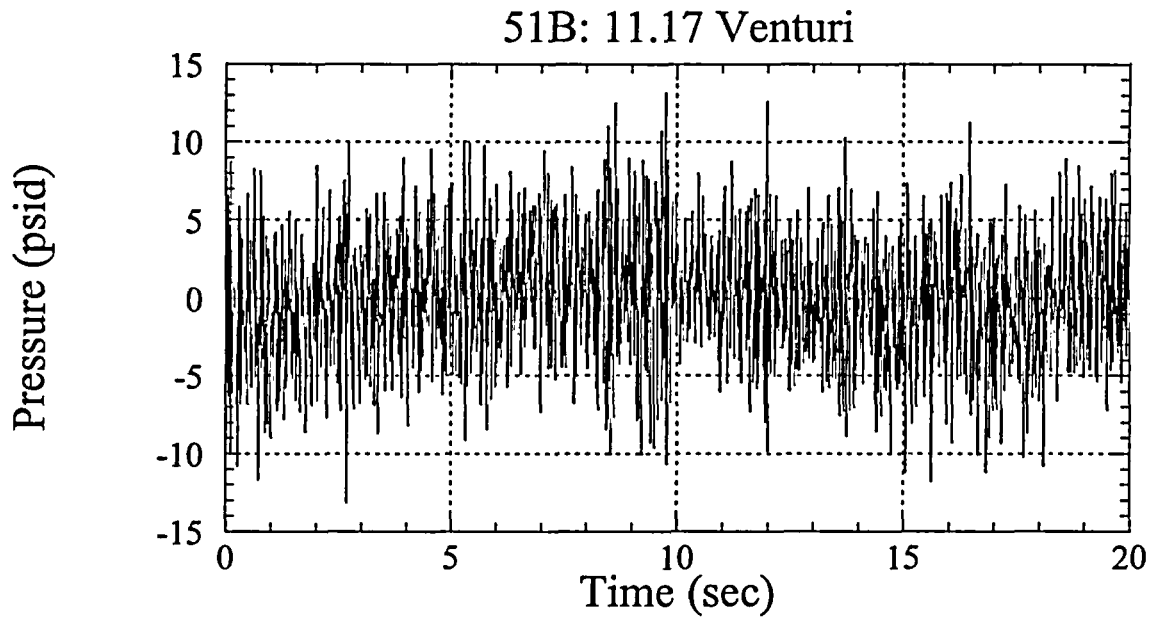


Figure 20-b

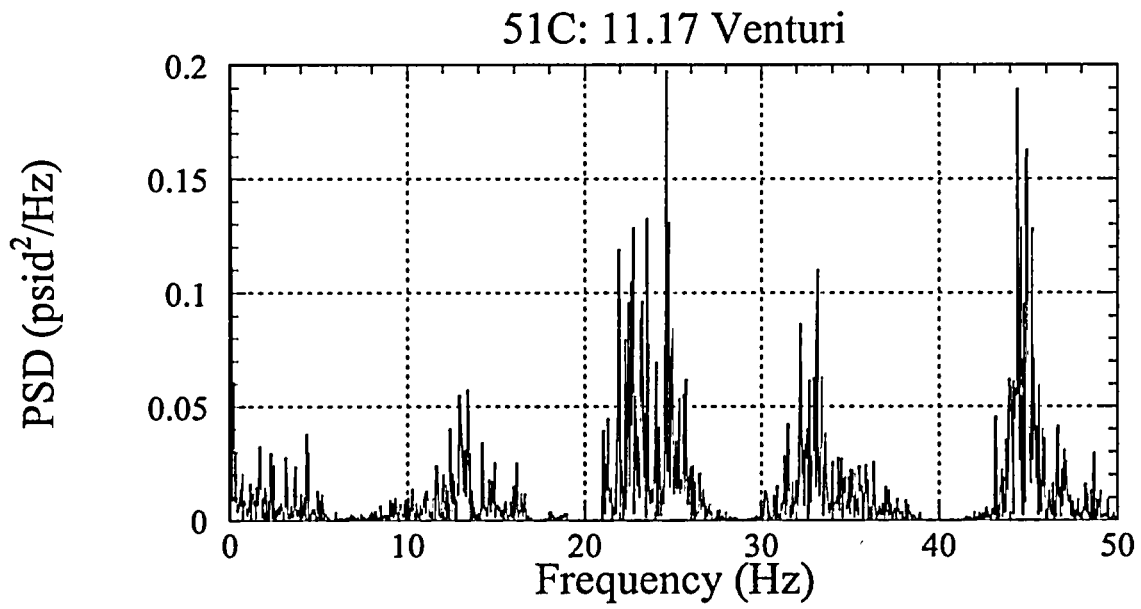
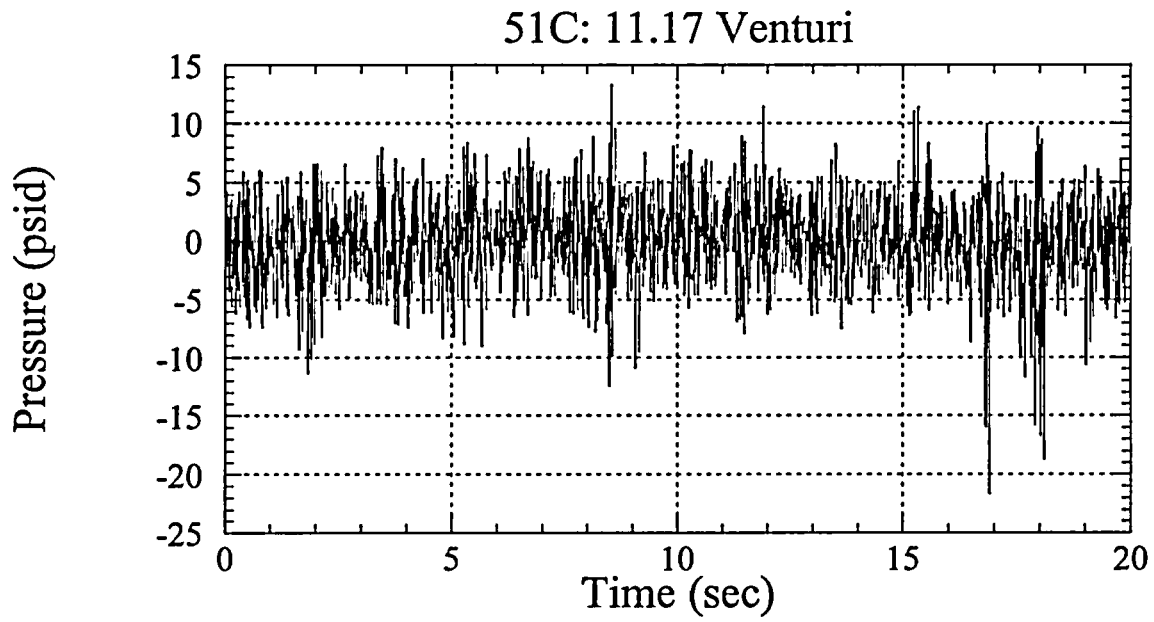


Figure 20-c

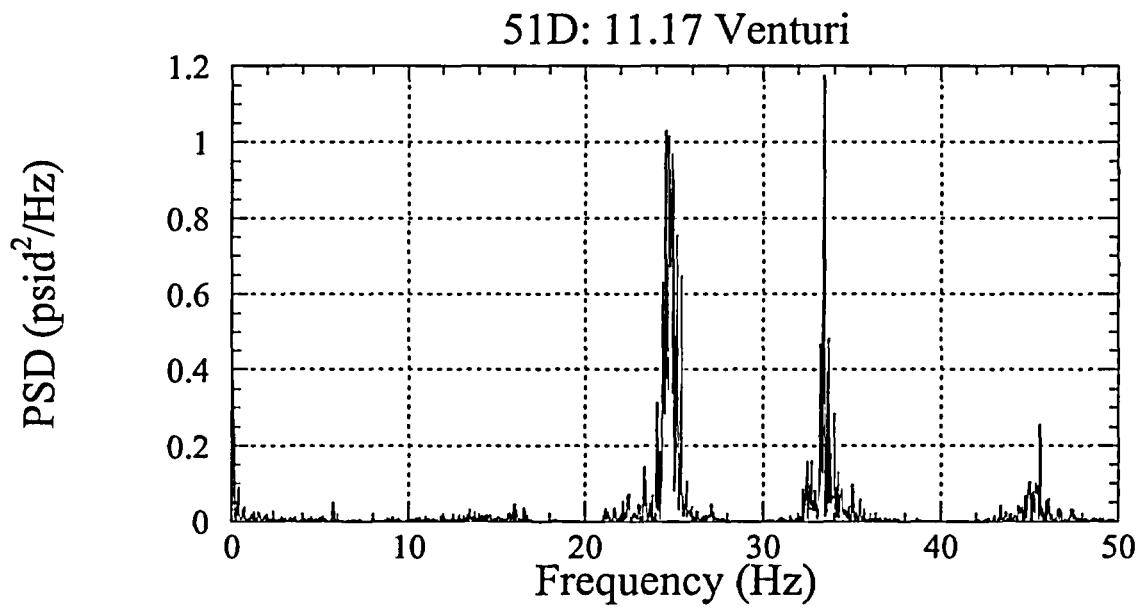
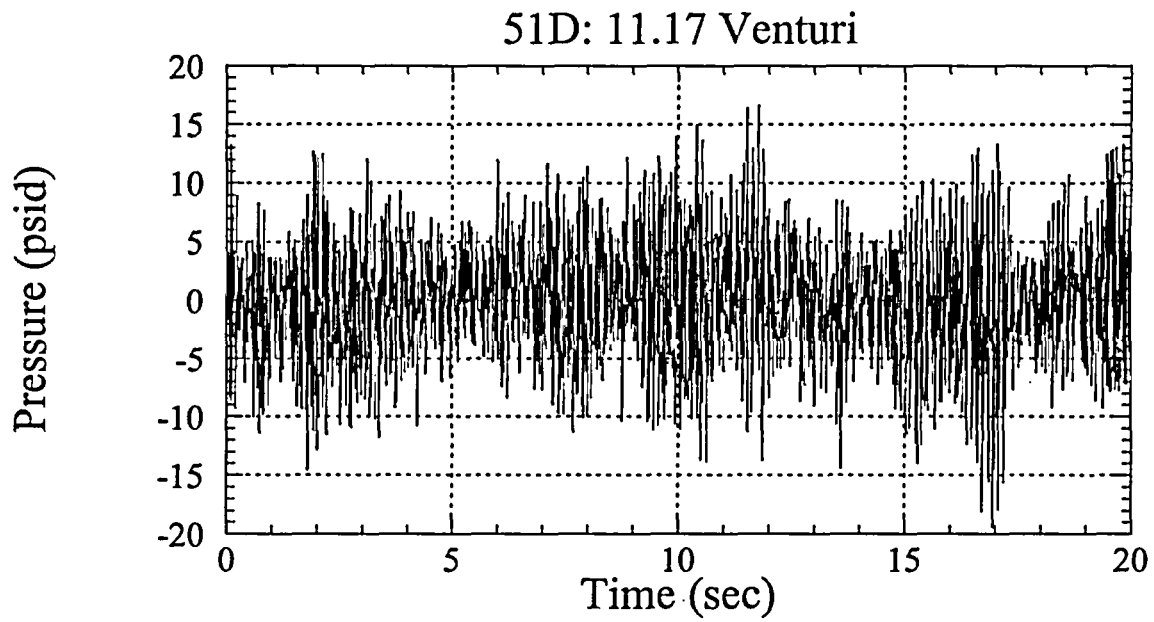


Figure 20-d

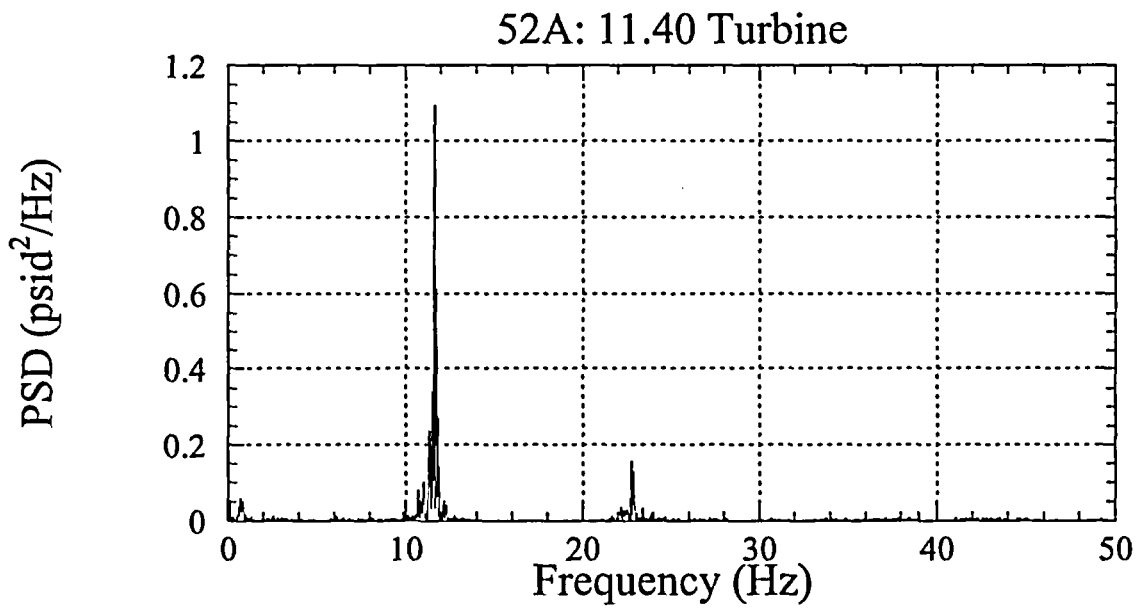
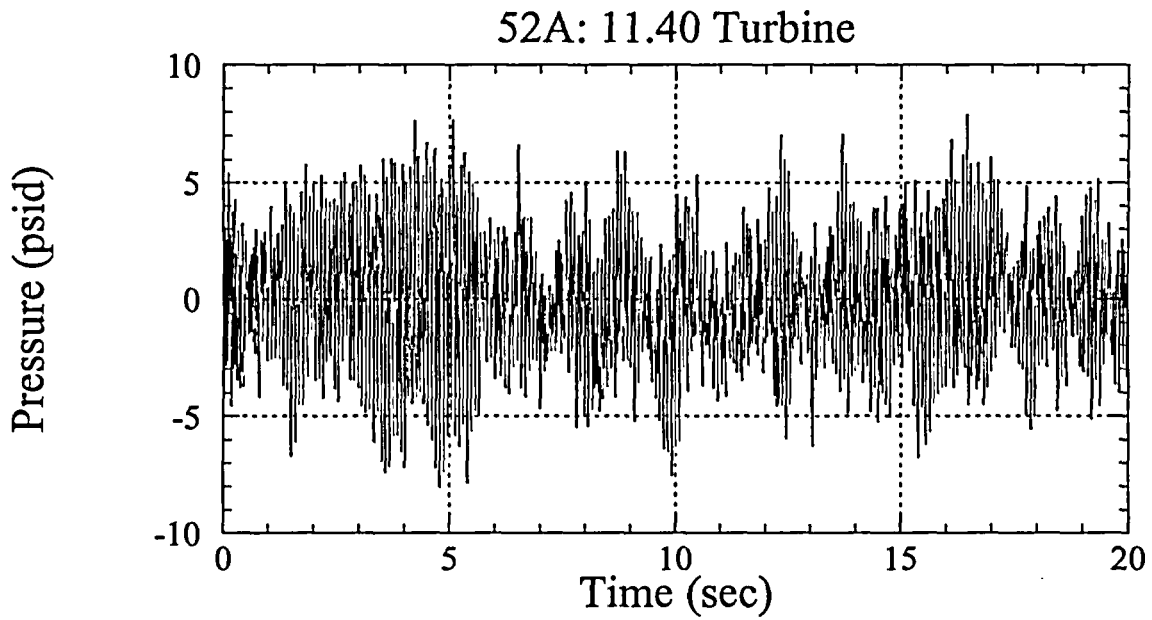


Figure 21-a

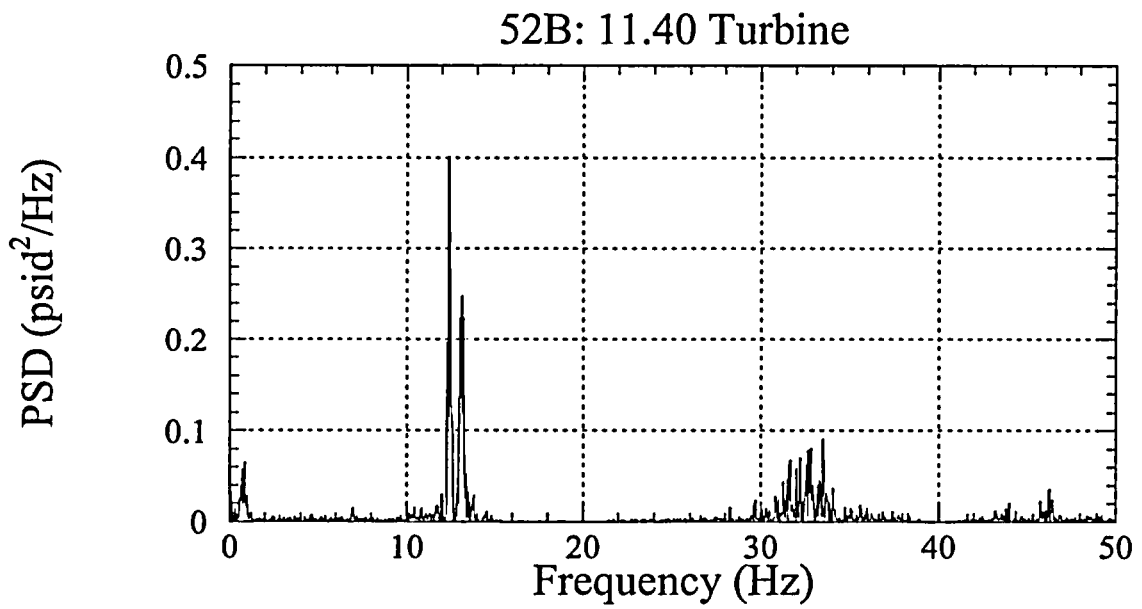
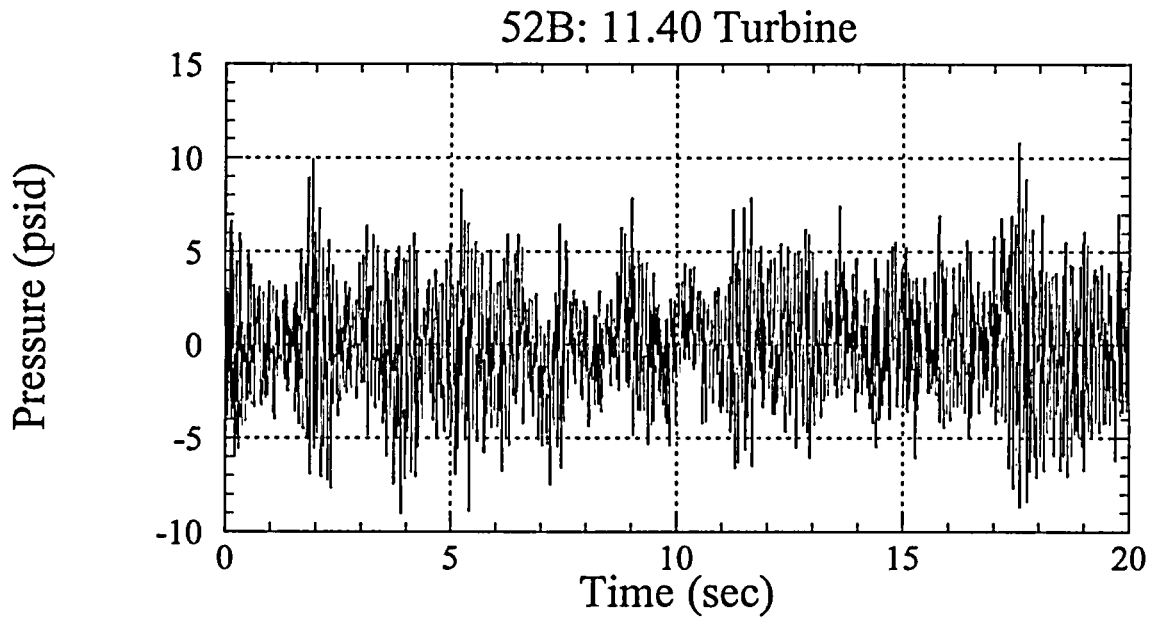


Figure 21-b

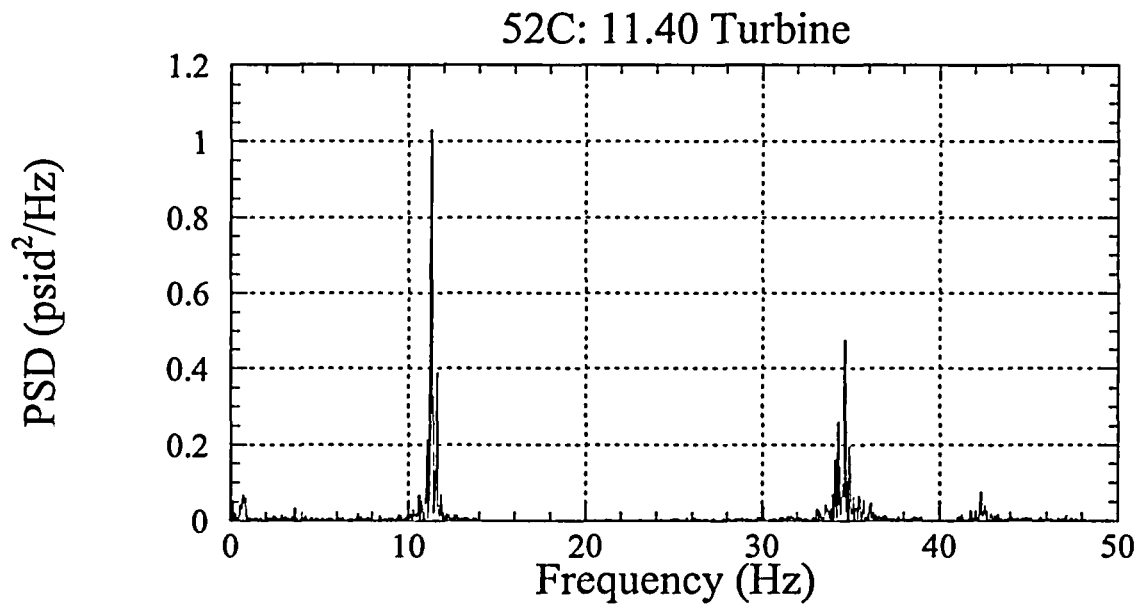
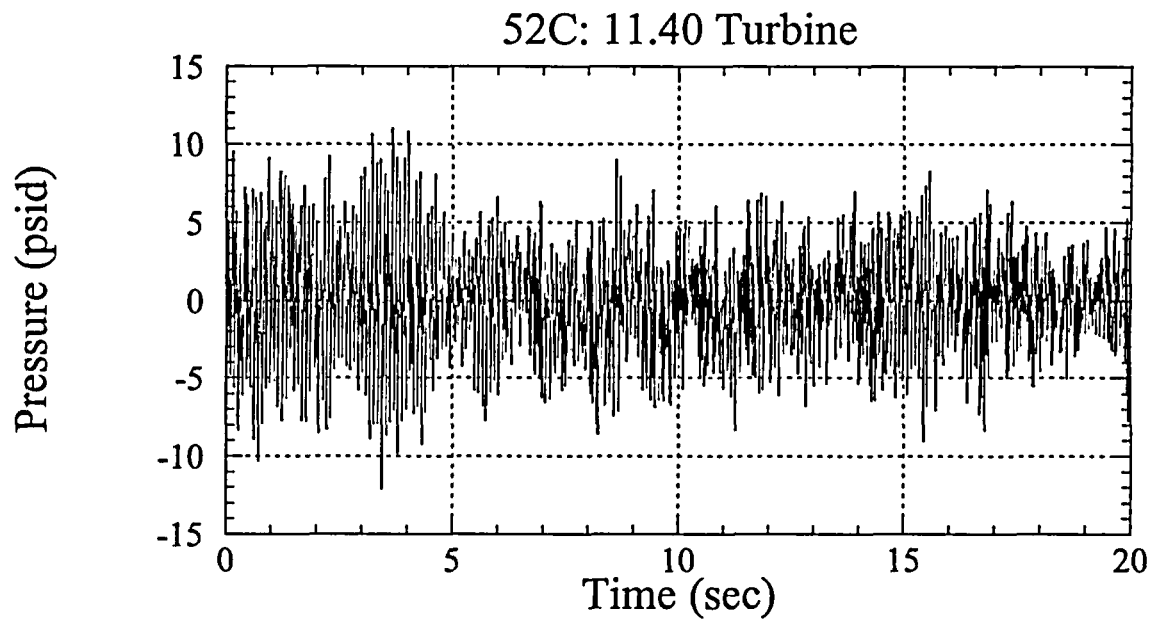


Figure 21-c

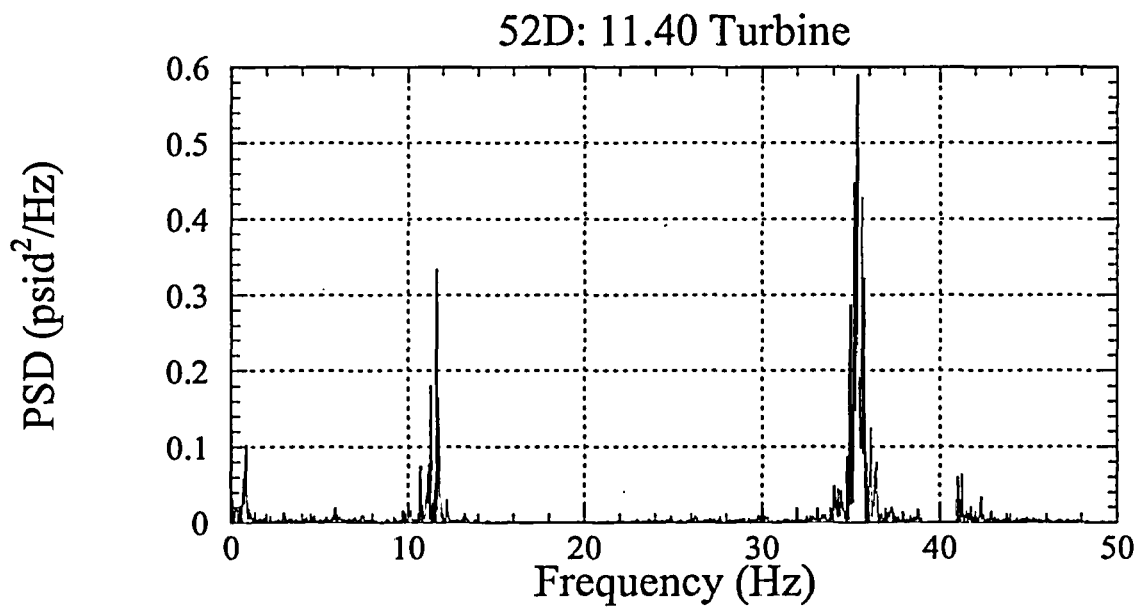
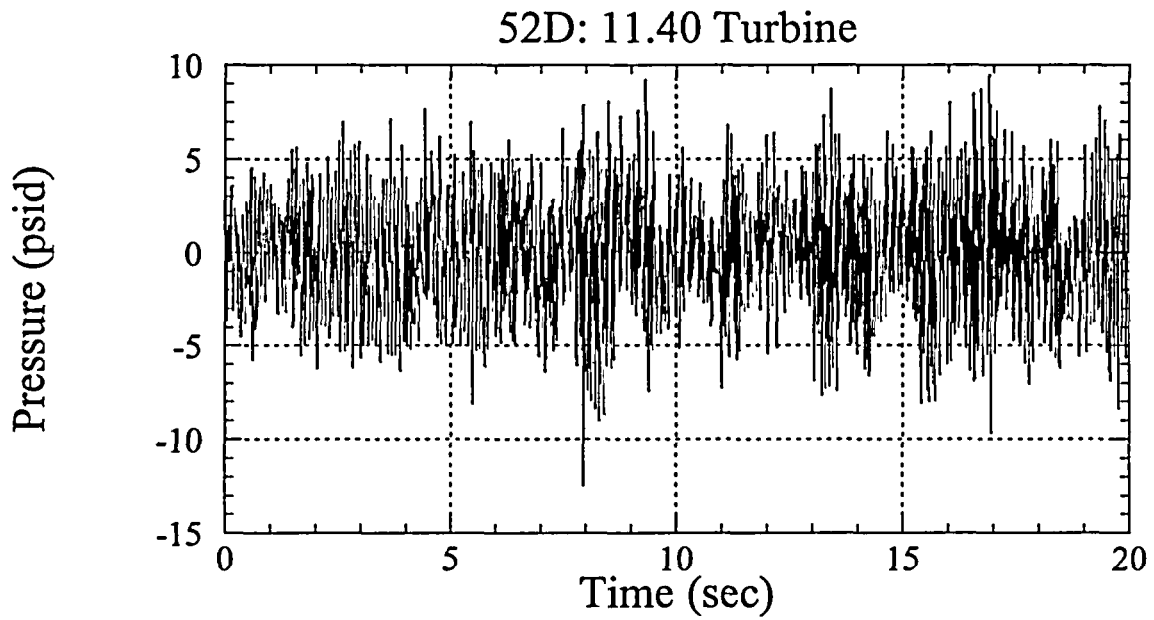


Figure 21-d

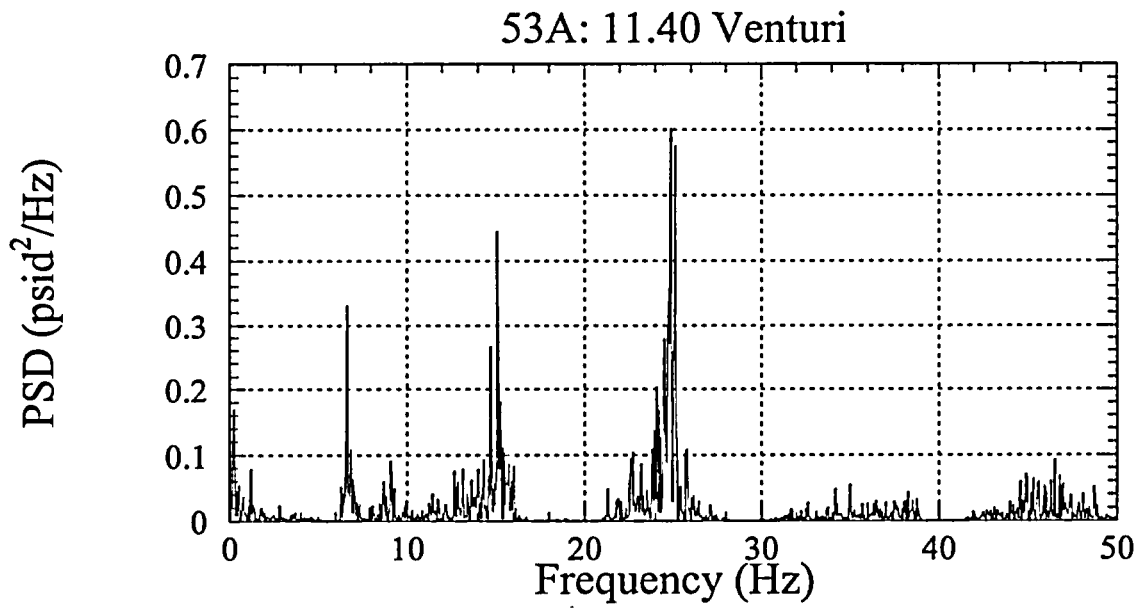
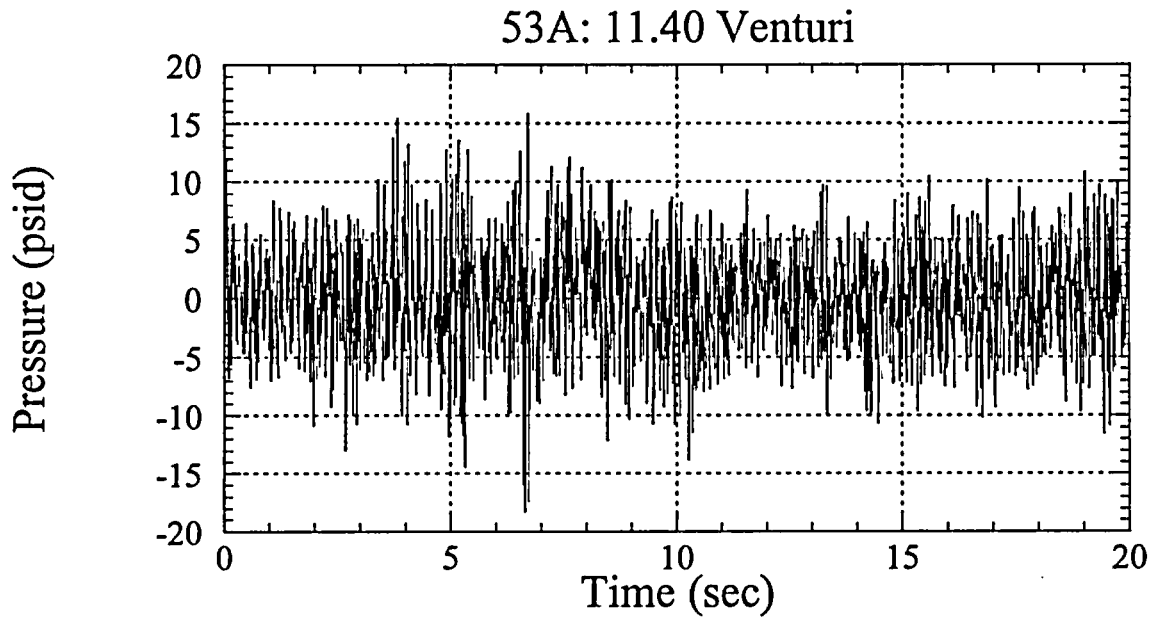


Figure 22-a

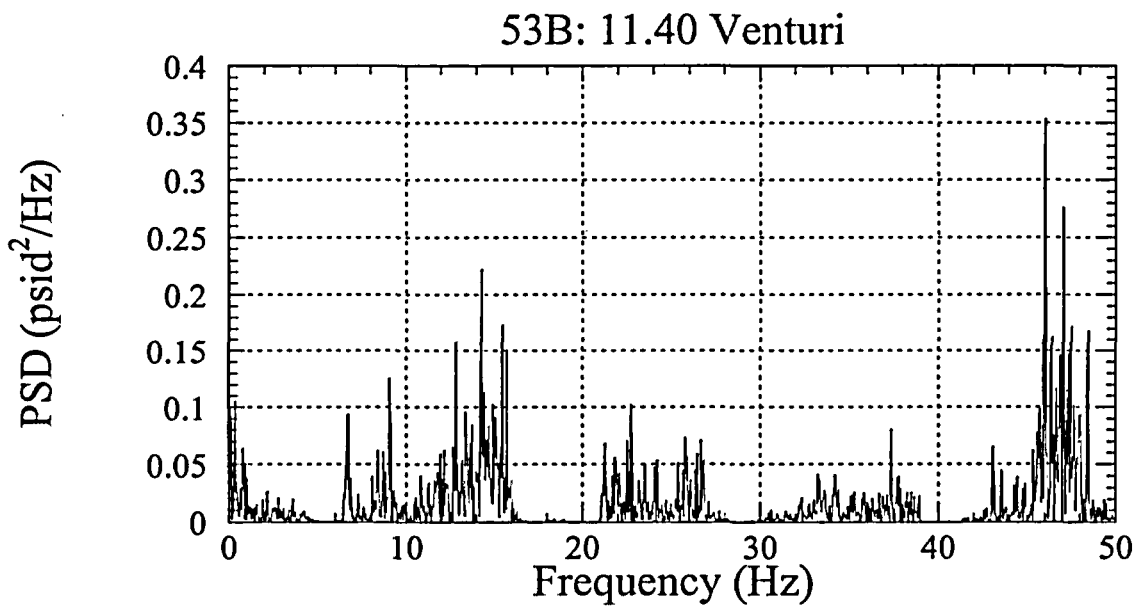
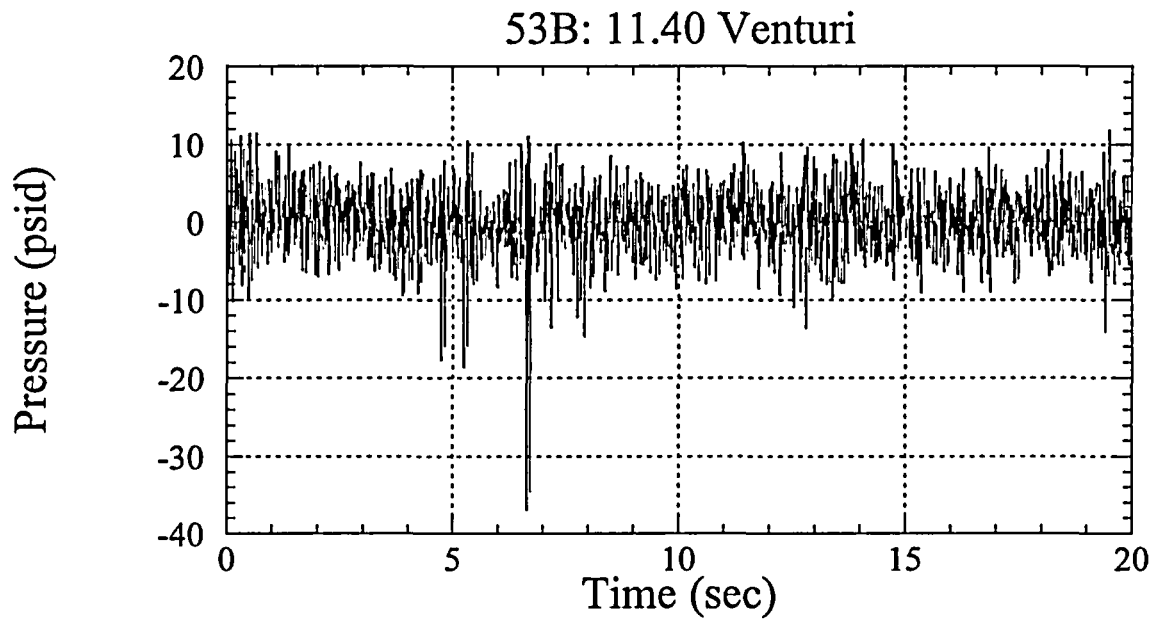


Figure 22-b

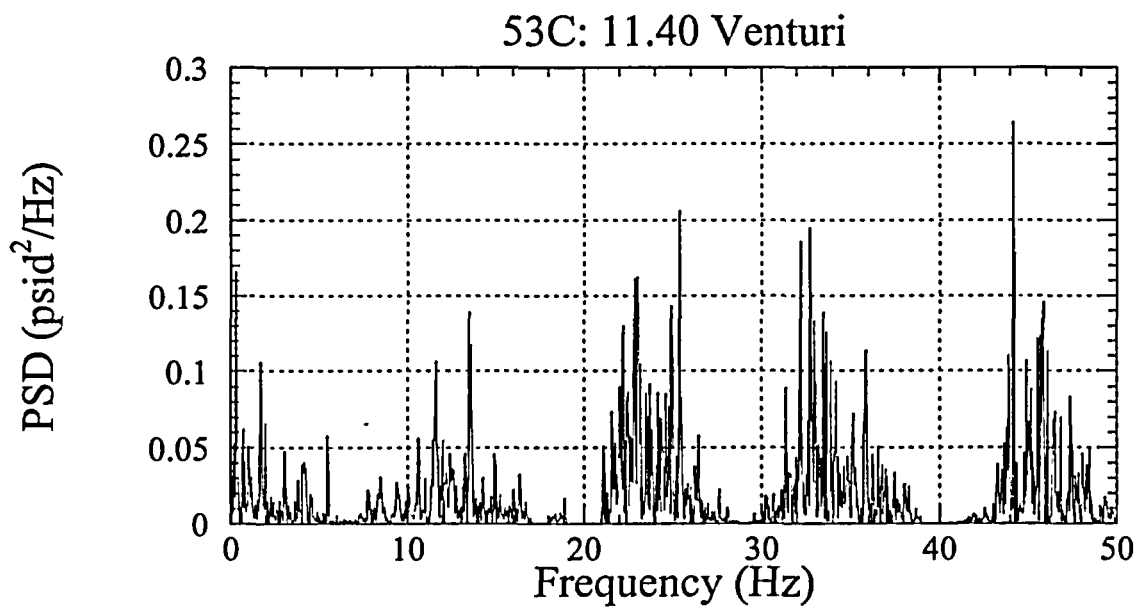
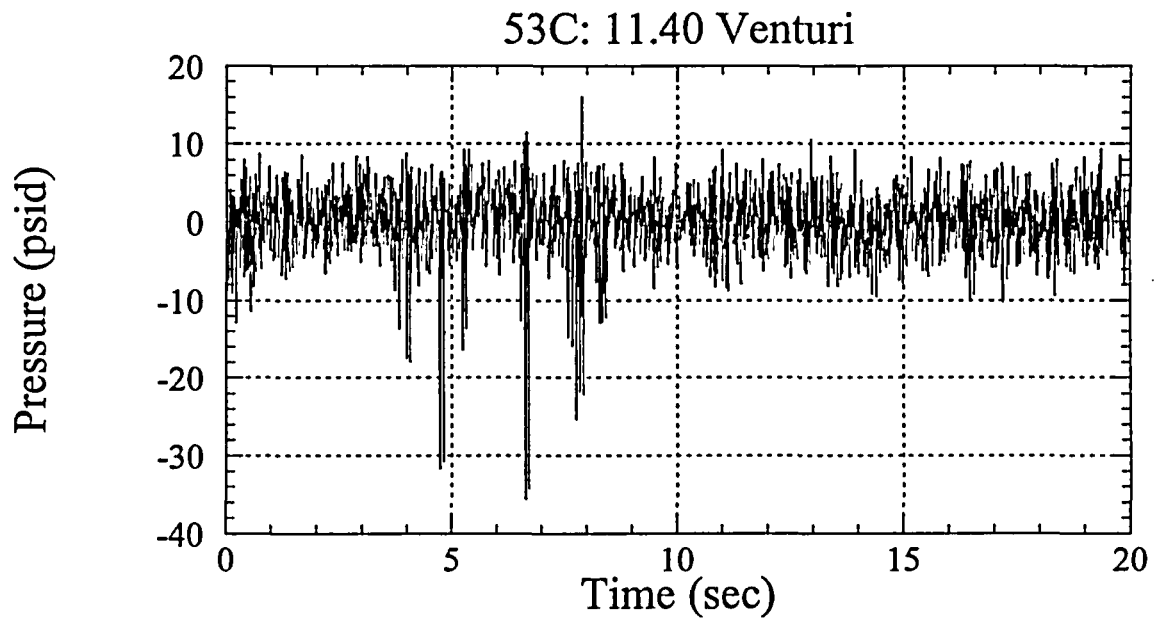


Figure 22-c

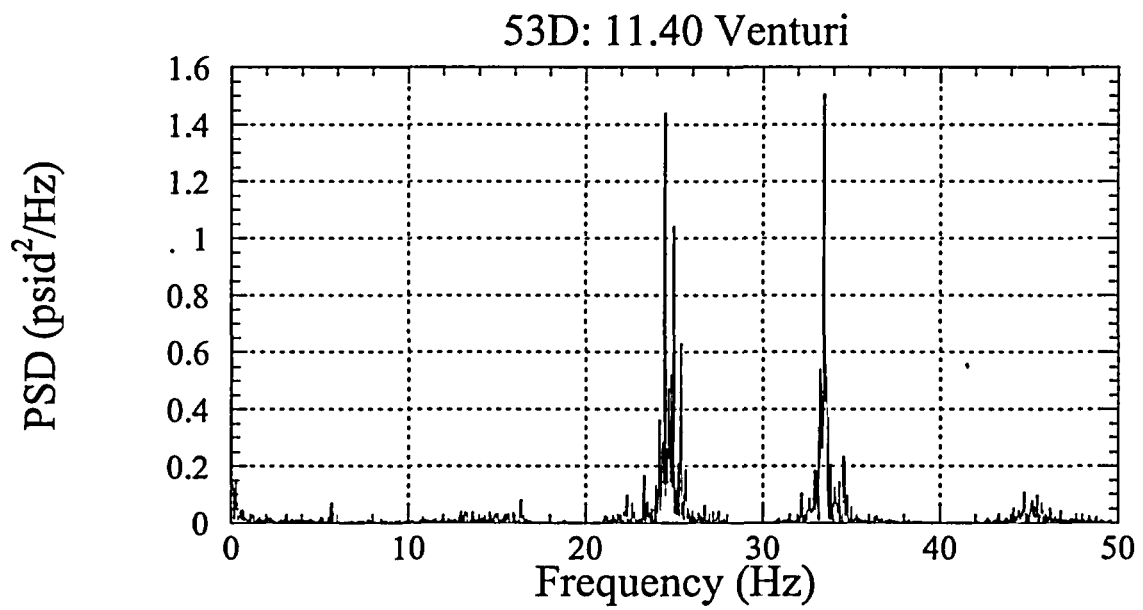
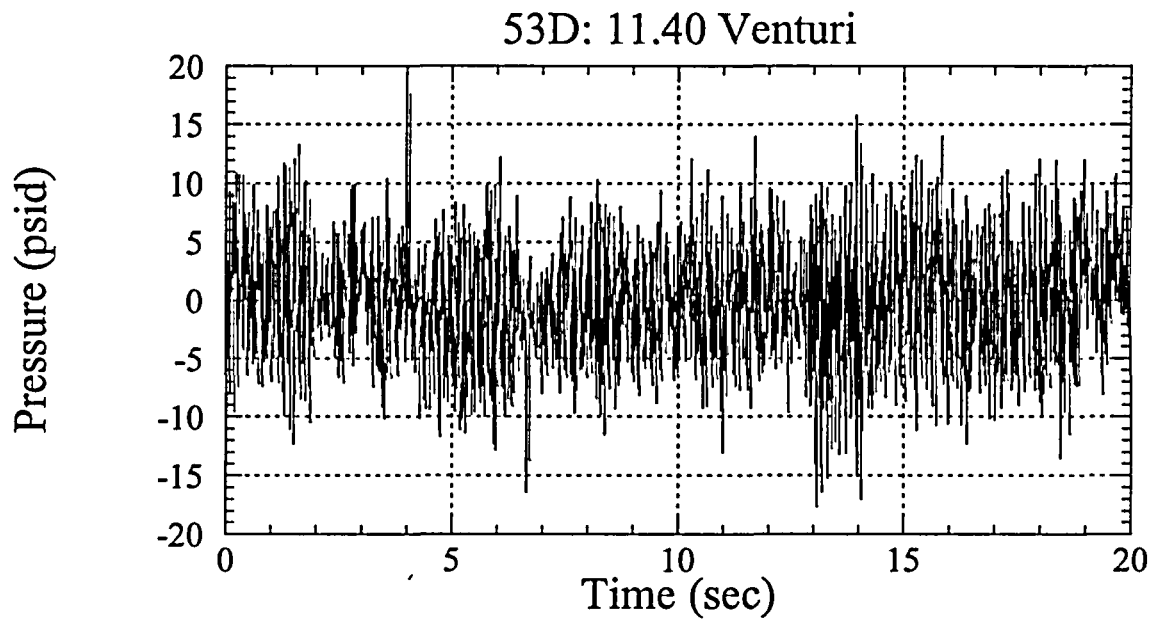


Figure 22-d

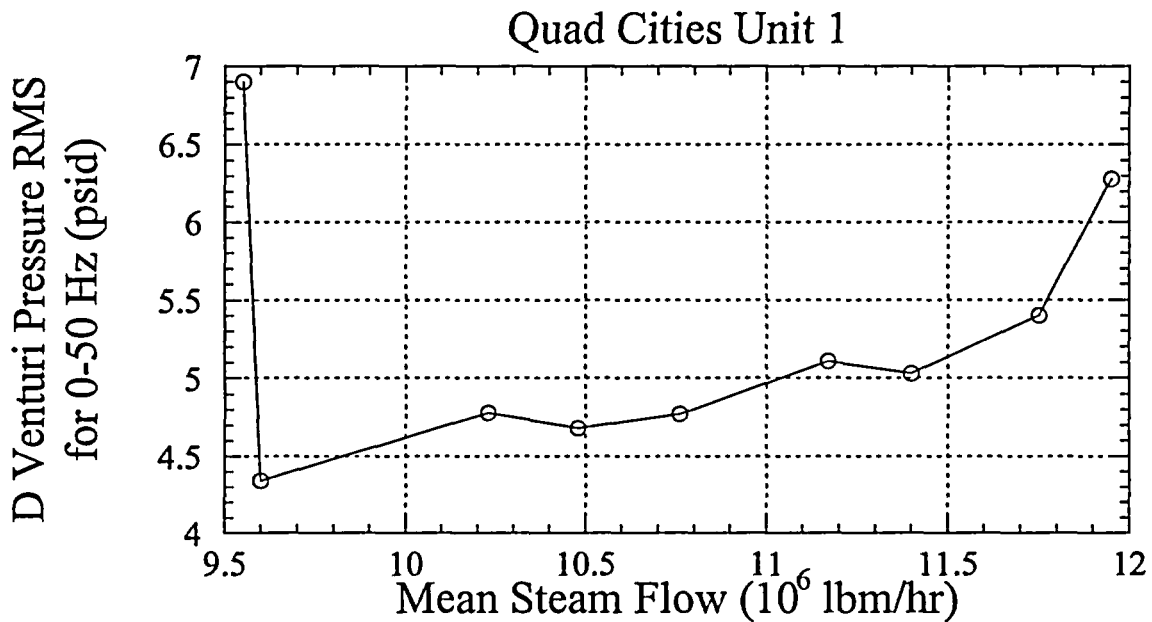


Figure 23. Comparison of RMS pressure data at the D venturi, corrected for instrument line length, for 0 to 50 Hz. The lowest mean steam flow rate ( $9.55 \times 10^6$  lbm/hr) includes nonphysical pressure data spikes that were not removed in the transfer from the end of the instrument line to the main steam vent. The highest mean steam flow rate ( $11.95 \times 10^6$  lbm/hr) is generated from data that were not taken in phase. Results for the mean steam flow rate of  $11.75 \times 10^6$  lbm/hr are detailed in the following figures.

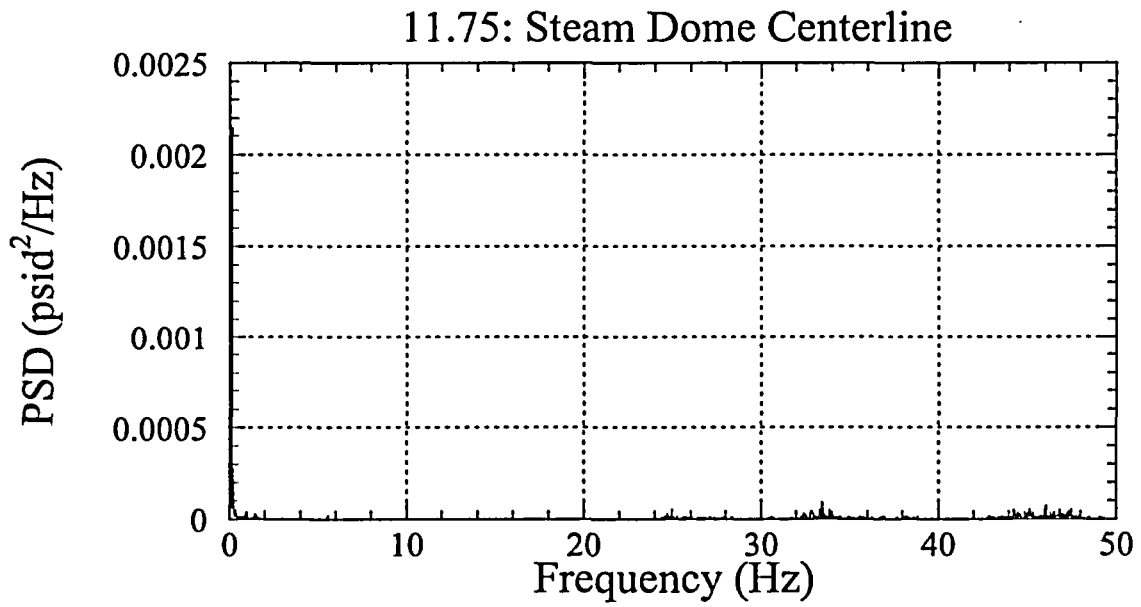
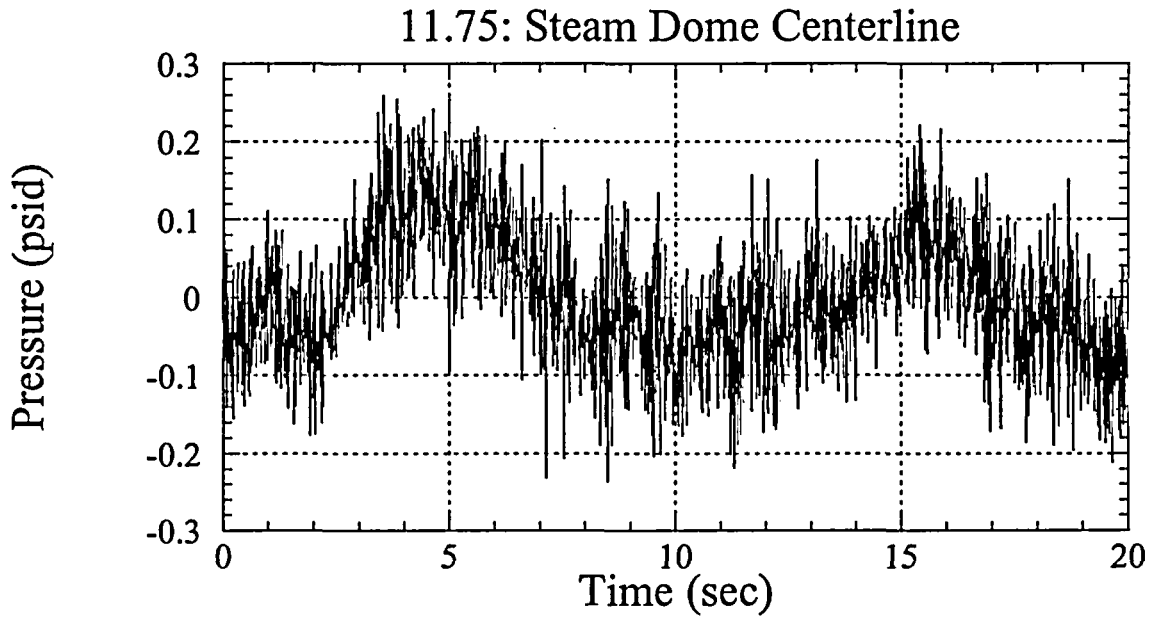


Figure 24. Predicted steam dome centerline pressures and associated PSD at a steam flow rate of  $11.75 \times 10^6$  lbm/hr.

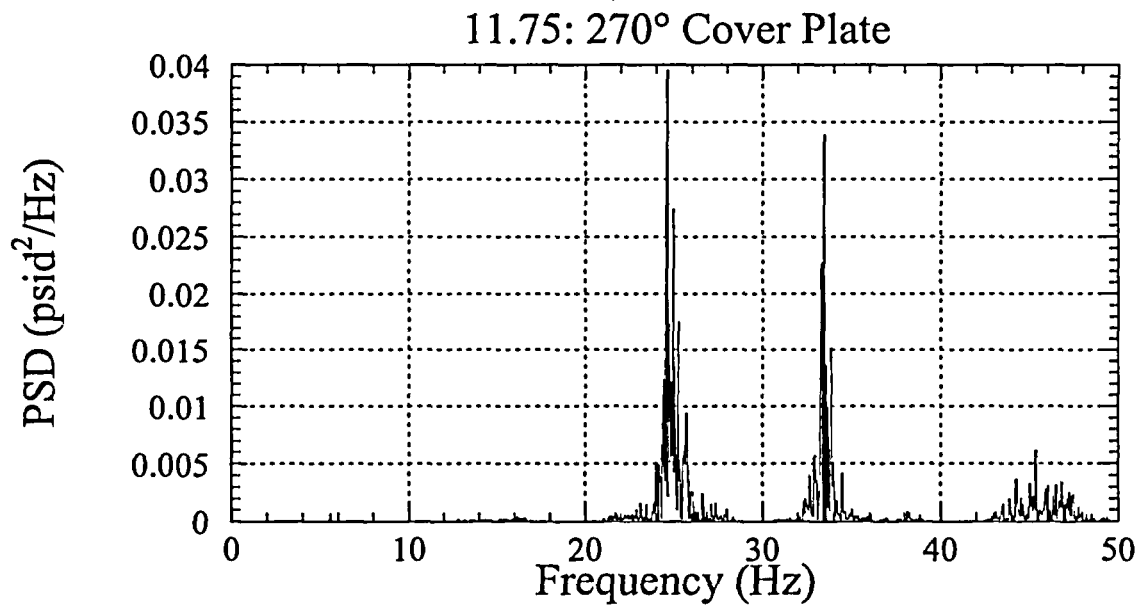
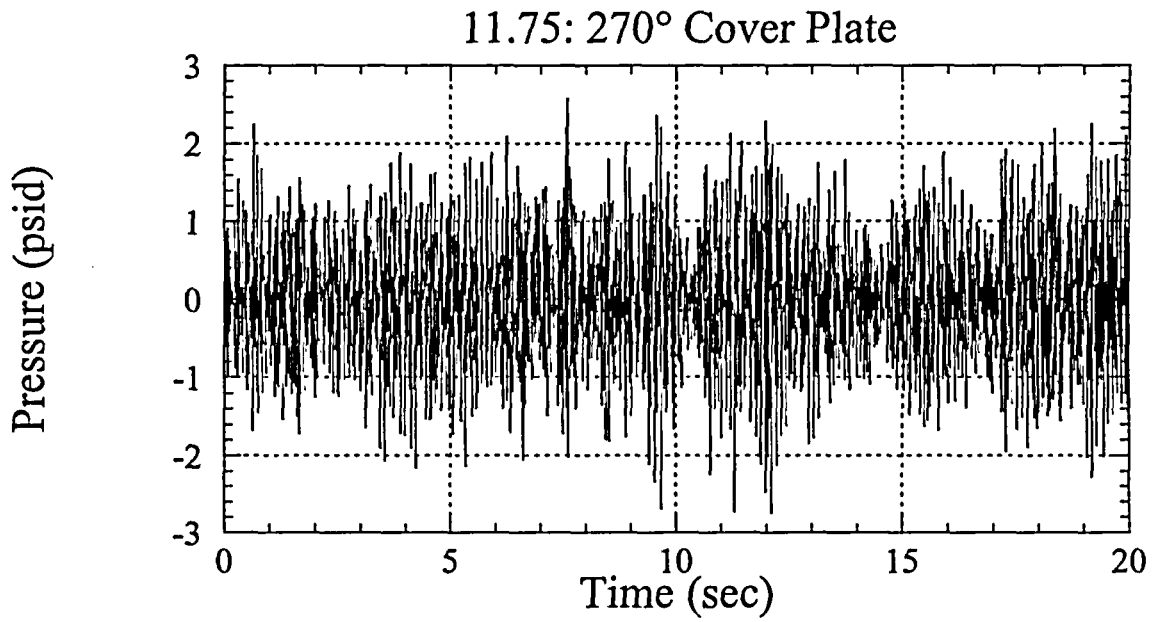


Figure 25. Maximum differential pressure load predicted across a dryer component.

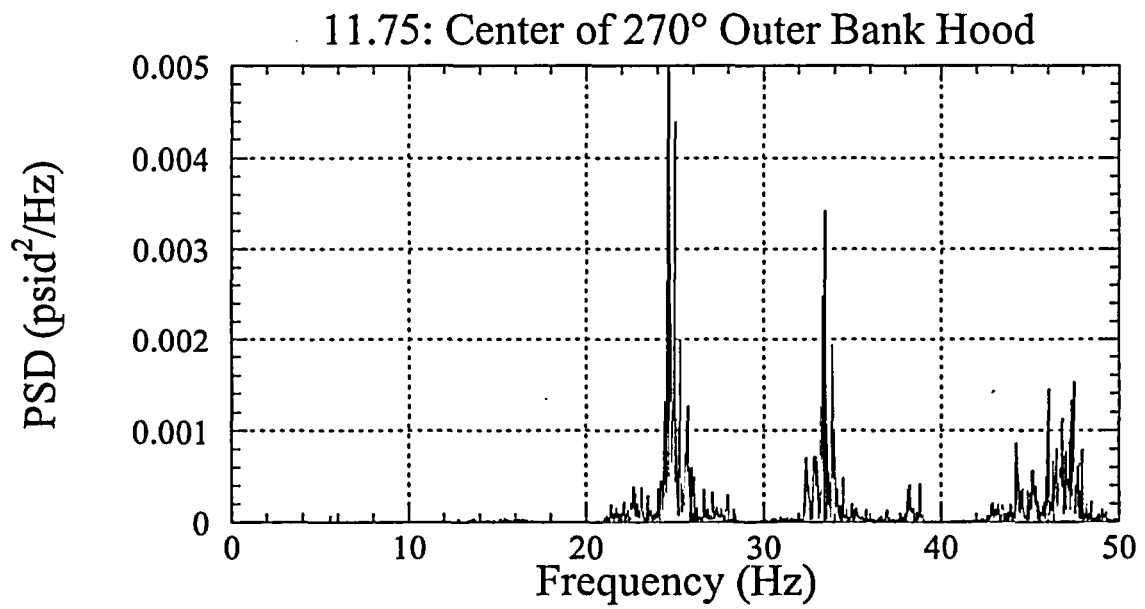
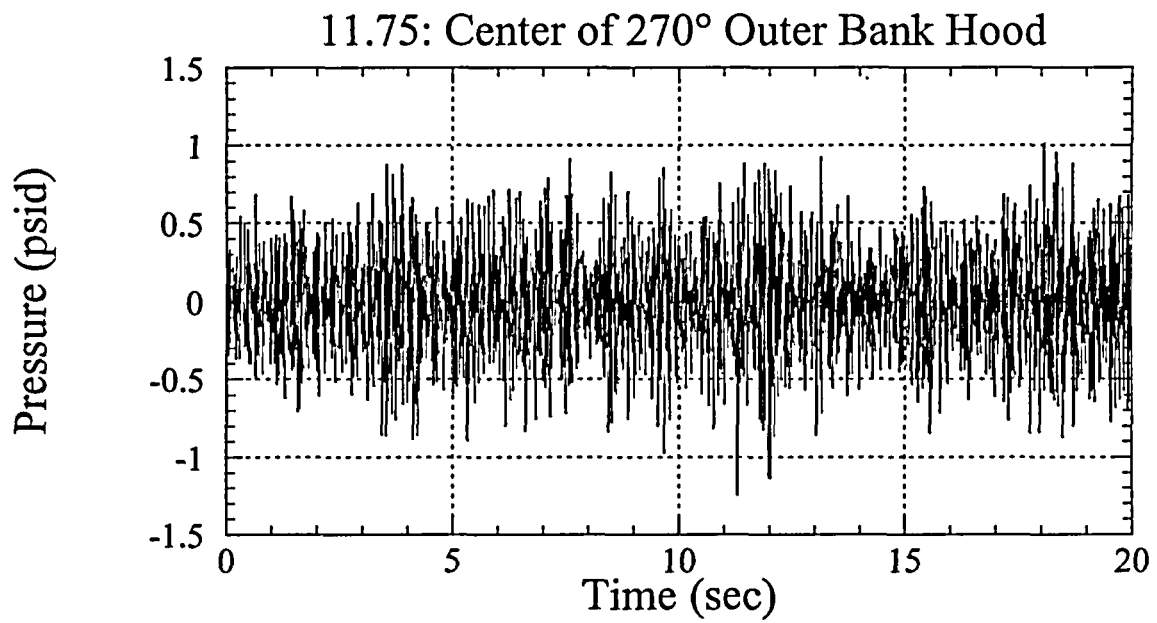


Figure 26.

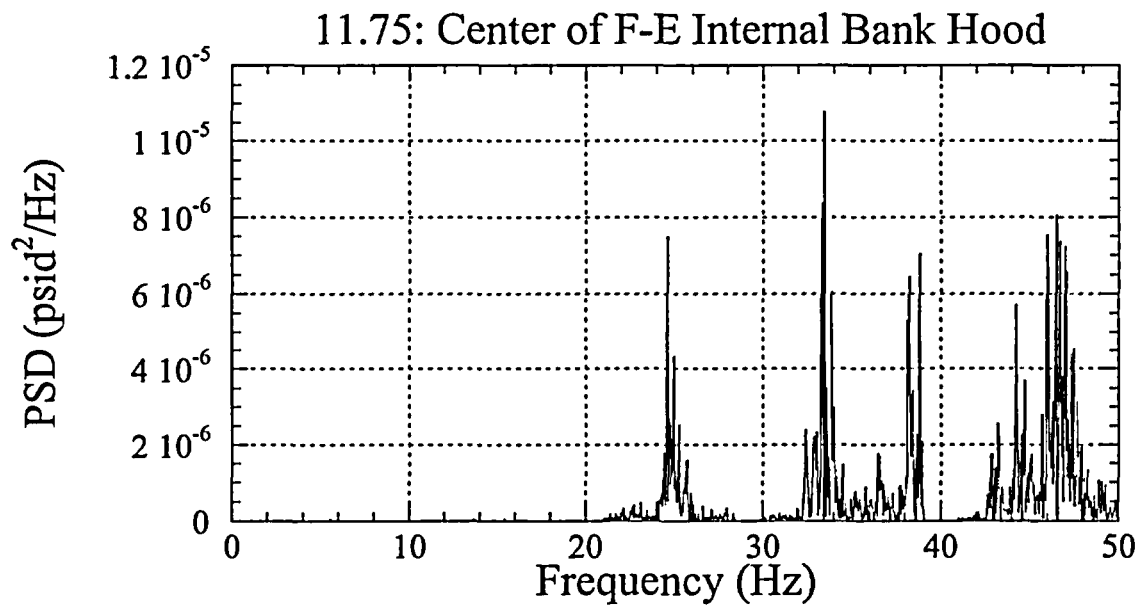
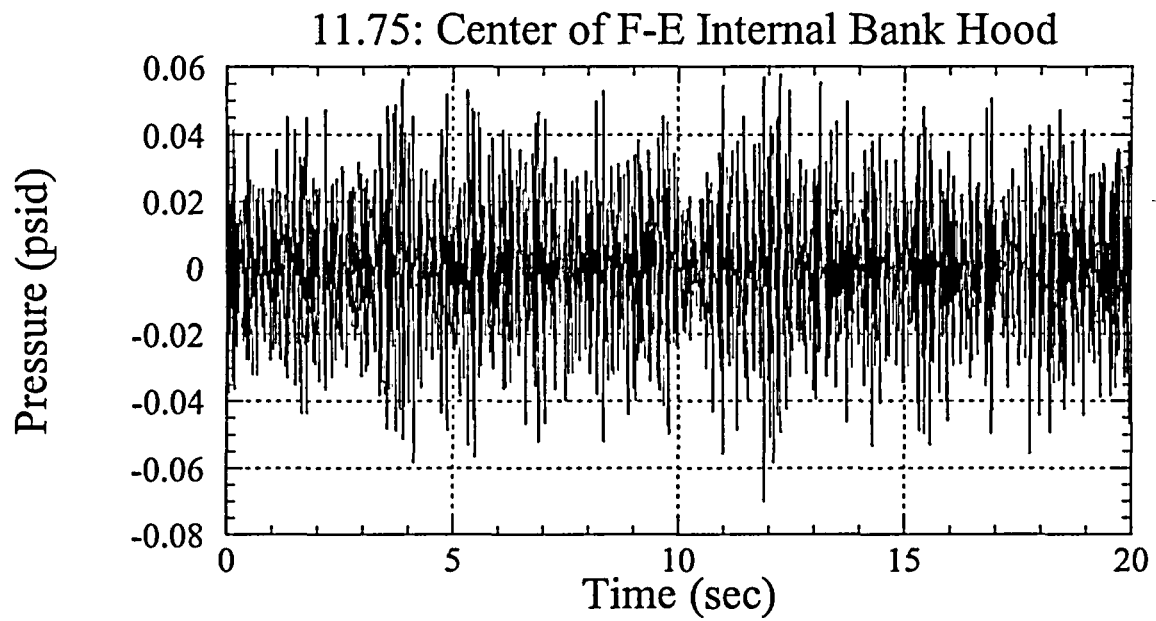


Figure 27.

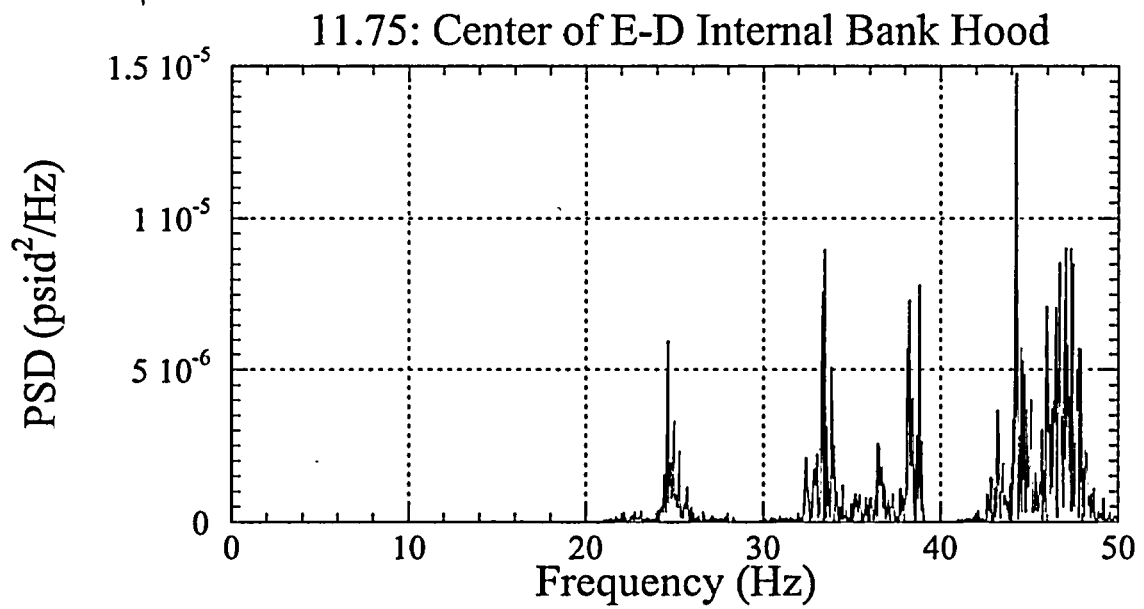
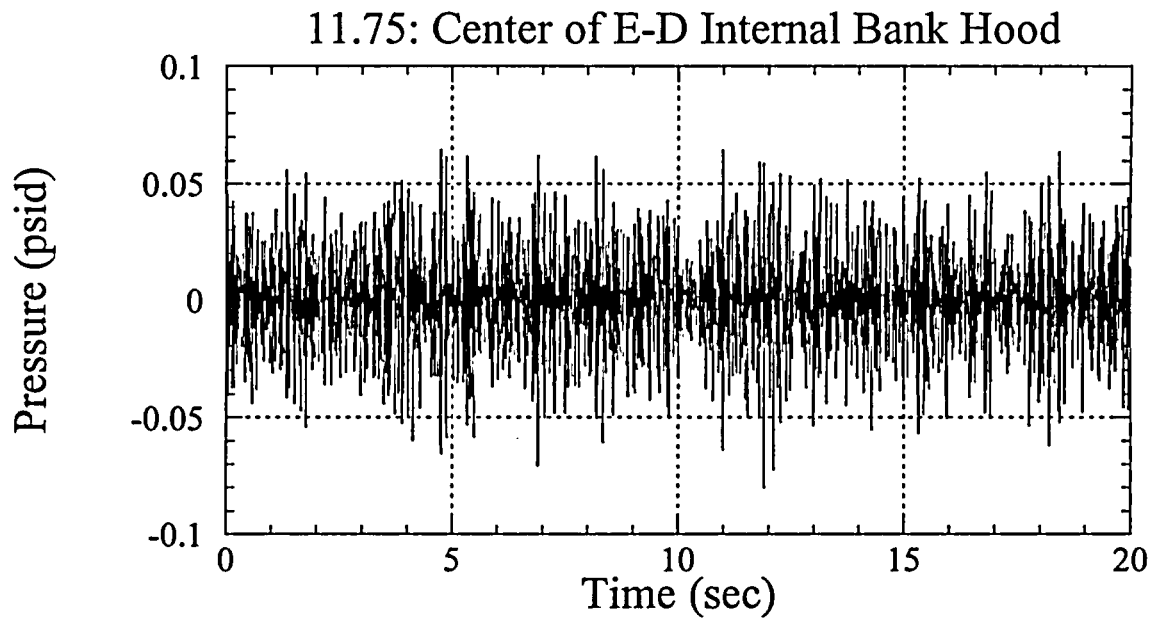


Figure 28.

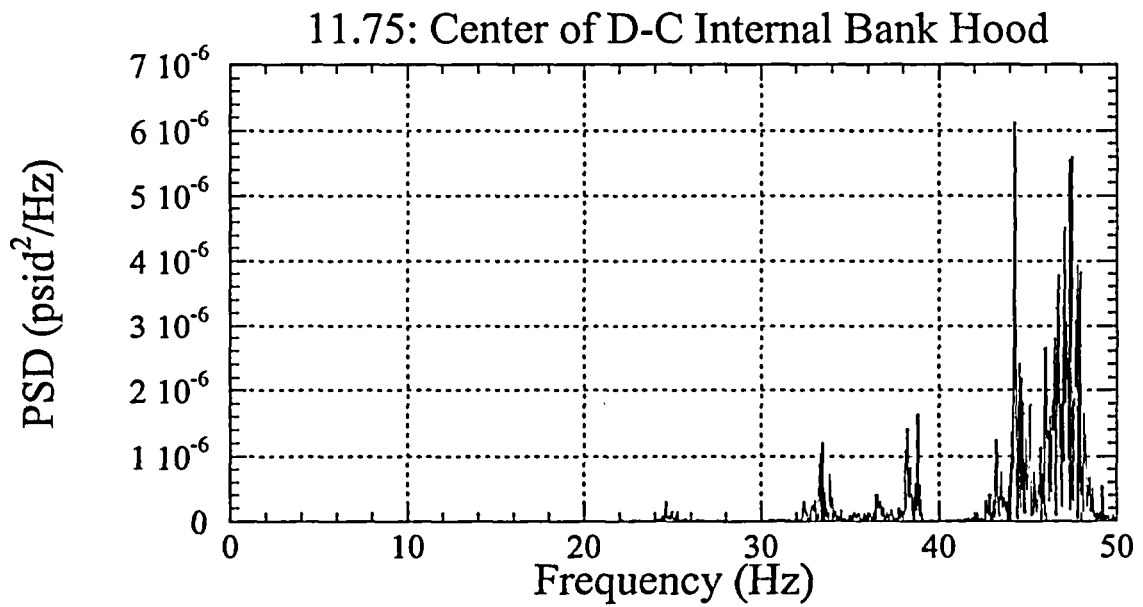
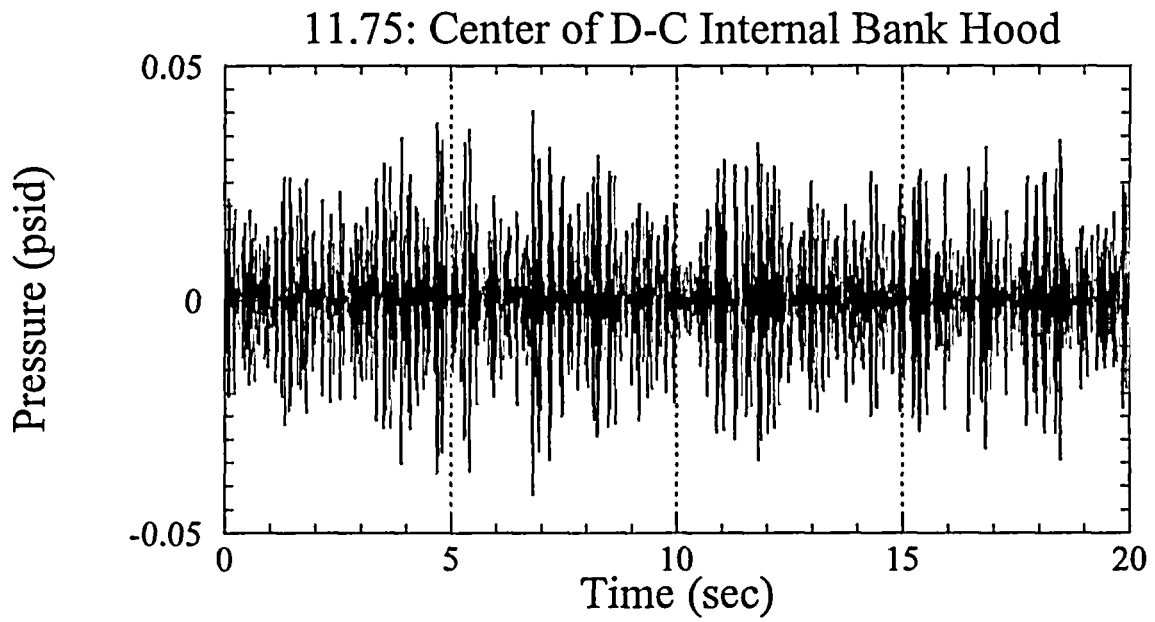


Figure 29.

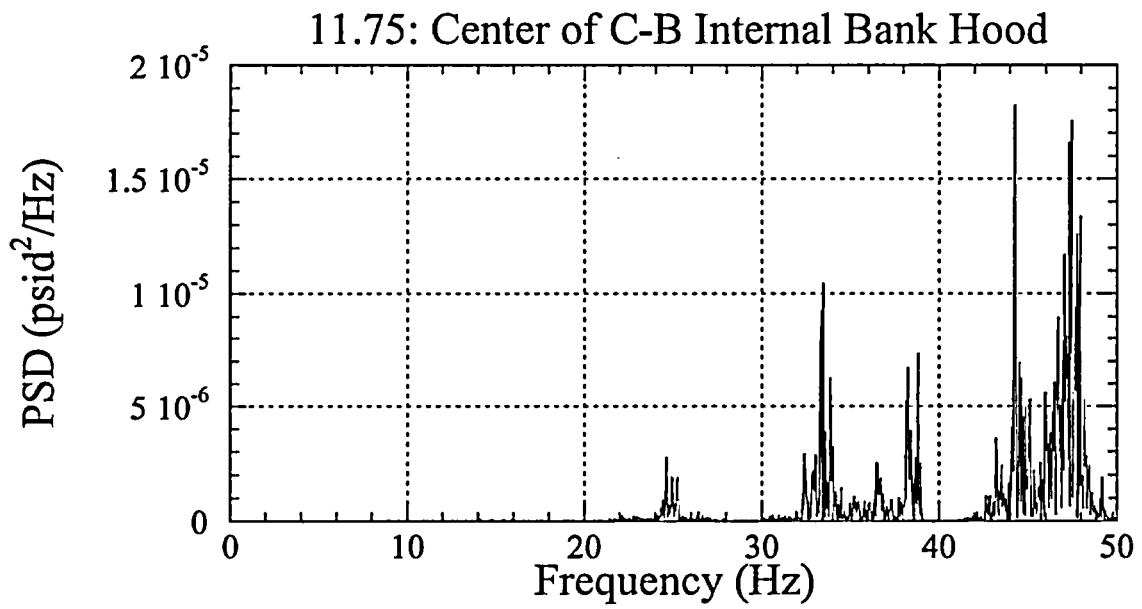
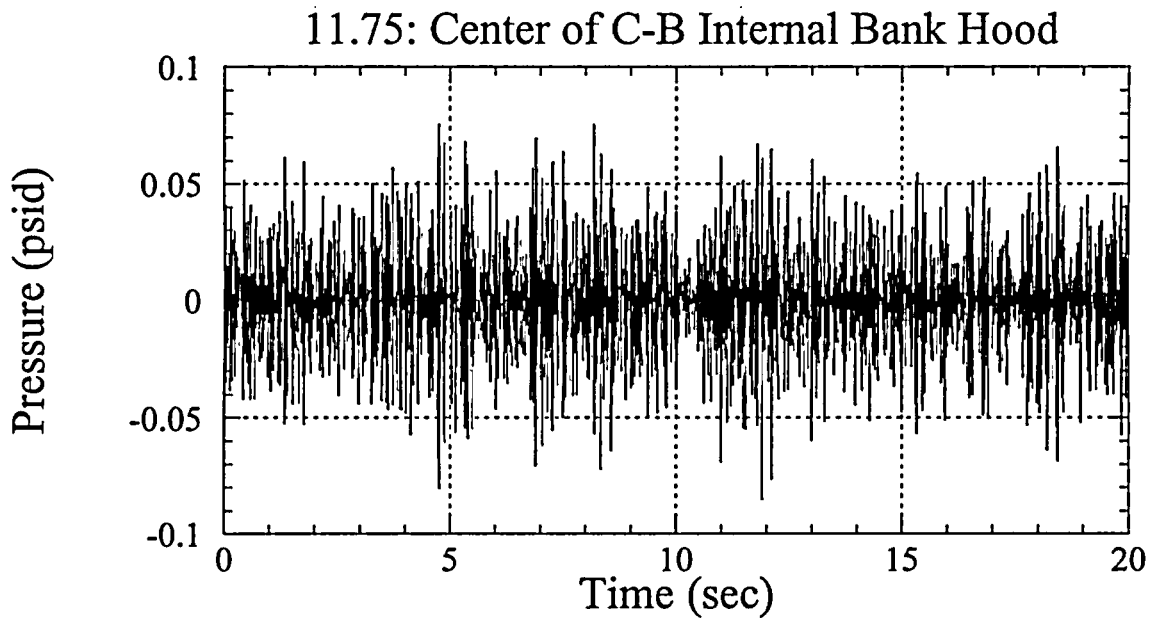


Figure 30.

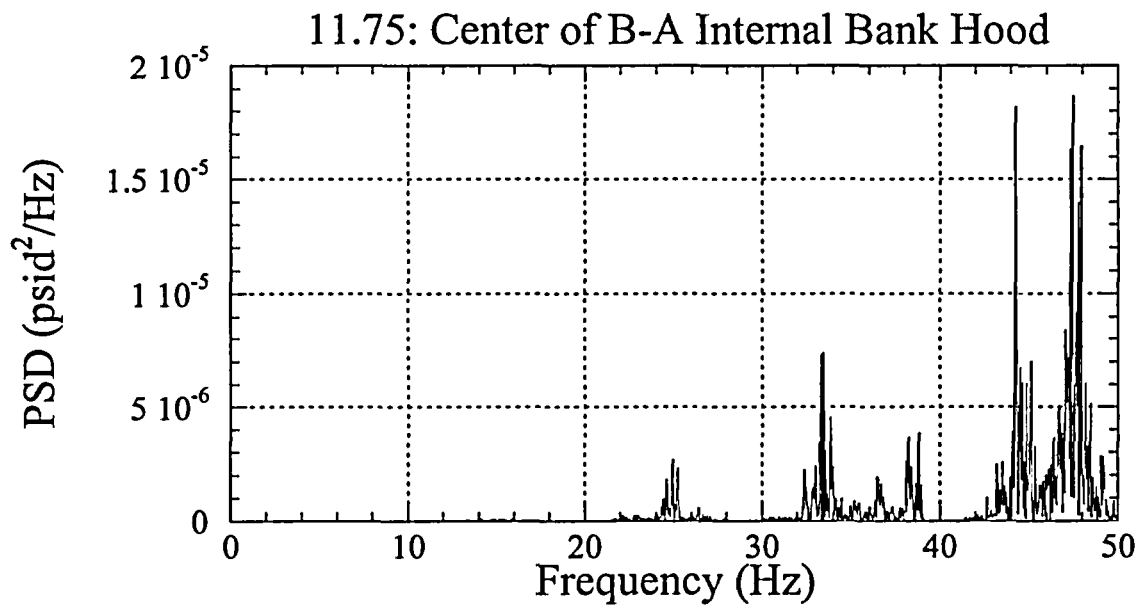
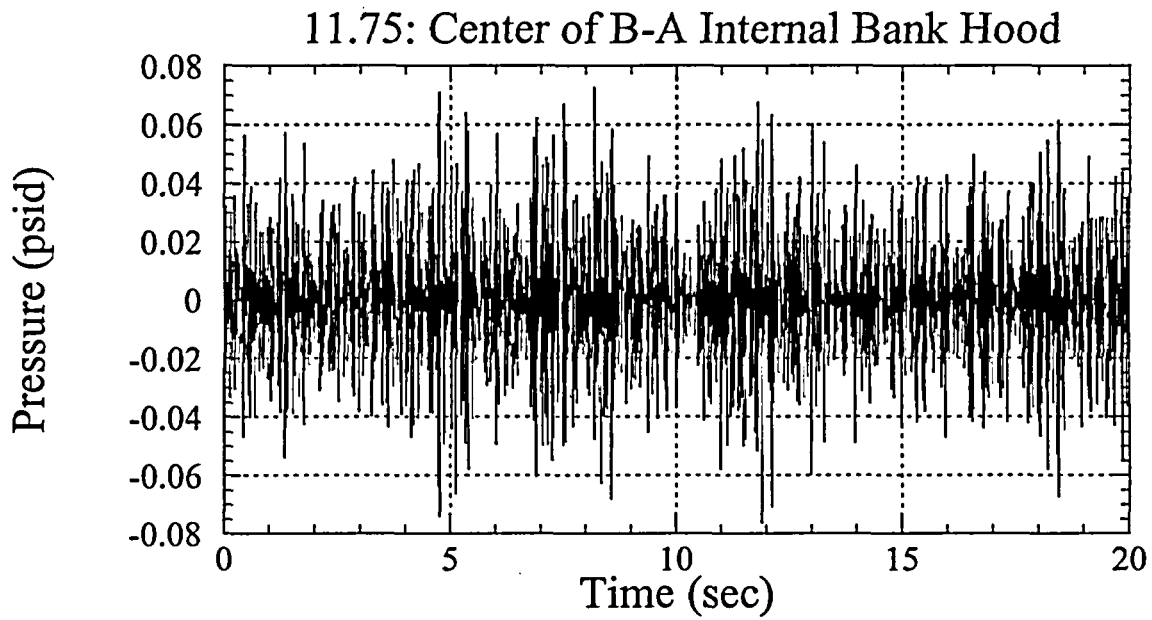


Figure 31.

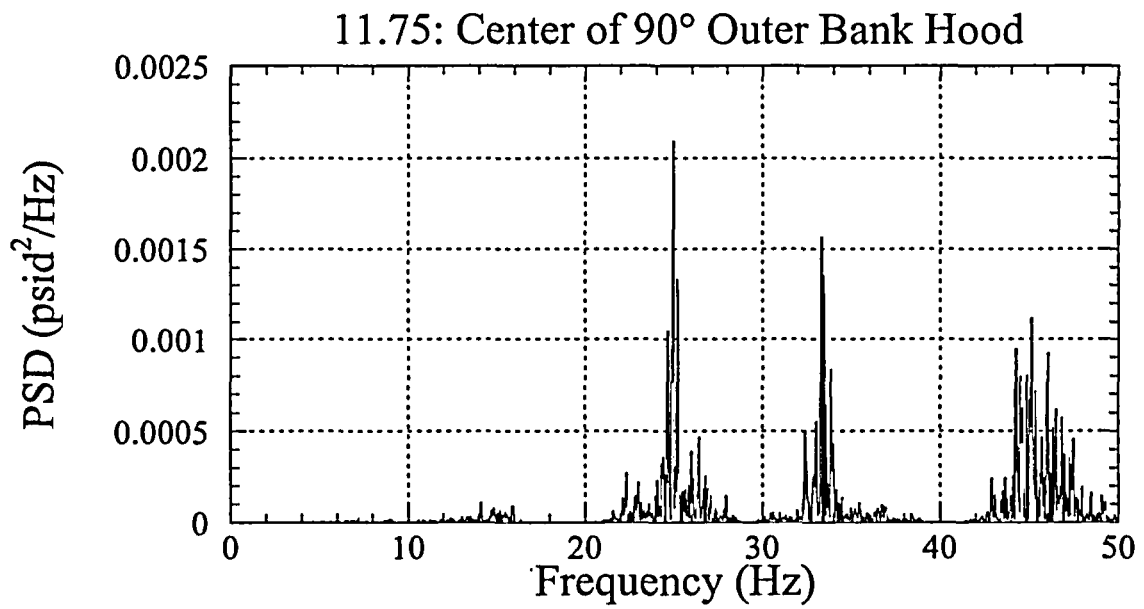
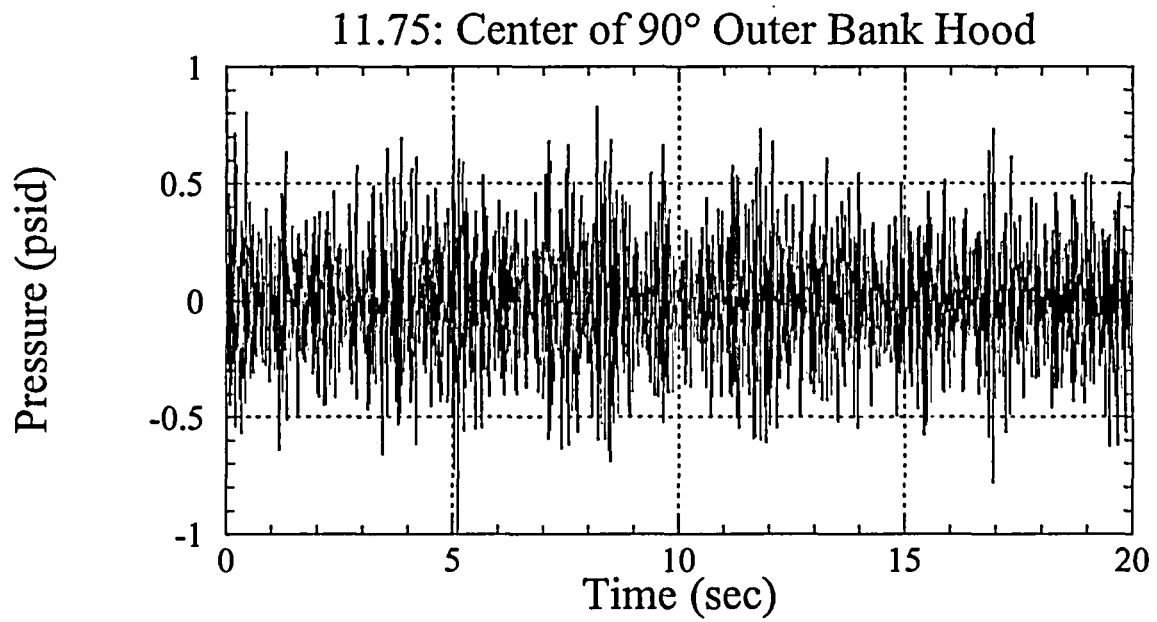


Figure 32.

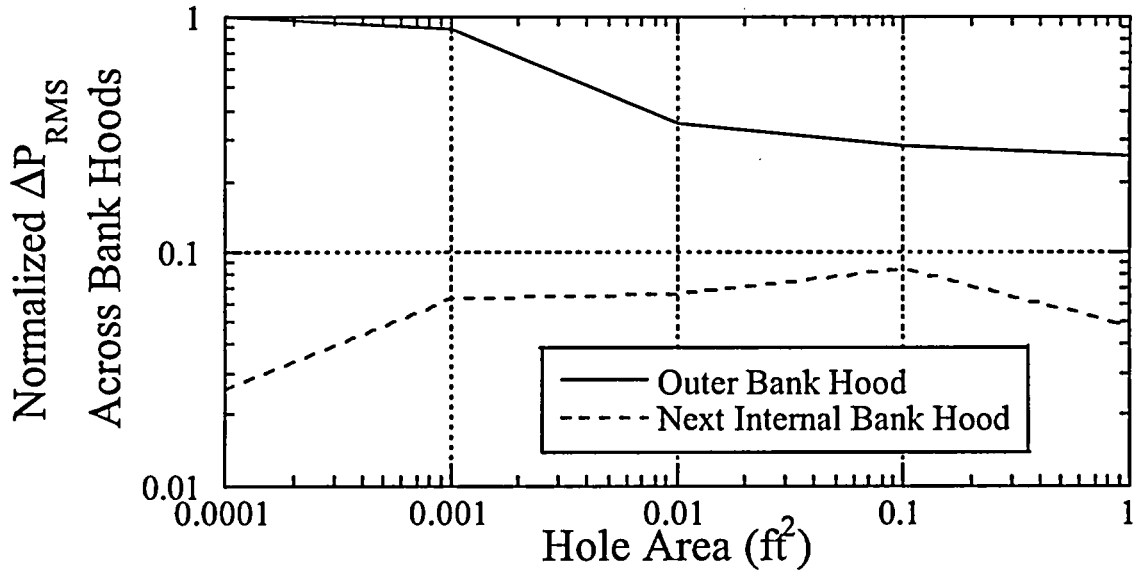


Figure 33.